Development of Photo-Induced Persulfate-Based Processes for Efficient Application in Water Treatment

BALPREET KAUR

TALLINN UNIVERSITY OF TECHNOLOGY
School of Engineering
Department of Materials and Environmental Technology
This dissertation was accepted for the defence of the degree 03/07/2020

Supervisor: Senior Research Scientist Dr. Niina Dulova
                            School of Engineering
                            Tallinn University of Technology
                            Tallinn, Estonia

Opponents: Prof. Laima Česonienė
                            Institute of Environment and Ecology
                            Vytautas Magnus University Agriculture Academy
                            Kaunas, Lithuania

                            Dr. Anne Menert
                            Chair of Genetics
                            University of Tartu
                            Tartu, Estonia

Defence of the thesis: 18/08/2020, Tallinn

Declaration:
Hereby I declare that this doctoral thesis, my original investigation and achievement, submitted for the doctoral degree at Tallinn University of Technology has not been submitted for doctoral or equivalent academic degree.

Balpreet Kaur

----
                                                    signature

European Union
European Regional
Development Fund

Investing
in your future

Foto-indutseeritud persulfaadi-põhiste protsesside väljatöötamine efektiivseks rakendamiseks vee puhastamisel

BALPREET KAUR

Contents

List of Publications

The list of author's publications, on the basis of which the thesis has been prepared:

I   Kattel, E., **Balpreet Kaur**, Trapido, M., Dulova, N. (2020). Persulfate-based photodegradation of a beta-lactam antibiotic amoxicillin in various water matrices. *Environmental Technology*, *41*, 202–210. doi.org/10.1080/09593330. 2018.1493149

II   **Balpreet Kaur**, Kuntus, L., Tikker, P., Kattel, E., Trapido, M., & Dulova, N. (2019). Photo-induced oxidation of ceftriaxone by persulfate in the presence of iron oxides. *Science of the Total Environment*, *676*, 165–175. doi.org/10.1016/j.scitotenv. 2019.04.277

III **Balpreet Kaur**, Dulova, N. (2020). UV-assisted chemical oxidation of antihypertensive losartan in water. *Journal of Environmental Management*, *261*, article id-110170. doi.org/10.1016/j.jenvman.2020.

IV   **Balpreet Kaur**, Kattel, E., Dulova, N. (2020). Insights into nonylphenol degradation by UV-activated persulfate and persulfate/hydrogen peroxide systems in aqueous matrices: a comparative study. *Environmental Science and Pollution Research*, *27*, 22499–22510. doi.org/10.1007/s11356-020-08886-y

Copies of these papers are included in Appendix.

Other publications related to the research:

Dulova, N.; Kattel, E.; **Balpreet Kaur**; Trapido, M. (2020). UV-induced persulfate oxidation of organic micropollutants in water matrices. *Ozone: Science & Engineering*, *42*, 13–23. 10.1080/01919512.2019.1599711.

Author's Contribution to the Publications

The contribution of the author to the papers included in the thesis is as follows:

I   The author carried out part of the experimental work and respective analyses, interpreted obtained data, and participated in writing of the paper.

II The author carried out experimental work, interpreted the results, and wrote the paper with the help of co-authors.

III The author carried out major part of the experimental work, supervised the experimental work of M.Sc. student, interpreted the results, and wrote the paper with the help of a co-author. She presented the results at the 4th International Conference on Photocatalytic and Advanced Oxidation Technologies for the Treatment of Water, Air, Soil, and Surfaces (PAOT-4).

IV The author carried out major part of the experimental work, supervised the experimental work of M.Sc. student, interpreted the results, and wrote the paper with the help of co-authors. She presented the results at the 6th European Conference on Environmental Applications of Advanced Oxidation Processes (EAAOP-6) and at the 20th European Meeting on Environmental Chemistry (EMEC-20).

Introduction

Over the years, emerging contaminants (ECs) are frequently detected in water matrices. Sources of such pollutants are the pharmaceutical industry, the cosmetic industry, the use of pesticides, etc. Effluent generated from these sources or surface runoff from agricultural areas allows the pollutants to enter different compartments of the environment. Therefore, conventional physical-biological water treatment techniques have been investigated to remove ECs from aqueous matrices. However, the effectiveness of most traditional three-step wastewater treatment plants (WWTPs) is insufficient to completely remove such pollutants and may lead to the formation of even more toxic by-products. As a result, residual ECs enter the drinking water resources as well as the food chain and can be a long-term risk to the ecosystem.

The application of advanced oxidation processes (AOPs) has demonstrated great potential for the treatment of water and wastewater in order to eliminate toxic, non-biodegradable, and recalcitrant organic compounds. Traditionally, the AOPs involved the generation of hydroxyl radicals (HO$^{\bullet}$) through different methods, including a combination of oxidizing agents (such as H_2O_2 and O_3), irradiation (such as ultraviolet (UV) light or ultrasound (US)), transition metal (such as Fe^{2+}, Co^{2+}, and Mn^{2+}), and heterogeneous activators. The non-selectivity of hydroxyl radical towards its target compound allows elimination of the contaminant along with its intermediate products. However, the HO$^{\bullet}$ based AOPs demonstrate lower efficiency in complex environmental matrices containing dissolved organic matters and carbonate/bicarbonate anions, which act as HO$^{\bullet}$ scavengers.

Recently, sulfate radicals (SO$_4^{\bullet-}$) based AOPs have proven to be a promising alternative to HO$^{\bullet}$ based AOPs for pollutant degradation in water treatment. Sulfate radicals are increasingly emerging as an oxidizing agent, which have a high redox potential as well as high selectivity and stability in aqueous solution.

The emphasis of this thesis was to evaluate the effectiveness of UV-induced persulfate (PS) oxidation processes in the degradation of various micropollutants that have been detected at very low concentrations (ng L^{-1}-μg L^{-1}) in different water matrices. The study aimed to enlarge the existing knowledge on the application of UV-activated PS system alone and in combination with other homogeneous and heterogeneous PS activators in different aqueous matrices treatment. Important parameters, such as the direct UV photolysis, pH value, activator dosage, oxidant concentration, and influence of water matrices, which determine emerging contaminants decomposition efficiency, were evaluated and optimized.

Among the emerging contaminants considered in this thesis were two β-lactam antibiotics, namely amoxicillin (AMX) and ceftriaxone (CTA), an endocrine disrupting compound, nonylphenol (NP), and angiotensin receptor blocker, losartan (LOR). The oxidation of AMX using UVC and UVC/Fe^{2+}-activated PS was studied in four different matrices, such as ultrapure water (UW), drinking water, groundwater (GW), and recycled wastewater. The removal of CTA from UW and GW was investigated using UV-activated PS and its combination with ferrous ions or heterogeneous iron oxides. The efficacy of UVC-induced PS and PS/H_2O_2 systems in NP decomposition in UW and GW was studied and compared. Finally, LOR oxidation in UW and GW was performed using UVC(/Fe^{2+})-activated PS processes.

The knowledge gained in this thesis contributes to the further development of the activated persulfate oxidation processes and their full-scale applications in water matrices treatment.

Abbreviations

AMX	Amoxicillin
AOPs	Advanced oxidation processes
AOTs	Advanced oxidation technologies
ARB	Angiotensin receptor blocker
CTA	Ceftriaxone
DW	Distilled water
EC	Emerging contaminant
EtOH	Ethanol
EU	European union
FDA	Food and drug administration
GW	Groundwater
HO$^{\bullet}$	Hydroxyl radical
HPLC	High-performance liquid chromatography
HPLC-MS	High-performance liquid chromatography combined with a mass spectrometry
LOR	Losartan
NOM	Natural organic matter
NP	Nonylphenol
NPEs	Nonylphenol-ethoxylates
PS	Persulfate
SO$_4^{\bullet-}$	Sulfate radicals
STWW	Secondary treated wastewater
t-BuOH	Tert-butanol
TOC	Total organic carbon
TP	Transformation products
US	Ultrasound
UV	Ultraviolet
UVA	Ultraviolet A (longwave UV, λ=315-400 nm)
UVC	Ultraviolet C (shortwave UV, λ=200-280 nm)
UW	Ultrapure water
WHO	World Health Organization
WWTPs	Wastewater treatment plants

1   Literature review

1.1   Emerging contaminants

The ECs have a detrimental impact on the aquatic ecosystem and human health. The past decades have seen an increasing number of organic contaminants such as pharmaceuticals and personal care products, steroids, pesticides, endocrine disruptor chemicals, artificial sweeteners, etc. The main routes of ECs entering into the environment are anthropogenic. As a result, the detection of ECs in water sources and associated potential toxic effect to ecosystems as well as human health has been issue of concern for the researchers (Martín-Pozo et al., 2019).

As shown in Figure 1, the untreated and concentrated wastewater generated from the pharmaceutical industries, chemical industries, and hospitals is eventually discharged into the sewer and ends up at a wastewater treatment plant. Moreover, pharmaceuticals after use are usually only partially metabolized in the body, and thus the original substances and their metabolites enter the sewer and then to the WWTPs. Since WWTPs are rarely equipped to detect or remove these pollutants from influent and effluent, treated wastewater from WWTPs is one of the main ECs sources in the environment. Micropollutants entering this way into receiving water bodies frequently can be detected in the drinking water supply system.
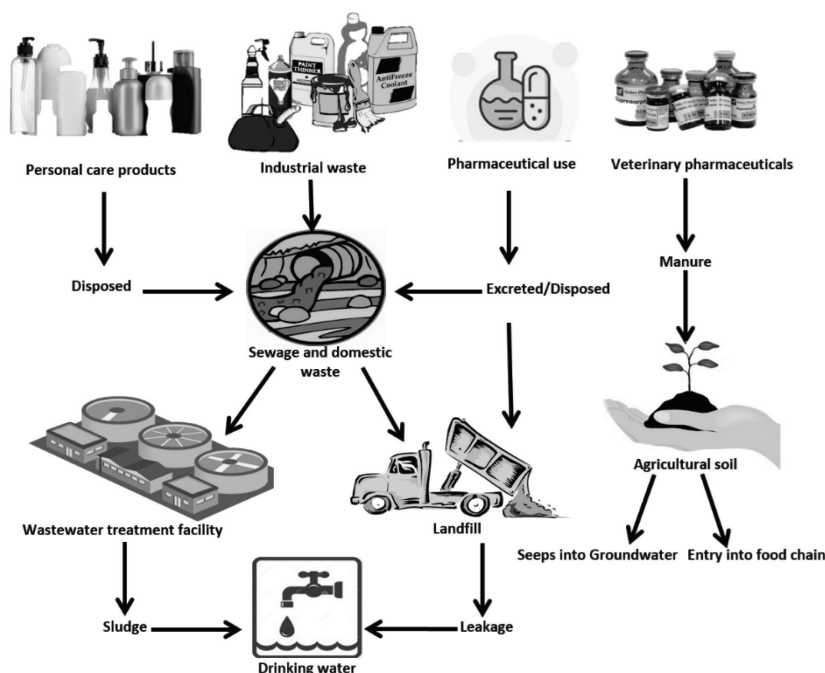
Figure 1. Sources and pathways of emerging contaminants in the environment

Another important ECs exposure pathway is the agricultural waste and manure, which contain excreted veterinary medicinal products and usually then used as compost. This reuse of manure allows residual drugs, including antibiotics, to enter the soil and finally the food chain. As a result, the traces of the organic pollutants or the transformation products are released into the environment. The continuous exposure to

low concentrations of the antibiotics (ng L^{-1} and μg L^{-1}) can lead to elevated antibiotic resistance in healthy individuals or in worst scenario cause "multidrug resistance". The antibiotic resistant microbes could be detected in both influent and effluent of municipal WWTPs.

Therefore, the focus of this thesis was to investigate the elimination of the following emerging contaminants from water matrices:

Amoxicillin

Amoxicillin (AMX), a semi-synthetic penicillin contributing to >50% consumption worldwide, is a widely consumed β-lactam antibiotic and has proved effective against an extensive range of gram-positive and gram-negative bacteria in both humans and animals (Bush et al., 2010). AMX is used to treat ear, nose and throat infections, infection of genitourinary and lower respiratory tract, infection of the skin and skin structure, sexually transmitted disease, and in the triple therapy of *Helicobacter pylori* infection (Graham et al., 2010; Rahmati et al., 2017). Numerous literature studies have detected the presence of AMX in different water matrices. For instance, AMX was detected in hospital effluent (80-900 ng L^{-1}) (Kasprzyk-Hordern et al., 2008; Kümmerer, 2001) WWTPs effluent (50 ng L^{-1}) (Fatta-Kassinos et al., 2011) raw sewage (280 ng L^{-1}) (Kasprzyk-Hordern et al., 2008), surface water (200 ng L^{-1}) (Fatta-Kassinos et al., 2011), and activated sludge (622 ng L^{-1}) (Castiglioni et al., 2005). The presence of AMX in the environment has adverse consequence on the ecosystem. Accordingly, AMX proved to have the noxious effect on the photosynthesis of *Synechocystis sp* (Pan et al., 2008) and on the larvae of fish (Yasser et al., 2015). Literatures have reported the antibiotic resistant microbial species and accordingly, *Enterobacteriaceae*, *Enterococcus spp.* and *Pseudomonas spp.* were up to 100% AMX resistant. Notably, among *Flavobacterium isolates*, resistance to AMX was 36% (Matsuo et al., 2011). *Escherichia coli spp.* were 18% and *Klebsiella* spp. were 13% resistant to AMX (Vazouras et al., 2020).

Ceftriaxone

Ceftriaxone (CTA), a broad-spectrum third-generation cephalosporin, was approved for clinical use by the FDA in 1984 and belongs to β-lactams. According to the antibiotic classification CTA is widely used to treat bacterial infections such as meningitis, respiratory tract, urinary tract, soft tissue, and joint infections due to its therapeutic efficacy against gram-positive and gram-negative bacteria (Kanwal et al., 2019). CTA is detected in hospital effluents (600 ng L^{-1}) (Diwan et al., 2010), wastewater influent (15.15 ng L^{-1}), and WWTP effluent (2.03 ng L^{-1}) (Yu et al., 2016). The adverse effects of CTA on the ecosystem have been investigated. For instance, the presence of CTA in ecosystem has proven to be hindering the photosynthesis of *Triticum aestivum* (Opriş et al., 2013). The gram-negative antimicrobial susceptibility test results indicated *Escherichia coli spp.* were 24% and *Klebsiella spp*. were 19% resistant to CTA (Yu et al., 2020).

Nonylphenol

Nonylphenol-ethoxylates (NPEs) are non-ionic surfactants contributing to 60% of total surfactant market (Loyo-Rosales et al., 2010). The widespread use of NPEs as emulsifiers, detergents, dispersants, lubricant etc., leads to their entry into the sewers and, as a result, to WWTPs. At the WWTPs the partial oxidation of NPEs can generate more toxic short-chain, synthetic compounds such as nonylphenol (NP), nonylphenol ethoxylate,

nonylphenol diethoxylate, and nonylphenoxyacetic acid (Kümmerer, 2009). Thus, NPs due to its ability to mimic the natural hormones of estrogen are recognized carcinogens (Guenther et al., 2002). For example, NPs are responsible for the multiplication of breast cancer cells as well as the hormonal disruption in animals (Karci et al., 2013). In year 2001, the European Union (EU) Water Framework Directive listed NP as a priority pollutant. As a result, the production and use of NP was restricted (Ince et al., 2009).

Several reports have indicated the presence of NP in surface and treated wastewater. For instance, NP at low concentrations was detected in tap water (1.98 ng L^{-1}) (Li et al., 2010), drinking water (2.7 ng L^{-1}) (Shao et al., 2005), wastewater influent (96.4 ng L^{-1}) (Klečka et al., 2010). Moreover, the NP has been detected in food chain and aquatic species (Jobling et al., 1993; Niu et al., 2015). Thus, the consumption of food and water contaminated with NP can lead to hormone-dependent cancers, as well as hormonal imbalances in humans and animals. Moreover, the toxic effect of NP on the plant growth in *Vigna radiate, Triticum aestivum, Brassica napus* and *Oryza sativa* was reported (Kim et al., 2019; Roberts et al., 2006).

Losartan

Losartan (LOR) is a widely used angiotensin receptor blocker (ARB) to treat high blood pressure, cardiovascular and neuroendocrine functions. According to the World Health Organization (WHO), LOR is listed as an essential pharmaceutical (Boslaugh, 2016). Due to the escalating consumption and partial metabolism of LOR in the body upon consumption, a significant amount of LOR is excreted as the parent compound. LOR is reported to be resistant to hydrolysis and biodegradation thus escape from WWTPs into the ecosystem (De Andrade et al., 2020). As a result, LOR were detected in seawater (0.60-8.70 ng L^{-1}) (Cortez et al., 2018), WWTP influent (19.7-2760 ng L^{-1}) (Ashfaq et al., 2017; Botero-Coy et al., 2018; Casado et al., 2014; Yuwen Wang et al., 2018), rivers (149 ng L^{-1}) (Barrera-Díaz et al., 2018), hospital effluent (Abu Jafar Khan et al., 1996) and wetlands (22.9 µg L^{-1}) (Bennett et al., 2018). The bioaccumulation of LOR in the environment and entry into the food chain can be hazardous to human and aquatic life. The toxicity of LOR was reported against *Drosophila melanogaster, Lemna minor* (Godoy et al., 2015; Silva-Oliveira et al., 2016).

1.2   Traditional water and wastewater treatment for removal of emerging contaminants

Due to ecological superiority, low economic cost, the biological methods are applied to eliminate organic load from wastewaters, though the degradation efficiency depends on the structural properties of the organic pollutant. In general, organic pollutants with high solubility in water, low acute toxicity are easily removed or demonstrate enhanced BOD reduction than micropollutants removal. In turn, it is known that pollutants with high bioaccumulation, biomagnification, and biotoxicity are resistant to complete biological oxidation (Kanaujiya et al., 2019). The efficacies of biological processes to degrade ECs in various water matrices are presented in Table 1.

Additionally, physico-chemical techniques namely coagulation, flocculation, filtration, membrane separation, ion exchange, adsorption, etc., have been extensively studied for the removal of ECs from water and wastewater (Table 2).

Table 1. Application of biological techniques to eliminate ECs in different water matrices

Classification	Category	Emerging compounds	Method	Water matrices	Removal Efficiency (%)	Reference
Pharmaceuticals	β-Lactam antibiotics	Ampicillin	Anaerobic baffled reactor	Wastewater	42	(Zhou et al., 2006)
		Ceftriaxone	Anaerobic membrane bioreactor	Pharmaceutical wastewater	48	(Huang et al., 2018)
		Ceftriaxone	Upflow anaerobic sludge blanket	Industrial wastewater	51	(Wen et al., 2011)
		Ceftriaxone	Anaerobic membrane bioreactor	Pharmaceutical wastewater	73	(Huang et al., 2018)
	Sulfonamides	Sulfamethoxazole	Anaerobic membrane bioreactor	Swine wastewater	68	(Cheng et al., 2018)
		Sulfamethoxazole	Sequencing batch reactor	Synthetic wastewater	92	(Yang et al., 2012)
		Sulfonamides	Biofilm membrane bioreactor	Swine wastewater	90	(Song et al., 2017)
		Sulfonamides	Sequencing batch reactor	Swine wastewater	78	(Cheng et al., 2018)
	Tetracycline	Tetracycline	Sequencing batch reactor	Synthetic wastewater	86	(Kim et al., 2005)
		Tetracycline	Sequencing batch reactor	Swine wastewater	85	(Kim et al., 2005)
		Chlortetracycline	Activated Sludge	Swine wastewater	90	(Song et al., 2017)
		Chlortetracycline	Activated Sludge	Swine wastewater	83	(Cheng et al., 2018)
		Tetracycline	Biofilm membrane bioreactor	Swine wastewater	87	(Cheng et al., 2018)
Hormones		Estradiol	Membrane bioreactor	Wastewater	15	(Joss et al., 2004)
		Estrone	Fixed bed reactor	Wastewater	90	(Joss et al., 2004)
Pesticides		MCPA	Membrane bioreactor	Wastewater	86	(González et al., 2006)
		2,4-D	Membrane bioreactor	Wastewater	87	(González et al., 2006)
		2,4-DP	Membrane bioreactor	Wastewater	87	(González et al., 2006)
		MCPP	Membrane bioreactor	Wastewater	90	(González et al., 2006)
Endocrine disrupting compounds		Nonylphenol	Sequencing batch reactor	Wastewater	91	(Kent et al., 2019)
		Bisphenol A	Membrane bioreactor	Wastewater	88	(Besha et al., 2017)
		Nonylphenol	Triple bed reactor	Wastewater	36	(Křesinová et al., 2018)

Table 2. Application of physico-chemical techniques to eliminate ECs in different water matrices

Classification	Category	Emerging contaminant	Physico-chemical techniques	Removal efficiency (%)	Reference
Pharmaceuticals	Analgesic	Hydrocodone	Coagulation	24	(Westerhoff et al., 2005)
		Acetaminophen		60	(Stackelberg et al., 2007)
	Anti-inflammatory	Naproxen		10	(Vieno et al., 2007)
	Beta-blocker	Acebutolol		8	(Vieno et al., 2007)
	Nonsteroidal anti-inflammatory drug	Diclofenac	Nanofiltration	>99	(Beier et al., 2010)
		Ibuprofen		>99	(Beier et al., 2010)
	Analgesic	Tramadol		>99	(Beier et al., 2010)
	Angiotensin receptor blockers	Telmisartan		>99	(Beier et al., 2010)
	Tetracycline	Oxytetracycline	Adsorption	68	(Choi et al., 2008)
		Minocycline		≤70	(Choi et al., 2008)
		Meclocycline-sulfosalicylate		>90	(Choi et al., 2008)
		Democlocycline-HCl		68	(Choi et al., 2008)
Pesticides		Metolachlor	Coagulation	28	(Stackelberg et al., 2007)
		Aldrin		49	(Westerhoff et al., 2005)
		Diazinon		34	(Stackelberg et al., 2007)
		Chlordane		24	(Westerhoff et al., 2005)
Textile dye		Direct red 80	Nanofiltration	99	(Akbari et al., 2002)
		Disperse blue 56		99	(Akbari et al., 2002)
		Acid red 4		>83	(Akbari et al., 2002)
		Basic blue 3		>21	(Akbari et al., 2002)
Hormones		Estriol	Adsorption	60	(Snyder et al., 2007)
		Estrone		72	(Snyder et al., 2007)
		Estradiol		80	(Snyder et al., 2007)

In general, the conventional physico-chemical treatment technologies are inefficient and slow in treating emerging pollutants containing wastewater. Moreover, the high-energy footprint of physico-chemical techniques makes application uneconomical and unsustainable on a large scale.
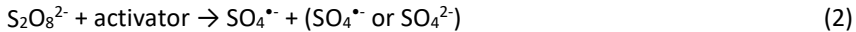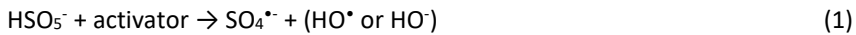
To fill the gaps, innovative chemical treatment specifically advanced oxidation techniques (AOTs) have gained a lot of attention for elimination of ECs from various water matrices. AOTs is a feasible choice as it is rapid, easy to optimize, simultaneously disinfects the wastewater, and cost-effective compared to other used processes of chemical, physical and biological treatment. Traditionally, AOTs involves the generation of hydroxyl radicals (E^0=2.73 V) (HO$^\bullet$) and has been used in water and wastewater treatment for effective removal of non-biodegradable ECs (Asghar et al., 2015). Over the last decade, technologies based on sulfate radicals (SO$_4^{\bullet-}$) have received much attention. The sulfate radicals have a high oxidation-reduction potential (E^0=2.5-3.1 V) and are comparatively stable in aqueous matrices as well as selective for oxidizing of the contaminants (Matzek et al., 2016).

1.3   Principles of persulfate oxidation processes

1.3.1   Persulfate activation mechanisms

In year 1878, a French chemist Marcelin Berthelot introduced peroxydisulfuric acid ($H_2S_2O_8$) (Kolthoff et al., 1951). Both peroxymonosulfate (PMS, HSO$_5^-$) and peroxydisulfate (PS, $S_2O_8^{2-}$) have been successfully applied to generate SO$_4^{\bullet-}$ (Eq. 1 and 2). The most common form of PMS used is KHSO$_5$, commercially known as Oxone® which is a triple potassium salt (2KHSO$_5$·KHSO$_4$·K$_2$SO$_4$).

The energy consumption to generate SO$_4^{\bullet-}$ by PS activation (140 kJ mol^{-1}) is lower than that by PMS (140-213.3 kJ mol^{-1}) (Miklos et al., 2018). Consequently, compared with PMS, PS is chosen as an oxidant for the elimination of organic pollutants. The three forms of PS, sodium persulfate (Na$_2$S$_2$O$_8$), potassium persulfate (K$_2$S$_2$O$_8$), and ammonium persulfate ((NH$_4$)$_2$S$_2$O$_8$) have been applied as oxidants for degradation of target pollutant (Yang et al., 2019). However, the sodium salt of PS (Na$_2$S$_2$O$_8$) is the most commonly used in the environmental pollution abatement and has a high solubility in water of 730 g L^{-1}. The bond length between peroxide (-O-O-) bond in persulfate molecule is 1.497 Å, and as presented in Figure 2 can be dissociated by thermal activation, UV radiations, alkaline activation, transition metals and strong oxidants such as hydrogen peroxide and ozone, etc. (Eq. 2 and 3) (Flanagan et al., 1984; Liang et al., 2003).

HSO$_5^-$ + activator → SO$_4^{\bullet-}$ + (HO$^\bullet$ or HO$^-$)	(1)
S$_2$O$_8^{2-}$ + activator → SO$_4^{\bullet-}$ + (SO$_4^{\bullet-}$ or SO$_4^{2-}$)	(2)
S$_2$O$_8^{2-}$ + radiation → 2SO$_4^{\bullet-}$	(3)

Consecutively, the oxidation-reduction reaction of PS with electron donor from the transition metal can generate SO$_4^{\bullet-}$ radicals following the Eq. 4 below (Anipsitakis et al., 2004).
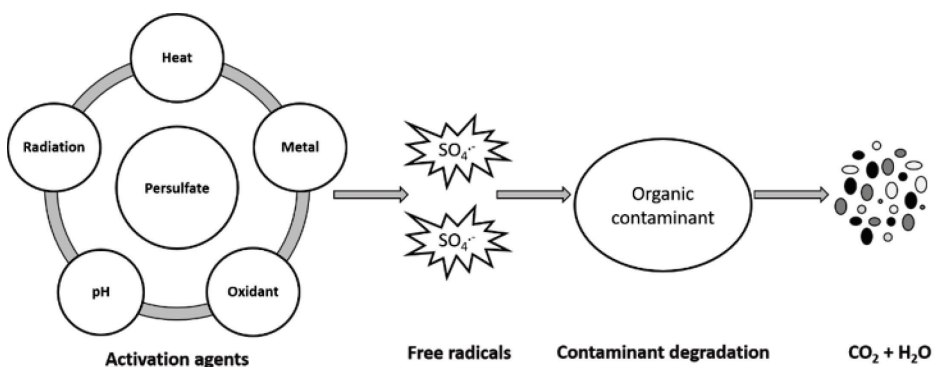
S$_2$O$_8^{2-}$ + e$^-$ → SO$_4^{\bullet-}$ + SO$_4^{2-}$	(4)

Figure 2. Overview of activated persulfate process.

1.3.2   Radiation activation

Ultraviolet, ultrasound, and gamma radiation have demonstrated the potential to eliminate the organic pollutants in aqueous solutions. As compared to the non-activated system, direct UV photolysis can be effective in degrading the majority of the contaminants in shorter reaction time due to high-energy input. However, photolysis has a limitation: it only works with photosensitive antibiotics (Shi et al., 2020).

As shown in Eq. 5, the combination of UV radiation with a strong oxidant such as PS produces radicals thus enhance target pollutant removal efficacy. The quantum yield is wavelength dependent and has been shown to decrease with increasing wavelength, typically in the range of 248-351 nm. Accordingly, the most commonly used radiation wavelength for the PS activation is 254 nm (Herrmann, 2007).

$$S_2O_8^{2-} + h\nu \rightarrow 2SO_4^{\bullet-} \tag{5}$$

Moreover, under the influence of UV radiation, dissociation of water molecule can produce the electron, which activates the PS by electron conduction and generate $SO_4^{\bullet-}$ as shown below (Wang et al., 2018):

$$H_2O + h\nu \rightarrow HO^\bullet + H^\bullet \tag{6}$$
$$S_2O_8^{2-} + H^\bullet \rightarrow SO_4^{\bullet-} + SO_4^{2-} + H^+ \tag{7}$$

The application of ultrasound enhances the mass transfer of chemical reactions due to the violent turbulence in aqueous solution. Cavitation, high temperatures and pressures caused by ultrasound have the potential for activating PS by homolysis of the peroxide bond, thus generating the $SO_4^{\bullet-}$ radicals as shown below:

$$S_2O_8^{2-} +))) \rightarrow 2SO_4^{\bullet-} \tag{8}$$

The application of the US/PS process can generate both $SO_4^{\bullet-}$ and $HO^\bullet$ radicals as shown in Eq. 9-11

$$SO_4^{\bullet-} + HO^- \rightarrow SO_4^{2-} + HO^\bullet \tag{9}$$
$$S_2O_8^{2-} + 2H_2O \rightarrow HO_2^- + 2SO_4^{2-} + 3H^+ \tag{10}$$
$$HO_2^- + S_2O_8^{2-} \rightarrow SO_4^{\bullet-} + SO_4^{2-} + H^+ + O_2^{\bullet-} \tag{11}$$

However, the US/PS is highly influenced by the ultrasonic amplitude. Studies suggest that the amplitude of ultrasound beyond the threshold amplitude can lead to the collapse

of cavitation bubbles leading to the recombination of $SO_4^{\bullet-}$ and a decrease in the efficiency of degradation (Wang et al., 2011).

Due to its high penetration efficiency, gamma radiation is a new technology for the elimination of toxic organic pollutants in water and wastewater. Reactive species, such as hydroxyl radicals, hydrated electron, and hydrogen atoms, are formed as a result of gamma radiations, which further activate PS by fission of the O-O bond. However, the simultaneous presence of the reactive species and PS can cause scavenging reactions (Wang, et al., 2017).

1.3.3 Thermal activation

As presented in Eq. 12, the energy input by the high temperature (> 50°C) can cause the fission of the O-O bond to form the $SO_4^{\bullet-}$.

$$S_2O_8^{2-} + heat \rightarrow 2SO_4^{\bullet-} \tag{12}$$

Accordingly, the activation energy to break the peroxide bond (O-O) at neutral, basic, and acidic conditions was 119-129 kJ mol^{-1}, 134-139 kJ mol^{-1}, and 100-116 kJ mol^{-1} respectively. The increase in temperature elevates the generation of the $SO_4^{\bullet-}$. Therefore, $SO_4^{\bullet-}$ rapidly increases the reaction rate thereby reducing the remediation time and increasing the mineralization of organic contaminations (Devi et al., 2016).

The elevated temperature might allow higher organic pollutant solubility in wastewater. However, the thermally activated reaction is highly pH-sensitive. At acidic conditions (pH< 3), the thermal decomposition of PS occurs without forming the $SO_4^{\bullet-}$ radicals. On the other hand, the alkaline conditions positively affect the reactivity of PS with the formation of $HO^{\bullet}$ as shown in Eq. 9. However, as to avoid the formation of potential scavengers such as chloride and bicarbonate ions, the thermal energy input needs to be optimized.

1.3.4 Alkaline activation

The change in pH can affect the predominance of radicals in the activated PS processes. Thus, at acid conditions (pH< 7) H^+ reacts with PS to generate SO_4^{2-} and $SO_4^{\bullet-}$. At neutral pH, both $HO^{\bullet}$ and $SO_4^{\bullet-}$ contributed to the degradation of organic pollutants (Eq. 13-15). The activation of persulfate by a base (NaOH) can favour positively the process efficiency (Furman et al., 2010).
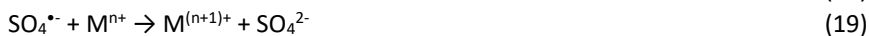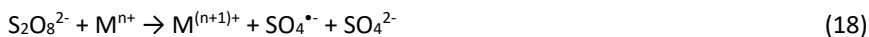
$$S_2O_8^{2-} + H^+ \rightarrow SO_4^{2-} + SO_4^{\bullet-} + H^+ \tag{13}$$
$$SO_4^{\bullet-} + H_2O \rightarrow SO_4^{2-} + HO^{\bullet} + H^+ \tag{14}$$
$$SO_4^{\bullet-} + HO^- \rightarrow SO_4^{2-} + HO^{\bullet} \tag{15}$$

However, this might also enhance the mutual reaction between co-existed $SO_4^{\bullet-}$ and $HO^{\bullet}$ as presented in Eq. 16 and 17 (Yang et al., 2019).

$$SO_4^{\bullet-} + SO_4^{\bullet-} \rightarrow S_2O_8^{2-} \tag{16}$$
$$SO_4^{\bullet-} + HO^{\bullet} \rightarrow HSO_5^- \tag{17}$$

1.3.5 Activation by transition metal ions

The utilization of transition metals such as Fe^{2+}, Cu^{2+}, Ce^{2+}, Mn^{2+}, Co^{2+}, Ni^{2+}, and Ag^+, etc. to activate PS has broad prospects for the degradation of organic contaminants and can be expressed via Eq. 18-20 (Yang et al., 2019).

$$S_2O_8^{2-} + M^{n+} \rightarrow M^{(n+1)+} + SO_4^{\bullet-} + SO_4^{2-} \tag{18}$$

$$SO_4^{\bullet-} + M^{n+} \rightarrow M^{(n+1)+} + SO_4^{2-} \tag{19}$$

$$S_2O_8^{2-} + 2M^{n+} \rightarrow 2M^{(n+1)+} + 2SO_4^{2-} \tag{20}$$

Fe^{2+} is the most commonly used transition metal and is a promising choice to activate PS owing to its low cost, low toxicity, and high abundance in the natural environment (Anipsitakis et al., 2004). Fe^{2+} requires low activation energy of 12 kcal mol^{-1} for the O-O bond dissociation. This consecutively increases the reaction rate and, thus, reduces overall operating costs (Xiao et al., 2020).

As shown in Eq. 21, Fe^{2+} initiates the PS activation via electron transfer, to form $SO_4^{\bullet-}$ thus facilitates the removal of the target pollutant and mineralization.

$$S_2O_8^{2-} + Fe^{2+} \rightarrow Fe^{3+} + SO_4^{\bullet-} + SO_4^{2-} \tag{21}$$

However, it is important to optimize the oxidant/activator molar ratio to inhibit the radical scavenging by generated $SO_4^{\bullet-}$. The results of numerous studies have shown that the most cost-efficient PS/Fe^{2+} molar ratio is 1/1 (Rastogi et al., 2009). As presented in Eq. 22, an excess concentration of activator dosage in the homogenous process has limitations associated with the conversion of a ferrous ion (Fe^{2+}) to a ferric ion (Fe^{3+}) (Xiao et al., 2020).

$$SO_4^{\bullet-} + Fe^{2+} \rightarrow Fe^{3+} + SO_4^{2-} \tag{22}$$

The organic radical ($R^{\bullet}$) (Eq. 23) formed in PS/Fe^{2+} system can regenerate Fe^{3+} to Fe^{2+}, although this is a rate-limiting step and at alkaline pH, the accumulation of iron can lead to lower reaction rate as a result of formation of hydroxide complex $Fe(OH)_3$ (Rodriguez et al., 2017).

$$R^{\bullet} + Fe^{3+} \rightarrow Fe^{2+} + intermediates \tag{23}$$
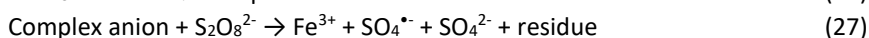
The availability of the dissolved iron ions in the PS/Fe^{2+} systems can be enhanced by the application of chelating or reducing agents such as citric acid (CA), oxalic acid (OA), ethylene diamine tetraacetic acid, (S, S)-ethylenediamine-N, N-disuccinic acid trisodium salt, hydroxylamine, gallic acid, tartrate (An et al., 2013). The proposed mechanism of Fe-chelate reaction (Eq. 24) shows the chelating agents (L) binds to iron resulting in imitation of Fenton-like reactions.

$$Fe^{3+} + L \rightarrow Fe^{3+}L \tag{24}$$

The chelates improve the solubility of non-polar and lipophilic pollutants. Moreover, at neutral pH chelates improve the dissolution of iron in aqueous matrices (Moreira et al., 2017). As shown in Eq. 25, the addition of ultraviolet radiation to the system promotes the release of reduced iron from the $Fe^{3+}L$ complex into the solution, which allows effective $SO_4^{\bullet-}$ generation from persulfate (Li et al., 2010).

$$Fe^{3+}L + h\nu \rightarrow Fe^{2+} + L \tag{25}$$

Inorganic reducing agent thiosulfate ($S_2O_3^{2-}$) serves as a chelating agent and the mechanism of persulfate-thiosulfate interaction is presented as Eq. 26-28:

$$XS_2O_3^{2-} + YFe^{2+} \rightarrow Complex\ anion \tag{26}$$

$$Complex\ anion + S_2O_8^{2-} \rightarrow Fe^{3+} + SO_4^{\bullet-} + SO_4^{2-} + residue \tag{27}$$

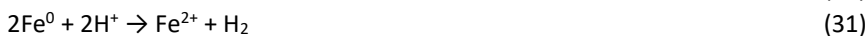$$S_2O_3^{2-} + Fe^{3+} \rightarrow Fe^{2+} + 0.5S_4O_6^{2-} \tag{28}$$

However, the addition of a chelating and/or reducing agent to the activated PS system must be carefully optimized, in order not to impede the oxidation process due to the unavailability of the soluble activator or become a source of secondary pollution (Xiao et al., 2020).

1.3.6 Transition metal-bearing species-activated persulfate

1.3.6.1 Zero-valent iron

Owing to the easy accessibility, high reducibility (Fe^0, E_0=-0.44 V), recoverability, and environmental friendliness, zero-valent iron (ZVI, Fe^0) is widely studied and applied as an activator of O-O bond containing oxidants in water matrices treatment (Al-Shamsi et al., 2013). In an acidic environment, ZVI in the presence of persulfate dissociates to form Fe^{2+} and acts as a source of slow-release of ferrous ions (Eq. 29-31) (Zhang et al., 2019; Zhen et al., 2018).

$$Fe^0 + 0.5O_2 + H_2O \rightarrow Fe^{2+} + 2HO^- \tag{29}$$
$$Fe^0 + 2H_2O \rightarrow Fe^{2+} + 2HO^- + H_2 \tag{30}$$
$$2Fe^0 + 2H^+ \rightarrow Fe^{2+} + H_2 \tag{31}$$

Additionally, the electron transfer on the surface of ZVI (Eq. 32) allows the activation of PS to generate $SO_4^{\bullet-}$.

$$Fe^0 + 2S_2O_8^{2-} \rightarrow \equiv Fe^{2+} + 2SO_4^{\bullet-} + 2SO_4^{2-} \tag{32}$$

In addition, ZVI has the advantage to reduce the Fe^{3+} formed in the Eq. (21) thus preventing the hydrolysis and precipitation of Fe^{3+} in the system. However, the formation of Fe^{2+} from ZVI surface dissolution is the rate-limiting step and is influenced by the particle size of ZVI. Therefore, it is important to optimize the particle size of ZVI (Zhong et al., 2015). However, the ZVI with optimized particle size is expensive to formulate and brings an additional cost to the treatment process (Zhang et al., 2019).

To elucidate this issue, nano zero-valent iron (nZVI) can be employed, as the particle size is small allowing high surface reactivity. Therefore, nZVI can rapidly activate PS and more likely to utilize Fe^0 completely. Moreover, the electron transfer on the surface of nZVI allows the elimination of target compounds and the electrostatic interaction on the core-shell enhances the adsorption of micropollutants (Yirsaw et al., 2016).

However, during the application of nZVI for contaminant reduction, the adsorption of natural organic substances may cause a change in the surface electrochemistry of nZVI thus affecting the reactivity and dissociation behavior of nZVI in the environment (Stefaniuk et al., 2016). Additionally, the persistent nature of the nanomaterials in the environment as well as associated health issues are raising the public concern and are serious barriers to their full-scale use.

1.3.6.2 Iron oxides and oxyhydroxides

Oxides and hydroxide minerals are abundantly found in the earth's crust. Iron oxides are composed mainly of Fe^{2+}, Fe^{3+} cations, and are widely used as oxidant activators for water/wastewater treatment and remediation of polluted groundwater and soil. As presented in Figure 3, the persulfate in PS/iron-bearing mineral systems can be activated to generate sulfate radicals and consequently hydroxyl radicals (Eq. 14) either on the surface of iron-bearing activator or in the bulk solution by Fe^{2+} leached from the surface of a heterogeneous activator (Aredes et al., 2012). The most commonly studied forms of

oxides and oxyhydroxides include magnetite (Fe_3O_4), goethite (α-FeO(OH)), maghemite (γ-Fe_2O_3), hematite (α-Fe_2O_3) and etc. (Aredes et al., 2012; Xiao et al., 2020).

Figure 3. Description of mineral-interface mechanism of heterogeneous persulfate activation

Magnetite (Fe_3O_4) is the most abundant iron oxide and has a higher dissolution rate compared to other iron oxides. The octahedral sites, mostly found on the surface of magnetite crystal accommodate Fe^{2+} and Fe^{3+} and are responsible for the catalytic activity of the oxide. Contrary to the ZVI, the PS activation by Fe_3O_4 occurs on the surface of solid, and thus providing continuous availability of Fe^{2+} and avoiding rapid utilization Fe^{2+} (Xiao et al., 2020).

In the case of the goethite activation, the reaction mechanism is similar to the Fenton-like system, i.e. electron reduction on the surface leads to the formation of persulfate radical ($S_2O_8^{\bullet-}$) (Eq. 33) or in the bulk solution by Fe^{2+} leached from the surface of a heterogeneous activator (Eq. 34).

$$\equiv Fe^{3+} + S_2O_8^{2-} \rightarrow \equiv Fe^{2+} + S_2O_8^{\bullet-} \tag{33}$$
$$\equiv Fe^{2+} + S_2O_8^{2-} \rightarrow \equiv Fe^{3+} + SO_4^{2-} + SO_4^{\bullet-} \tag{34}$$

The advantages of using iron oxides as activators are environmental friendliness, relatively low cost, applicability in a wide pH range, and the possibility of their repeated use for the decomposition of pollutants.

1.4 Application of activated persulfate oxidation for water and wastewater treatment

Persulfate-based advanced oxidation processes have been reported to eliminate dyes, pharmaceuticals, etc. in various water matrices (Wang et al., 2018). Activated persulfate systems are promising and cost-effective technologies for the elimination of organic contaminants from water and wastewater. The examples of the application of PS/Fe^{2+} based oxidation systems to oxidize ECs in water are summarized in Table 3, and the results showed practically complete elimination of ECs in various water matrices. However, the composition of real water matrices undoubtedly reduced the efficacy of ECs degradation in studied activated PS systems. Irrespective of the applied UV-induced PS-based process, the ECs mineralization was less effective than the target compound degradation.

Table 3. Summary of emerging contaminants elimination in various water matrices by Fe^{2+}-activated persulfate oxidation

Emerging contaminants	Contaminant concentration (mM)	Oxidant concentration (mM)	Reaction time (min)	Removal efficiency (%)	Water matrices	Reference
Acetaminophen	0.05	0.8	30	81	Ultrapure water	(Wang et al., 2019)
Sulfadiazine	0.1	4	120	>99	Ultrapure water	(Yang et al., 2018)
Trimethoprim	1	4	240	73	Wastewater	(Wang et al., 2018)
Chlortetracycline	1	5	120	76	Wastewater effluent	(Pulicharla et al., 2018)
Sulfamethoxazole	0.05	4	120	>99	Wastewater	(Wang, 2017)
Atrazine	0.02	0.4	10	50	Ultrapure water	(Bu et al., 2016)
Carbamazepine	0.02	1	40	78	Distilled water	(Rao et al., 2014)
Diuron	0.05	0.04	180	>99	Distilled water	(Vicente et al., 2011)
Diuron	0.09	2	180	>99	Distilled water	(Romero et al., 2010)
2-chlorobiphenyl	0.02	0.22	240	>99	Distilled water	(Rastogi et al., 2009)
Bisphenol A	0.088	4.3	60	>99	Distilled water	(Gao et al., 2018)
Trichloroethylene	0.15	2.25	60	>99	Distilled water	(Wu et al., 2014)
Orange G	0.1	4	120	97	Activated sludge	(Niu et al., 2012)
Iopamidol	0.02	0.2	150	80	Ultrapure water	(Dong et al., 2017)
Cephalexin	0.1	1	120	90	Wastewater effluent	(Qian et al., 2020)
Cefradine	0.1	1	120	91	Wastewater effluent	(Qian et al., 2020)
Ciprofloxacin	0.03	0.06	240	96	Groundwater	(Ji et al., 2014)
Sulfamethoxazole	0.03	0.03	240	50	Groundwater	(Ji et al., 2014)

The effectiveness of AOTs is strongly affected by the composition of the water matrix. For example, natural organic matter (NOM), which is composed of humic and fulvic acids and is an integral part of the composition of real water, also reacts with free radicals and thus competes with ECs in the oxidation process. Similarly, the inorganic anions such as bicarbonate (HCO_3^-), carbonate (CO_3^{2-}), phosphate (PO_4^{3-}), nitrite (NO_2^-), nitrate (NO_3^-) and chloride (Cl^-) present in water can have neutral, positive or inhibitory effect on the elimination of target compound resulting in the formation of radicals with lower oxidation potential.

1.4.1   Natural organic matter

Natural organic matter composed of humic substances is a well-known absorber of UV radiation (Matzek et al., 2016). In addition, the chemical structure of NOM, containing available hydrogen as well as valence electrons, binds with free radicals and, thus, reduces the efficiency of decomposition (Xiao et al., 2020). However, depending on the concentration and composition of humic substances, as well as the treatment conditions used, NOM may have an inhibitory (Eq. 35 and 36) or a stimulating effect on the removal of contaminants by activated PS systems.

$$NOM + SO_4^{\bullet-} \rightarrow products \tag{35}$$
$$NOM + HO^\bullet \rightarrow products \tag{36}$$

However, the photosensitizer behavior of NOM may display the synergistic effect in the elimination of organic contaminants. Moreover, the composition and origin have a significant impact on the amount, character, and properties of NOM in the waters (Yang et al., 2019).

1.4.2   Anions

Carbonates and bicarbonates are commonly present in natural water and wastewater matrices and are well-known scavengers of the $SO_4^{\bullet-}$ and $HO^\bullet$ radicals (Devi et al., 2016). The influence of the carbonates on the applied AOP system rises with increasing pH (Asghar et al., 2015). Accordingly, CO_3^{2-} and HCO_3^- compete with the target compound for the sulfate and hydroxyl radicals to form carbonate radicals ($CO_3^{\bullet-}$), which are much less reactive species of radicals (Eq. 37-40) (Romero et al., 2010).

$$SO_4^{\bullet-} + HCO_3^- \rightarrow SO_4^{2-} + H^+ + CO_3^{\bullet-} \tag{37}$$
$$SO_4^{\bullet-} + CO_3^{2-} \rightarrow SO_4^{2-} + CO_3^{\bullet-} \tag{38}$$
$$HO^\bullet + HCO_3^- \rightarrow H_2O + CO_3^{\bullet-} \tag{39}$$
$$HO^\bullet + CO_3^{2-} \rightarrow HO^- + CO_3^{\bullet-} \tag{40}$$
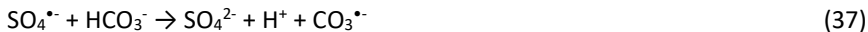
Similarly, phosphate ion and nitrate ions are well known $SO_4^{\bullet-}$ and $HO^\bullet$ radical scavenger, and as a result, a less reactive phosphate radical ($H_2PO_4^\bullet$) and nitrate radical ($NO_3^\bullet$) are formed, respectively (Eq. 41-44) (Yang et al., 2019).

$$H_2PO_4^- + SO_4^{\bullet-} \rightarrow SO_4^{2-} + H_2PO_4^\bullet \tag{41}$$
$$H_2PO_4^- + HO^\bullet \rightarrow HO^- + H_2PO_4^\bullet \tag{42}$$
$$NO_3^- + SO_4^{\bullet-} \rightarrow SO_4^{2-} + NO_3^\bullet \tag{43}$$
$$NO_3^- + HO^\bullet \rightarrow HO^- + NO_3^\bullet \tag{44}$$

In heterogeneously activated PS systems, carbonates, bicarbonates, and phosphate ions tend to absorb onto the metal surface thus blocking the active sites. Moreover, both

bicarbonate and phosphate ions have a strong buffering capacity and, thereby, inhibiting the decrease in the pH of the solution during oxidation, suppressing the dissolution of iron and lowering the oxidation potential of radical species (Xiao et al., 2020).

Chlorine ions commonly exist in the water and wastewater system. Several reports have identified highly toxic and refractory chlorinated by-products in the wastewater as a result of the AOPs application (Bennedsen et al., 2012; Lutze et al., 2015). Decomposition of such by-products leads to the formation of more toxic halogenated products such as chlorophenol, chlorobenzene, and chlorobenzoate (Bennedsen et al., 2012). In general, the reaction between of Cl^- and $SO_4^{\bullet-}$ or $HO^\bullet$ radicals leads to the generation of weaker chlorine containing radicals, such as $Cl^\bullet$, $Cl_2^{\bullet-}$, and $HOCl^{\bullet-}$ (Eq. 45-57) (Xiao et al., 2020).

Initiation:

$$Cl^- + SO_4^{\bullet-} \leftrightarrow SO_4^{2-} + Cl^\bullet \tag{45}$$

$$Cl^- + HO^\bullet \leftrightarrow HOCl^{\bullet-} \to Cl^\bullet + HO^- \tag{46}$$

Propagation:

$$Cl^\bullet + H_2O \to HOCl^{\bullet-} + H^+ \tag{47}$$

$$Cl^\bullet + Cl^- \leftrightarrow Cl_2^{\bullet-} \tag{48}$$

$$Cl^\bullet + HO^- \to HOCl^{\bullet-} \tag{49}$$

$$Cl_2^{\bullet-} + HO^- \to HOCl^{\bullet-} + Cl^- \tag{50}$$

$$OCl^- + HO^\bullet \to ClO^\bullet + HO^- \tag{51}$$

$$2ClO^\bullet + H_2O \to ClO^- + ClO_2^- + 2H^+ \tag{52}$$

$$ClO_2^- + HO^\bullet \to ClO_2^\bullet + HO^- \tag{53}$$

Termination:

$$Cl_2^{\bullet-} + Cl_2^{\bullet-} \to Cl_2 + 2Cl^- \tag{54}$$

$$Cl_2^{\bullet-} + HO^\bullet \to HOCl + Cl^- \tag{55}$$

$$ClO_2^\bullet + HO^\bullet \to ClO_3^- + H^+ \tag{56}$$

$$HO^\bullet + HO^\bullet \to H_2O_2 \tag{57}$$
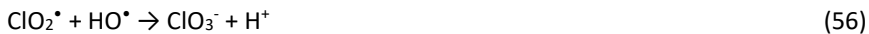
Overall, the presence of anions at certain concentrations in the system might facilitate the elimination of the target compound. However, the identification of the optimum concentration of anions in the system is a challenge.

1.5   Aim of the study

Over the past decade, numerous studies have extensively reviewed the application of $SO_4^{\bullet-}$-based processes for the oxidation of emerging contaminants in water and wastewater. This work dedicates to identify and fill the knowledge gaps related to the applications of activated persulfate oxidation technologies for the degradation of emerging contaminants in water matrices.

The current doctoral thesis provides a critical evaluation on the main aspects involving the degradation and mineralization of ECs such as β-lactam antibiotics, endocrine disrupting compounds, and angiotensin receptor blockers in water by application of UV-induced persulfate-based oxidation processes. The efficiency of PS activation by UV radiation was studied both individually and in combination with other activation methods, such as ferrous ions, iron oxides, hydrogen peroxide, for the decomposition of

selected contaminants. During the study, special attention was paid to evaluating the environmental impact of the applied processes.

The objectives of this study were as follows:

- to investigate and compare the efficiency of β-lactam antibiotic AMX decomposition by UVC- and UVC/Fe^{2+}-activated PS systems;
- to study the effectiveness of UVA/PS and UVC/PS systems separately and in combination with homogenous activator (Fe^{2+}) and heterogeneous activators (α-FeO(OH) and Fe$_3$O$_4$) for the oxidation of β-lactam antibiotic CTA;
- to study the UVC-induced PS, PS/Fe^{2+}, PS/H$_2$O$_2$ and PS/H$_2$O$_2$/Fe^{2+} systems for the degradation of endocrine disrupting compound NP;
- to investigate and compare the efficiency of UVC- and UVC/Fe^{2+}-activated PS systems for the degradation and mineralization of angiotensin receptor blocker LOR;
- to evaluate the effect of operating parameters, such as pH value, dosage of activator, oxidant concentration and the composition of real water matrices, on the efficiency of UV-induced persulfate systems;
- to identify AMX and LOR transformation products in the studied PS-based systems; in the case of LOR, also evaluate acute toxicity to luminous bacteria (*Vibrio fischeri*).

2 Materials and Methods

2.1 Chemicals and materials

All the chemicals were of analytical grade used without further purification. All stock solutions were prepared in ultrapure water (Millipore Simplicity®UV System, Merck) or in double-distilled water with purity equal to ultrapure water (UW). Sodium hydroxide, sulfuric acid, or phosphate buffered aqueous solutions were used to adjust pH.

Water samples collected from various sources were used as natural and processed aqueous matrices for the target compound degradation. Drinking water (DW) was obtained from a drinking water treatment plant (Tallinn, Estonia) (*Paper I*). Groundwater (GW) was used without preceding purification and was collected from a 19-m deep borehole (Harjumaa, Estonia) (*Paper I-IV*). Secondary treated wastewater (STWW) was collected from the outlet of the secondary treatment of a municipal wastewater treatment plant (Tallinn, Estonia) (*Paper I*). All water samples were stored at 4°C. The main parameters of real water matrices are presented in Table 4.
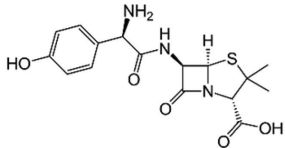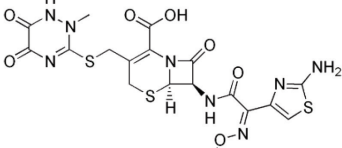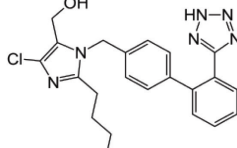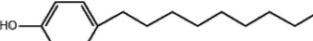
Table 4. Chemical composition and main parameters of water samples

Parameter	Unit	AMX			CTA	LOR	NP
		GW	DW	STWW	GW	GW	GW
pH	-	8.1	7.4	7.4	7.9	7.71	7.94
Alkalinity	$mgCaCO_3$ L^{-1}	308	130	186	366	350	342
Conductivity	μS cm^{-1}	730	390	1275	763	820	763
TOC	mg L^{-1}	0.15	6.4	7.85	16.9	2.2	16.4
Fe^{2+}	μg L^{-1}	60	30	250	10	12	5
Total Fe	μg L^{-1}	170	50	570	68	175	38
F^-	mg L^{-1}	-	3.5	2.4	-*	-*	0.3
Cl^-	mg L^{-1}	90.4	102.1	794.1	128.2	83.5	73.6
NO_2^-	mg L^{-1}	-*	-*	-*	-*	0.82	0.63
NO_3^-	mg L^{-1}	-*	-*	38.7	2.25	2.1	1.13
SO_4^{2-}	mg L^{-1}	42.1	15.7	68.2	36	34	34.9

*Below detection limit.

A stock NP solution of 4.54 mM was prepared in methanol and stored in the dark at 4°C. The synthetic solutions of AMX (*Paper I*), CTA (*Paper II*), LOR (*Paper III*) and NP (*Paper IV*) were prepared in ultrapure water or in a real aqueous matrix to obtain the target compound concentration of 40 µM, 50 µM, 40 µM, and 50 µM, respectively. The structure and main properties of the studied micropollutants are given in Table 5.

Table 5. Studied emerging contaminants

Properties	AMX	CTA	LOR	NP
Molecular structure				
IUPAC name	(2S,5R,6R)-6-[[(2R)-2 amino-2-(4-hydroxyphenyl)acetyl]amino]-3,3-dimethyl-7-oxo-4-thia-1-azabicyclo[3.2.0]heptane-2-carboxylic acid	6R,7R)-7-[[(2Z)-2-(2-amino-1,3-thiazol-4-yl)-2-methoxyiminoacetyl]amino]-3-[(2-methyl-5,6-dioxo-1H-1,2,4-triazin-3-yl)sulfanylmethyl]-8-oxo-5-thia-1-azabicyclo[4.2.0]oct-2-ene-2-carboxylic acid	[2-butyl-5-chloro-3-[[4-[2-(2H-tetrazol-5-yl)phenyl]phenyl]methyl]imidazol-4-yl]methanol	4-nonylphenol, p-nonylphenol
Classification	β-lactam antibiotic	β-lactam antibiotic	Angiotensin receptor blocker	Endocrine disruptor
CAS nr.	26787-78-0	73384-59-5	114798-26-4	68081-86-7
Molecular formula	$C_{16}H_{19}N_3O_5S$	$C_{18}H_{18}N_8O_7S_3$	$C_{22}H_{23}ClN_6O$	$C_{15}H_{24}O$
Molecular weight (g mol^{-1})	365.4	554.58	422.9	220.36
Solubility (mg ml^{-1})	0.958 (Singh et al., 2018)	0.105 (Yu et al., 2016)	0.0033 (Salazar et al., 2016)	0.005 (Brix et al., 2001)
pKa	2.68,7.49,9.63 (Demirezen et al., 2019)	3.19, 4.17 (Ruzza et al., 2018)	4.9 (Salazar et al., 2016)	10.7 (Al-Ahmari et al., 2018)

2.2 Experimental procedure

The experiments (Table 6) were conducted in a batch mode in non-buffered solution (*Paper I, III, and IV*) or in 0.1 M potassium phosphate buffered solution (*Paper II*) at ambient room temperature (22 ± 1 °C). The trails were conducted in a cylindrical glass reactor with a permanent agitation speed (300-400 rpm) for 2 h (*Paper I, II, and III*) or 3 h (*Paper IV*). The pH of the sample was not adjusted, if not stated otherwise. The activator was added first in UV/PS/activator systems and after its complete dissolution ($FeSO_4 \cdot 7H_2O$) (*Papers I-IV*) or establishment of adsorption/desorption equilibrium between the target compound and the iron oxide (α-FeO(OH), Fe_3O_4) particles (*Paper II*). The oxidation was initiated by adding the oxidant followed by the exposure to the UV lamp.

Table 6. Studied activated persulfate systems and water matrices with respect to the selected emerging contaminants

Emerging contaminant	Water matrix	Processes	Paper
AMX	UW GW DW STWW	UVC/PS, UVC/PS/Fe²⁺	I
CTA	UW GW	UVA/PS, UVC/PS, UVA/PS/Fe²⁺, UVC/PS/Fe²⁺, UVA/PS/α-FeO(OH), UVC/PS/α-FeO(OH), UVA/PS/Fe₃O₄, UVC/PS/Fe₃O₄	II
LOR	UW GW	UVC/PS, UVC/PS/Fe²⁺,	III
NP	UW GW	UVC/PS, UVC/PS/Fe²⁺, UVC/PS/H₂O₂, UVC/PS/H₂O₂/Fe²⁺	IV

A low-pressure mercury germicidal lamp (11 W, Philips TUV PL-S) (*Papers I-IV*) or a low-pressure mercury lamp (11 W OSRAM Dulux S BLUE) (*Paper II*) located in a quartz tube inside the reactor were used as an UVC and UVA source, respectively. The average irradiance entering the solution in the reactor measured by a spectrometer (Ocean Optics USB2000+) equipped with SpectraSuite software was 7.1 mW cm^{-2} (*Paper I*), 2.68 mW cm^{-2} (*Paper II*), and 2.7 mW cm^{-2} (*Papers III, IV*). In the case of UVA lamp, the average irradiance entering the solution in the reactor was 3.89 mW cm^{-2}. The lamps were turned on at least 5 min prior to the trial to provide a constant output. A water cooling jacket was used to keep the constant temperature in the reactor.

Samples were withdrawn at pre-determined time intervals (*Papers I-IV*). The groundwater or secondary treated wastewater samples were filtered through a 0.45-μm pore size filter (CA, Millipore™) (*Papers I-IV*). The oxidation quenching was done by the addition of EtOH (sample/EtOH volume ratio of 10/1) for HPLC analysis and by the addition of Na_2SO_3 ([PS]$_0$/[SO$_3^{2-}$] molar ratio of 1/10) for TOC analysis. Two radical probes *t*-BuOH and EtOH were used to identify the main radicals involved in the degradation of the studied target compounds using UV-induced PS-based systems (*Papers I-IV*). An excessive amount of scavenger was spiked into the reaction solutions before the

addition of activator and oxidant at a target pollutant/scavenger molar ratio of 1/500. All experiments were duplicated. The results of the analysis are presented as the mean with a standard deviation of at least two parallel replicates less than 5%.

2.3 Analytical methods

The concentration of AMX, CTA, NP, and LOR were quantified using a high-performance liquid chromatography combined with diode array detector (HPLC-PDA, SPD-M20A, Shimadzu) equipped with a Phenomenex Gemini (150 × 2.0 mm, 1.7 mm) NX-C18 (110 Å, 5 µm) column. All samples were analyzed at the flow rate of 200 µL min^{-1} and at λ=230 nm (*Papers I, II*) or 210 nm (*Papers III, IV*). The AMX (*Paper I*) sample analysis were performed using an isocratic method with a mobile phase mixture of 10% acetonitrile (with 0.3% formic acid) and 90% formic acid (0.3%) aqueous solution. The CTA (*Paper II*) sample analysis were performed using an isocratic method with a mobile phase mixture of 15% acetonitrile (with 0.3% formic acid) and 85% formic acid (0.3%) aqueous solution. The LOR (*Paper III*) sample analysis were performed using an isocratic method with a mobile phase mixture of 40% acetonitrile (with 0.3% formic acid) and 60% formic acid (0.3%) aqueous solution. The NP (*Paper IV*) sample analysis were performed using an isocratic method with a mobile phase mixture of 85% acetonitrile (with 0.3% formic acid) and 15% formic acid (0.3%) aqueous solution. The by-products formed during AMX and LOR oxidation were identified by the HPLC combined with mass spectrometer (HPLC-MS, LC-MS 2020, Shimadzu) (*Papers I, III*). Mass spectra were acquired in full-scan mode (scanning in the range 50-500 m/z). The instrument was operated in positive ESI mode, and the results obtained with MS detector were handled using Shimadzu Lab Solutions software.

The pH was measured using a digital pH/Ion meter (Mettler Toledo S220). The electrical conductivity was measured using a digital EC meter (HQ 430d flexi, HACH Company). The total organic carbon (TOC) was measured by a TOC analyzer multi N/C® 3100 (Analytik Jena). The concentration of anions was measured using ion chromatography with chemical suppression of the eluent conductivity (761 Compact IC, Metrohm Ltd.). The alkalinity of groundwater was measured by titration with hydrochloric acid (0.1 M) in the presence of methyl orange. The residual hydrogen peroxide concentration in the treated samples was measured spectrophotometrically at λ=410 nm with titanium sulfate by a H_2O_2-Ti^{4+} complex formation (Eisenberg, 1943) by a GENESYS 10S spectrophotometer (Thermo Scientific). The measurement of residual PS concentration in the treated samples was done spectrophotometrically (Genesys 10S, Thermo Scientific) at λ=352 nm by an excess KI reaction with PS towards the formation of I_2 (Liang et al., 2008). The residual concentration of PS was determined by using the standard multipoint calibration.

The acute toxicity of LOR solution (*Paper III*) was investigated using the Microtox® method (Model 500 Analyzer SDI) (ISO (International Organization for Standardization), 2007).

3 Results and discussion

The obtained results indicated that irrespective of the applied UV-assisted process, the target ECs degradation followed a pseudo-first order reaction kinetics ($r^2 \geq 0.95$) under studied experiment conditions and may be described with regard to the EC concentration through Eq. 58.

$$\frac{dC_{EC}}{dt} = -k_{obs} \times C_{EC} \qquad (58)$$

Where k_{obs} is the observed pseudo-first-order rate constant and C_{EC} is the EC concentration. The k_{obs} constants were calculated from the slopes of the straight lines by plotting ln (C_t/C_0) as a function of time t through linear regression.

3.1 UV-activated persulfate oxidation

The application of UV photolysis and UV/PS processes was investigated in various water matrices to eliminate AMX (*Paper I*), CTA (*Paper II*), LOR (*Paper III*), and NP (*Paper IV*). The oxidant utilization and TOC removal results are presented in Table 7.

As presented in Figure 4, the application of UVC photolysis to eliminate AMX (*Paper I*) in various water matrices indicated the highest k_{obs} value in UW (0.108 min^{-1}) and lowest k_{obs} in STWW (0.056 min^{-1}). Irrespective of the studied water matrix, the mineralization of AMX was in the range of 9-12%.
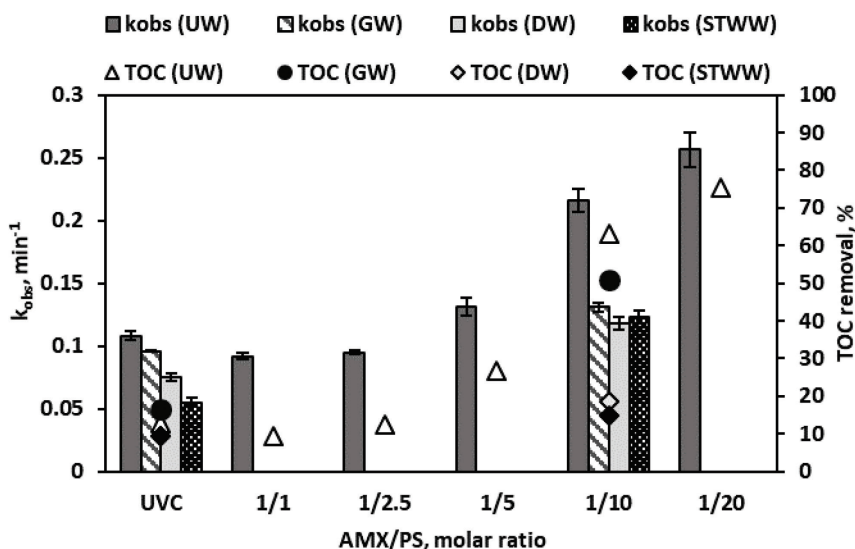
Figure 4. AMX degradation observed reaction rate constants and TOC removal by UVC photolysis and UVC/PS process at different PS concentrations at unadjusted pH in UW ([AMX]$_0$=40 μM, t=2 h)

In UW, the blank PS oxidation trial at an AMX/PS molar ratio of 1/10 resulted in only 40% degradation and negligible mineralization of AMX after 2 h of treatment. Thus, the subsequent addition of UVC radiation into PS system was justified. The application of UVC/PS process at various molar ratios of AMX/PS (1/1, 1/2.5, 1/5, 1/10, and 1/20) improved the target compound degradation (≥99%) in UW. An increase in the applied PS

concentration led to faster degradation of AMX, and thus k_{obs} values of 0.091 min^{-1} and 0.216 min^{-1} were obtained at $[PS]_0$=40 µM and $[PS]_0$=400 µM, respectively.

A comparison of the k_{obs} values obtained for different water matrices, at an AMX/PS molar ratio of 1/10, showed the inhibitory effect of the composition of real water samples on the degradation and mineralization of AMX (Figure 4). Overall, the oxidant consumption (*Paper I, Table 3*) was 76%-98% for all studied UV-assisted PS systems in UW. The obtained results suggested that a PS concentration of 400 µM was the most effective for AMX decomposition by the UVC/PS system.

Table 7. Oxidant utilization and mineralization in UV photolysis and UV/PS systems for elimination of emerging contaminants in UW

Studied emerging contaminant and treatment conditions	Process	EC/PS, molar ratio	PS utilized,%	TOC removal, %
AMX $[AMX]_0$=40 µM, t=2 h	UVC photolysis		-	12.9
	UVC/PS	1/1	76	9.3
		1/2.5	78	12.6
		1/5	90	26.9
		1/10	92	63
		1/20	98	75.4
CTA $[CTA]_0$=50 µM, t=2 h	UVA photolysis	-	-	0.14
	UVA/PS	1/1	8	1.1
		1/5	10	1.25
		1/10	11	1.1
		1/20	13	2.54
		1/40	14	4
	UVC photolysis	-	-	16.9
	UVC/PS	1/1	57	19.5
		1/5	82	25.3
		1/10	79	38.3
		1/20	94	48.5
		1/40	82	73.7
LOR $[LOR]_0$=40 µM, t=2 h	UVC photolysis		-	7.8
	UVC/PS	1/1	28	11.3
		1/5	49	19
		1/10	66	45
		1/20	93	88.6
NP $[NP]_0$=50 µM, t=3 h	UVC photolysis		-	-
	UVC/PS	1/1	61	-
		1/2	73	-
		1/4	76	-
		1/10	90	-

Further, the performance of UV-assisted PS system to degrade CTA (*Paper II*) was investigated in artificial buffered solution (pH_0=7.4, UW) and in GW. To investigate the influence of pH, UV/PS oxidation trials were also conducted at adjusted pH_0=3 in both studied water matrices.

The application of direct UVC photolysis indicated a higher CTA degradation efficiency (≥99% in first 15 min) in both water matrices compared to UVA photolysis (8.5% in UW and 35% in GW after 2 h of treatment). Further, the use of UVA/PS (Figure 5a) and UVC/PS (Figure 5b) systems at different PS concentrations ($[PS]_0$=50-2000 µM) was studied in UW. The effect of groundwater composition on CTA degradation was evaluated at a CTA/PS molar ratio of 1/10.

For all studied CTA/PS molar ratios, the use of UVA/PS system led to incomplete (19-72%) target compound degradation after 2 h of oxidation in UW. It is noteworthy that the $k_{obs} \times 10^2$ value was slightly higher in GW (0.475 min^{-1}) compared to UW (0.438 min^{-1}) at the same treatment conditions. Overall, CTA mineralization in the UVA-activated PS system was ≤4% at buffered pH_0=7.4 and ≤7% at adjusted pH_0=3 (*Paper II, Figure 2a, Figure 8a*).
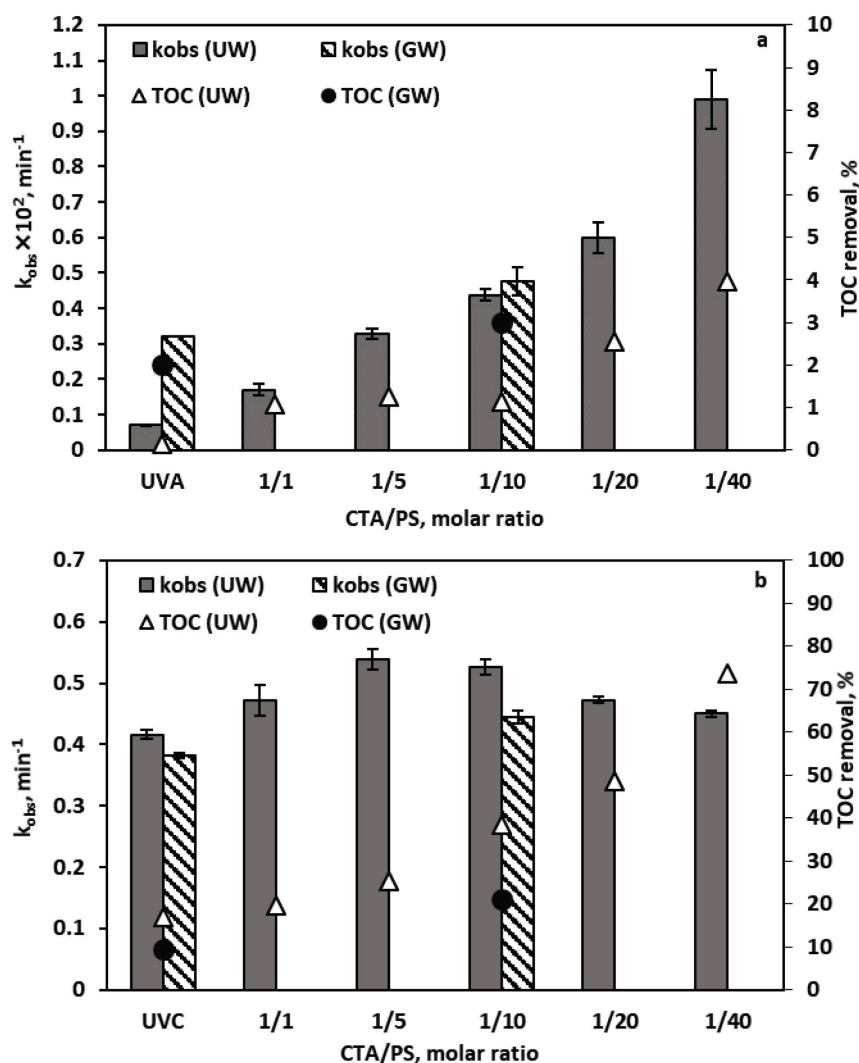
Figure 5. CTA degradation observed reaction rate constants and TOC removal by UV photolysis and UV/PS process (a for UVA, b for UVC) at different PS concentrations ($[CTA]_0$=50 µM, t=2 h)

In the case of UVC/PS systems, an increase in the concentration of PS from 50 µM to 250 µM led to an improvement in k_{obs} value. A further increase in PS concertation ($[PS]_0 \geq 500$ µM) showed a stable decrease in k_{obs} values most likely due to the PS scavenging reactions or/and the recombination of both $SO_4^{\bullet-}$ and $HO^{\bullet}$ radicals (*Paper II, Eq. 10-18*). The use of persulfate photolysis slightly improved the efficiency of CTA degradation (k_{obs}=0.44 min^{-1}) compared to direct UVC photolysis (k_{obs}=0.38 min^{-1}) in GW. However, the k_{obs} value in GW was lower compared to the k_{obs} value in UW (0.53 min^{-1}) at $[PS]_0$=500 µM. Similar to the results of decomposition of the target compound, TOC removal was considerably higher in UVC/PS systems (20%-74%) compared with UVA/PS processes (1.1%-4%).

In general, the results of oxidant consumption in UVA/PS systems (8%-14%) were substantially lower than in UVC-induced PS oxidation processes (57%-94%). In the latter systems, oxidant consumption increased simultaneously with an increase in $[PS]_0$ used up to 1000 µM (94%) (Table 7). A further increase in $[PS]_0$=2000 µM led to a decline in oxidant activation efficacy with around 20% of PS remained in solution. The latter observation can be explained by the limited activation capacity of the used source of UV irradiation in the case of elevated PS concentrations.

As presented in Figure 6, the UVC photolysis and UVC/PS system ($[PS]_0$=40-800 µM) were performed to eliminate LOR (*Paper III*) in UW and GW. The direct UVC photolysis proved more efficient in GW (k_{obs} value of 0.106 min^{-1}) along with 25% of TOC removal compared to results in UW (0.081 min^{-1}) with 8% mineralization. In UW, the application of UVC-assisted PS oxidation indicated $\geq$95% LOR degradation in 60 minutes. This observation can be explained by the fact that the photolysis of persulfate at high doses of the latter led to an increase in the formation of radicals, which, in turn, led to an improvement in the removal of LOR. The groundwater composition had an inhibitory effect on the removal of LOR by the UVC/PS system. Thus, the k_{obs} value and the removal of TOC were lower compared to the results obtained in UW at $[PS]_0$=400 µM.
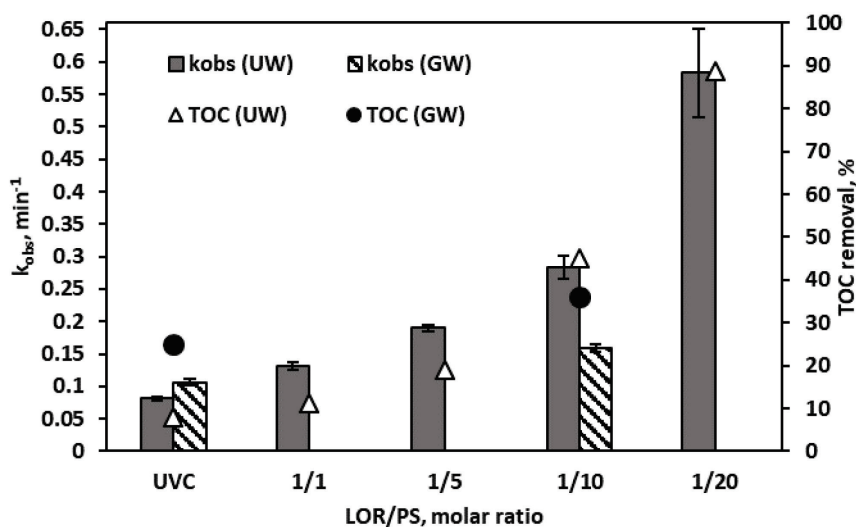

Figure 6. LOR degradation observed reaction rate constants and TOC removal by the UVC photolysis and UVC/PS processes in different water matrices ($[LOR]_0$=40 µM, t=2 h)

Consistent with the results of LOR degradation, the oxidant consumption was higher in UW compared with the results in GW (Table 7). In addition, more effective utilization of the oxidant was observed when using higher initial dosages of PS in UW. Accordingly, 93% PS was consumed after 2 h of UVC/PS oxidation at the highest studied LOR/PS molar ratio of 1/20. The acidic nature of the oxidant used and the formation of acidic intermediates led to a decrease in pH in the non-buffered UW matrix (*Paper III, Table 2*).

As presented in *Paper IV, Figure 2*, the direct UVC photolysis resulted in considerably higher ≥90% NP decomposition compared to the non-activated persulfate oxidation (<15%) in both matrices after 3 h of treatment. In addition, the use of UVC-induced PS systems for the decomposition of NP in UW and GW was evaluated at various oxidant concentrations ([PS]$_0$=50-1000 µM) corresponding to NP/PS molar ratios from 1/1 to 1/20.

The use of direct UVC photolysis led to a faster NP decomposition in UW (k_{obs}=0.017 min^{-1}) compared to GW (k_{obs}=0.012 min^{-1}) (*Paper IV*). As presented in *Paper IV, Figure 2*, increasing the PS dosage from 50 µM to 200 µM improved k_{obs} values in both water matrices. However, the obtained k_{obs} were generally lower in GW compared to UW results under the same treatment conditions, indicating the inhibitory effect of a real water matrix. Finally, the detected drop in k_{obs} at the highest applied PS concentration ([PS]$_0$=500 µM) indicated the scavenging effect of the increased oxidant dose and emphasized the need for careful optimization of the dosage of persulfate to obtain the most practicable outcomes. Contrary, to the NP degradation results, the oxidant utilization improved along with an increase in oxidant dosage, with the highest PS utilization of 82% and 90% in GW and UW, respectively, at [PS]$_0$=500 µM. The buffering capacity of the natural water sample resulted in negligible change in pH value in GW, while in UW a decrease in pH was observed. In conclusion, the PS dosage of 200 µM (NP/PS molar ratio of 1/4) proved the most efficient for NP degradation at all the studied UV/PS systems in both water matrices.

3.2   UV/Fe^{2+}-activated persulfate oxidation

The efficacy of target contaminants degradation using various iron-activated UV/PS systems was studied. The results of PS consumption and mineralization of emerging contaminants in the studied systems are presented in Table 8.

Oxidation of AMX by the PS/Fe^{2+} system at an AMX/PS/Fe^{2+} molar ratio of 1/10/1 led to incomplete degradation of the target compound (72.5%), negligible mineralization, and only 17.5% of oxidant utilization after 2 h of treatment (*Paper I*). As shown in Figure 7, the application of UVC/Fe^{2+}-activated PS system for the decomposition of AMX was investigated in various water matrices. Accordingly, the addition of iron activator ([Fe^{2+}]$_0$=40 µM) to the UVC/PS system showed an improvement in the k_{obs} value (0.531 min^{-1}) compared to the UV/PS system (0.216 min^{-1}) only in UW. In the case of TOC removal results, the efficiency was as follows: UW (75.4%) > GW (56.2%) > DW (24.1%) > STWW (14.3%).

In UW, the fastest decomposition of AMX (k_{obs}=1.38 min^{-1}) and the most complete mineralization (85%) were obtained with the highest studied dose of activator 80 µM at a fixed AMX/PS molar ratio of 1/10. Irrespective of the applied Fe^{2+} dose, the results of PS utilization showed ≥94% of oxidant consumption in the studied UVC/PS/Fe^{2+} systems. A decrease in pH was observed in all the UVC/Fe^{2+}-activated PS systems to a final value of about 3, indicating the acidity of added chemicals and the formation of acidic by-products (*Paper I, Table 3*).

Table 8. Oxidant utilization and mineralization in iron-activated UV/PS systems for elimination of emerging contaminants in UW

Studied emerging contaminant and treatment conditions	Process	EC/PS, molar ratio	PS utilized, %	TOC removal, %
AMX [AMX]$_0$=40 µM, t=2 h	UVC/PS/Fe^{2+}	1/10/0.25	96	63
		1/10/0.5	94	62.1
		1/10/1	96	75.4
		1/10/2	97	85.4
CTA [CTA]$_0$=50 µM, [PS]$_0$=500 µM, [α-FeO(OH)]$_0$=0.1-2.5 g L^{-1}, [Fe$_3$O$_4$]$_0$=0.01-0.5 g L^{-1}, t=2 h	UVA/PS/α-FeO(OH)	0.1	18	0.8
		0.2	14	1.23
		0.5	15	0.5
		1	14	0.6
		2	10	0.25
		2.5	12	2.1
	UVC/PS/α-FeO(OH)	0.1	34	75.1
		0.2	35	71.8
		0.5	36	68.3
		1	38	73.6
		2	37	68.7
		2.5	36	70.6
	UVA/PS/Fe$_3$O$_4$	0.01	16	-
		0.05	11	0.14
		0.1	13	-
		0.2	12	0.22
		0.5	8	-
	UVC/PS/Fe$_3$O$_4$	0.01	67	-
		0.05	65	15.8
		0.1	53	-
		0.2	45	23.9
		0.5	45	-
LOR [LOR]$_0$=40 µM, t=2 h	UVC/PS/Fe^{2+}	1/1/1	56	22.1
		1/5/0.5	98	17.3
		1/5/1	91	36.5
		1/5/2	98	45.4
		1/10/1	96	73.9
		1/10/2	94	84.7
NP [NP]$_0$=50 µM, t=3 h	UVC/PS/Fe^{2+}	1/1/0.25	35	-
		1/1/1	69	-
		1/2/1	9	-
		1/4/1	93	-
		1/10/0.25	95	-
		1/10/0.5	97	-
		1/10/1	97	-
		1/10/2	97	-
		1/10/10	98	-
		1/20/1	97	-

The application of UVA/PS/α-FeO(OH) system at a fixed CTA/PS molar ratio of 1/10 and different goethite dosages ranging from 0.1 g L^{-1} to 2.5 g L^{-1} was examined (*Paper II, Figure 5a*) to eliminate CTA in UW. Regardless of the goethite concentration used, the efficiency of the UVA/PS/α-FeO(OH) system in CTA degradation was lower compared to the UVA/PS system at the same $[PS]_0$=500 μM. Most likely, due to the amplified impact of radicals scavenging reactions in the combined UVA/α-FeO(OH)-activated PS systems. AMX mineralization was low (0.2%-2.5%) in all the studied UVA/PS/α-FeO(OH) systems after 2 h of treatment.
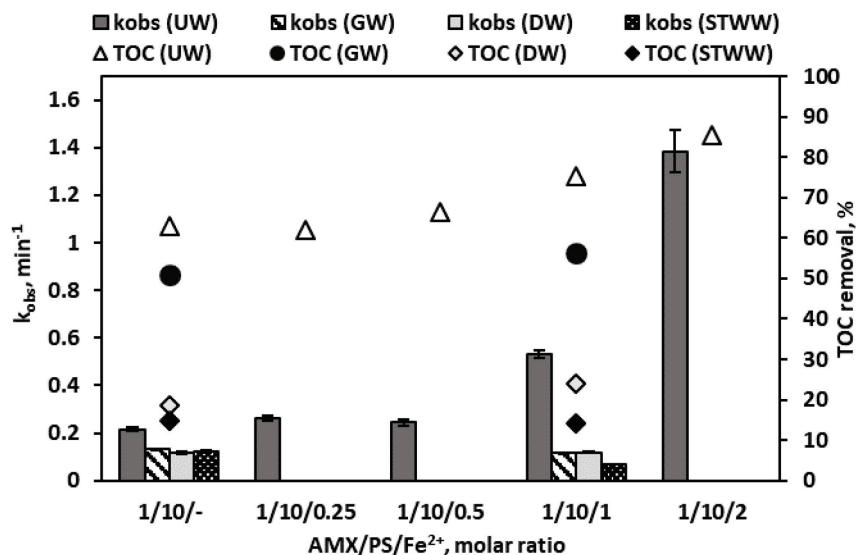
Figure 7. AMX degradation observed reaction rate constants and TOC removal by UVC/PS and UVC/PS/Fe²⁺ process at different Fe²⁺ concentrations at unadjusted pH ($[AMX]_0$=40 μM, t=2 h)

On the other hand, the UVC/α-FeO(OH)-activated PS oxidation trials conducted at the same treatment conditions led to some acceleration of CTA degradation and a substantial improvement in TOC removal compared to the UVC/PS systems in UW (*Paper II, Figure 5b*). Accordingly, the k_{obs} values were in the range 0.57 min^{-1}-0.61 min^{-1}, with the exception of k_{obs}=0.50 min^{-1}, obtained at $[α-FeO(OH)]_0$=2.5 g L^{-1}. Irrespective of the applied goethite dosages, the extent of CTA mineralization after 2 h of UVC/PS/α-FeO(OH) treatment was in the range 68%-75%.

The efficacy of the UVA/PS/Fe₃O₄ system in CTA degradation and mineralization was studied at the same fixed CTA/PS molar ratio of 1/10 and at different Fe₃O₄ dosages in the range of 0.01-0.5 g L^{-1} (*Paper II, Figure 6a*). Similar to the results obtained for the UVA /PS/α-FeO(OH) system, the addition of Fe₃O₄ to the UVA/PS system reduced the efficiency of CTA degradation. In addition, an increase in the used dosage of Fe₃O₄ led to a further decrease in the $k_{obs} \times 10^2$ value. In all studied UVA/Fe₃O₄-activated PS systems, negligible mineralization of CTA was observed (0.14%-0.22%).

The application of UVC/PS/Fe₃O₄ (*Paper II, Figure 6b*) process indicated complete CTA degradation (≥97%) within a 2-h treatment. However, the addition of magnetite to the UVC/PS system has led to a decrease in the decomposition efficiency of CTA. Similarly, the removal of TOC in all the studied UVC/PS/Fe₃O₄ systems was lower (up to 24%) compare to the UVC/PS (39%) process.

The performance of dual activated heterogeneous PS-based systems in the target compound oxidation was also studied in GW (*Paper II, Figure 7a, Figure 7b*). Irrespective of the UV radiation used, the efficiency of CTA degradation by the UV/PS/α-FeO(OH) system was higher than in the UV/PS/Fe_3O_4 system, but lower than in the UV/PS system.

Overall, the results of UV-induced heterogeneous PS-based systems suggested that the application of UVC/α-FeO(OH)-activation is the most effective technology for the $SO_4^{\bullet-}$-based CTA oxidation among the studied processes. It is noteworthy that the utilization of PS was ≤68% (Table 8) in all the heterogeneous systems studied. The oxidation trials conducted at adjusted pH_0=3 (*Paper II, Figure 8a, Figure 8b*) showed improved TOC removal in both water matrices. Irrespective of the UV radiation used, the UV/PS/Fe^{2+} and UV/PS/α-FeO(OH) systems proved to be more efficient in TOC removal compared to the UV/PS and UV/PS/Fe_3O_4 systems.

The application of PS/Fe^{2+} system at a LOR/PS/Fe^{2+} molar ratio of 1/10/1 resulted in only 28% of LOR decomposition, negligible mineralization, and around 90% of PS consumption after 2 h of treatment (*Paper III*). The efficacy of the UVC/Fe^{2+} system for the decomposition of LOR at a LOR/Fe^{2+} molar ratio of 1/1 was also investigated. The results indicated the k_{obs} value of 0.12 min^{-1} and 21% of TOC removal after 2 h of treatment (Figure 8).
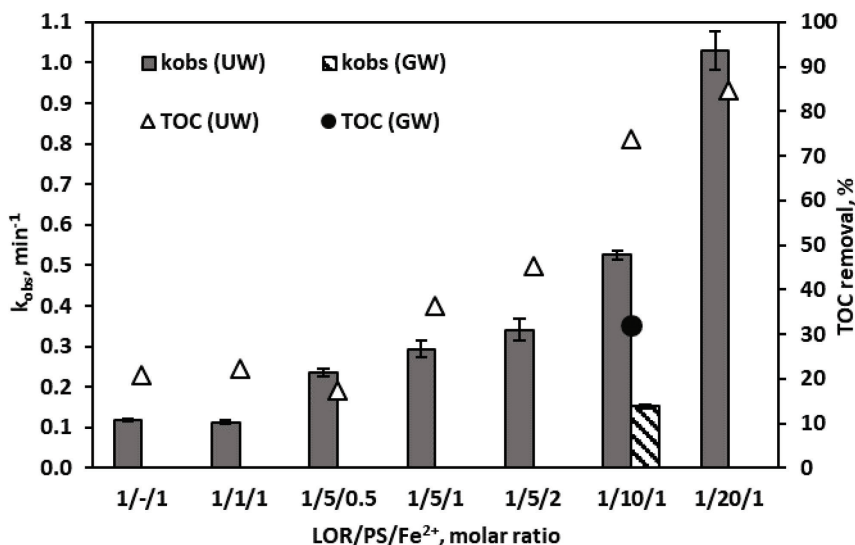
Figure 8. LOR degradation observed reaction rate constants and TOC removal by the UVC/Fe^{2+} and UVC/PS/Fe^{2+} processes in different water matrices ([LOR]$_0$=40 µM, t=2 h)

In the case of combined UVC/PS/Fe^{2+} system, the use of a higher oxidant concentration at a fixed activator concentration ([Fe^{2+}]$_0$=40 µM) led to a faster LOR decomposition (Figure 8). For example, k_{obs} values of 0.113 min^{-1} and 0.526 min^{-1} were obtained for [PS]$_0$=40 µM and [PS]$_0$=400 µM, respectively, in UW. It should be noted that the UVC/PS/Fe^{2+} oxidation at a LOR/PS/Fe^{2+} molar ratio of 1/10/1 led to a 3.5-fold decrease in the k_{obs} value (0.152 min^{-1}) in GW. In addition, the effect of Fe^{2+} concentration on the efficacy of degradation and mineralization of LOR in the UVC/Fe^{2+}-activated PS system ([PS]$_0$=200 µM) was also investigated. The results showed the need for careful optimization of Fe^{2+} in order to increase the cost-effectiveness of the process. Overall,

the highest k_{obs} value (1.03 min^{-1}) and the most complete mineralization (85%) were obtained at a LOR/PS/Fe^{2+} molar ratio of 1/20/1.

As presented in *Paper IV, Figure 3,* the application of UVC/Fe^{2+}-activated PS system with a variable concentration of PS ranging from 50-1000 μM at a fixed concentration of activator ([Fe^{2+}]$_0$=50 μM) was investigated to eliminate NP in various water matrices. In general, the use of combined UVC/Fe^{2+}-activated PS systems retarded the decomposition of NP compared with the results of UVC/PS treatment in UW. A slight improvement in NP degradation efficiency was observed at a NP/PS/Fe^{2+} molar ratio of 1/4/1 (k_{obs}=0.016 min^{-1}). Notably, the application of the same treatment conditions in GW led to lower NP decomposition efficiency (k_{obs}=0.014 min^{-1}). A further increase in the oxidant concentration in UW led to a slower degradation of NP in the UVC/PS/Fe^{2+} system.

To investigate the effect of Fe^{2+} activator dosage on NP degradation in the UVC/PS/Fe^{2+} system, oxidation experiments were conducted at a fixed concentration of oxidant ([PS]$_0$=500 μM) along with varying concentration of Fe^{2+} (5-500 μM) (*Paper IV, Figure 4)*. Irrespective of the activator dosage used, lower k_{obs} values (0.003 min^{-1}-0.01 min^{-1}) were obtained in the UVC/PS/Fe^{2+} system compared to the UVC/PS system (k_{obs}=0.02 min^{-1}). Though, almost complete (~95%) PS utilization was observed after 3 h of UVC/PS/Fe^{2+} oxidation.

3.3   H$_2$O$_2$- and H$_2$O$_2$/Fe^{2+}-activated persulfate oxidation

The UVC-activated dual oxidant (PS/H$_2$O$_2$) system was investigated to eliminate NP (*Paper IV*) in UW and at optimized concentrations in GW. The efficacy of the UVC/PS/H$_2$O$_2$ system was considered at a fixed [PS]$_0$=50 μM and varying [H$_2$O$_2$]$_0$=5-50 μM. The results demonstrated ≥90% NP degradation in all studied systems after 3 h of treatment.

The use of direct oxidation of H$_2$O$_2$ was ineffective in the decomposition of NP (15%) with more than 90% residual H$_2$O$_2$ in both matrices after 3 h of oxidation. In turn, the photolysis of H$_2$O$_2$ at [H$_2$O$_2$]$_0$=50 μM showed higher efficiency with 96% NP degradation and a higher k_{obs} value of 0.024 min^{-1} compared to the UV/PS system (k_{obs} value of 0.019 min^{-1}) at the same oxidant concentration. As presented in *Paper IV, Figure 5*, a slight improvement in the obtained k_{obs} value (0.022 min^{-1}) was observed at [H$_2$O$_2$]$_0$=12.5 μM in UW. It is noteworthy that the oxidation of NP at the same treatment conditions in GW led to a 3.5 times lower value of k_{obs} (0.006 min^{-1}).

The application of PS/H$_2$O$_2$/Fe^{2+} oxidation at a NP/PS/H$_2$O$_2$/Fe^{2+} molar ratio of 1/1/0.25/0.25 in UW and GW showed substantially lower efficiency (26% and 33% NP degradation, respectively) compared to the UVC/Fe^{2+}-activated PS/H$_2$O$_2$ system (96% and 93%, respectively). In turn, the results of combined UVC/PS/H$_2$O$_2$/Fe^{2+} system at a NP/PS/H$_2$O$_2$/Fe^{2+} molar ratio of 1/1/0.25/0.25 showed a negligible improvement in the efficiency of NP degradation in UW and 3.5 times faster decomposition of the target compound in GW compared to the UVC/PS/H$_2$O$_2$ system.

The H$_2$O$_2$ utilization results showed a low consumption (18%-28%) at all studied NP/PS/H$_2$O$_2$ molar ratios in UW and GW. Irrespective of the water matrix studied, the highest H$_2$O$_2$ utilization was observed in the UVC/PS/H$_2$O$_2$/Fe^{2+} system with 52% and 32% of H$_2$O$_2$ consumed in UW and GW, respectively. This observation indicated the predominance of different radicals scavenging reactions over NP oxidation reactions.

3.4 Radical scavenging studies

The prevalence of $SO_4^{\bullet-}$ or $HO^{\bullet}$ was determined by observing the degradation of target compounds in UW after the addition of the molecular probe EtOH or *t*-BuOH into various systems. EtOH a well-studied scavenger for $SO_4^{\bullet-}$ $(1.6\text{-}7.7) \times 10^7$ M^{-1} s^{-1} and $HO^{\bullet}$ $(1.2\text{-}2.8) \times 10^9$ M^{-1} s^{-1}, while *t*-BuOH is an effective scavenger for $HO^{\bullet}$ $(3.8\text{-}7.6) \times 10^8$ M^{-1} s^{-1} than for $SO_4^{\bullet-}$ $(4\text{-}9.1) \times 10^5$ M^{-1} s^{-1}.

As presented in *Table 9,* the addition of EtOH resulted in additional residual AMX *(Paper I)* in the UVC/PS (23.4%) and UVC/PS/Fe^{2+} (37.3%) system compared to *t*-BuOH in the UVC/PS (2%) and UVC/PS/Fe^{2+} (6.8%) suggesting the predominance of $SO_4^{\bullet-}$ oxidative species in the studied systems.

The addition of *t*-BuOH inhibited the degradation of CTA (*Paper II*) by the UV/PS, UV/PS/α-FeO(OH), and UV/PS/Fe_3O_4 systems to some extent. As a result, residual CTA concentration increased by about 3% and 6% in the UVA/PS and UVC/PS systems respectively suggesting the participation of $HO^{\bullet}$ in all cases.

Table 9. Degradation of emerging contaminants by the studied UV-activated PS systems in UW

Emerging contaminants	Treatment conditions	Process	$[EC]t/[EC]_0$,%		
			Without scavenger	*t*-BuOH	EtOH
AMX	$[AMX]_0$=40 μM $[Fe^{2+}]_0$=40 μM, $[PS]_0$=400 μM, $[t\text{-}BuOH]_0$=20 mM, $[EtOH]_0$=20 mM, t=5 min	UVC/PS	30	32	54
		UVC/PS/Fe^{2+}	6	13	43
CTA	$[CTA]_0$=50 μM, $[PS]_0$=500 μM, $[\alpha\text{-}FeO(OH)]_0$=1 g L^{-1}, $[Fe_3O_4]_0$=0.2 g L^{-1}, $[EtOH]_0$=25 mM, $[t\text{-}BuOH]_0$=25 mM, t_{UVA}=60 min, t_{UVC}=5 min	UVA/PS	76	79	86
		UVA/PS/α-FeO(OH)	79	88	90
		UVA/PS/Fe_3O_4	93	99	100
		UVC/PS	5	11	13
		UVC/PS/α-FeO(OH)	10	12	13
		UVC/PS/Fe_3O_4	14	15	19
LOR	$[LOR]_0$=40 μM, $[Fe^{2+}]_0$=40 μM, $[PS]_0$=200 μM, $[t\text{-}BuOH]_0$=20 mM, $[EtOH]_0$=20 mM, t=7 min	UVC	46	71	-
		UVC/PS	22	54	72
		UVC/PS/Fe^{2+}	8	33	60
NP	$[NP]_0$=50 μM, $[PS]_0$=50 μM, $[H_2O_2]_0$=12.5 μM, $[Fe^{2+}]_0$=50 μM (UV/PS/Fe^{2+}), $[Fe^{2+}]_0$=12.5 μM (UV/PS/H_2O_2/Fe^{2+}), $[t\text{-}BuOH]_0$=25 mM, $[EtOH]_0$=25 mM, t=15 min	UVC/PS	63	80	82
		UVC/PS/Fe^{2+}	68	72	73
		UVC/PS/H_2O_2	67	80	81
		UVC/PS/H_2O_2/Fe^{2+}	58	72	73

On the other hand, the addition of EtOH to the UV/PS systems resulted in 10.5% (UVA) and 8% (UVC) additional residual CTA concentration. The obtained results suggested that both hydroxyl and sulfate radicals contributed to the degradation of CTA in the UV-induced persulfate systems, while $SO_4^{\bullet-}$ proved the predominant radical in all studied systems.

The addition of excess t-BuOH in UVC-induced PS-based systems decreased the efficiency of LOR (*Paper III*) degradation by 32% and 25% in the UVC/PS and UVC/PS/Fe^{2+} system, respectively, indicating the active participation of HO$^{\bullet}$ in the oxidation process. Whereas, the addition of excess EtOH substantially inhibited the decomposition of LOR in the UVC/PS (50%) and UVC/PS/Fe^{2+} (52%) system, which, in turn, indicated the important role of $SO_4^{\bullet-}$ in the degradation of the target compound. The outcomes of scavenging studies suggested that both free radicals contributed to the degradation of LOR in the UVC/PS/Fe^{2+} system, while HO$^{\bullet}$ proved dominant oxidative species in the UVC/PS system.

The addition of excess t-BuOH decreased the efficacy of NP (*Paper IV*) degradation in the UVC/PS (17%), UVC/PS/Fe^{2+} (3%), UVC/PS/H$_2$O$_2$ (13%) and UVC/PS/H$_2$O$_2$/Fe^{2+} (14%) systems suggesting that HO$^{\bullet}$ was involved in the oxidation of the target compound by all processes. Irrespective of the studied system, the addition of excess EtOH led to only 1-2% supplementary inhibition of the decomposition of NP compared to the use of t-BuOH. The results of the scavenging studies for the degradation of NP suggested that both HO$^{\bullet}$ and $SO_4^{\bullet-}$ contributed to the degradation of NP in the studied systems, while HO$^{\bullet}$ turned out to be the predominant radical species.

3.5   Transformation products and acute toxicity

During the degradation of AMX by the UVC/PS and UVC/PS/Fe^{2+} system, the formation of transformation products was observed in the water matrices (UW, GW, DW, and STWW) using LC-MS as presented in *Paper I, Figure 5*. Accordingly, hydroxylation of the target compound resulted in a hydroxylated AMX with m/z 382 (route A) and the hydrolysis on the β-lactam ring led to the formation of AMX-diketopiperazine-2',5' with m/z 366 (route B). The opening of the β-lactam ring followed by demethylation, decarboxylation, opening of the thiazole ring and loss of S atom (route C) can lead to the formation of a penicilloic acid derivate with m/z 122. In addition, the decarboxylation, demethylation and opening of the thiazole ring may result in the formation of an AMX derivative with m/z 208 (route D).

The transformation products were identified during the oxidation of LOR (*Paper III, Table 5*) by the UVC/PS, UVC/H$_2$O$_2$, UVC/PS/Fe^{2+}, and UVC/H$_2$O$_2$/Fe^{2+} systems using LC-MS analysis and proposed degradation pathway is presented in *Figure 9*.

In accordance with the radicals scavenging studies results, the formation of TP1 (route A) and TP2 (route D) was result of the attack of HO$^{\bullet}$ on the alcohol moiety and carbon double bond of LOR, respectively (Serna-Galvis et al., 2019). In addition, TP3 (route C) is formed as a result of hydroxylation of the alkyl chain, followed by its oxidation to generate TP4 (Gao et al., 2016). TP5 (route B) was formed by the removal of chlorine. The hydroxylation of carbon atoms 2 and 5 in the imidazole ring led to the formation of TP6. Similarly, TP7 and TP8 are isomers formed from the opening of the imidazole ring (Carpinteiro et al., 2019).

Supplementary, to the formation of toxic intermediates, the acute toxicity of LOR (*Paper III*) aqueous solutions treated by the UVC/PS/Fe^{2+} system at a LOR/PS/Fe^{2+} molar ratio of 1/5/1 was studied using *Vibrio fischeri* bioluminescence inhibition assay.

The obtained results were compared with the UVC/H_2O_2/Fe^{2+} system at the same treatment conditions. Accordingly, the EC_{20} of the initial LOR solution was low (55.6% of the sample). However, the application of UVC/Fe^{2+}-activated H_2O_2 process led to the detoxification of the LOR solution (EC_{20} at >100% of the solution). On the other hand, the sample treated with the UV/PS/Fe^{2+} system showed an increase in the inhibition of *Vibrio fischeri* bioluminescence (EC_{20} at 16.5% of the solution). This observation can be explained by the toxic effect of residual PS concentration in the system (Moreno-Andrés et al., 2019). Therefore, unused PS must be removed from treated water/wastewater prior to discharge into receiving water bodies.
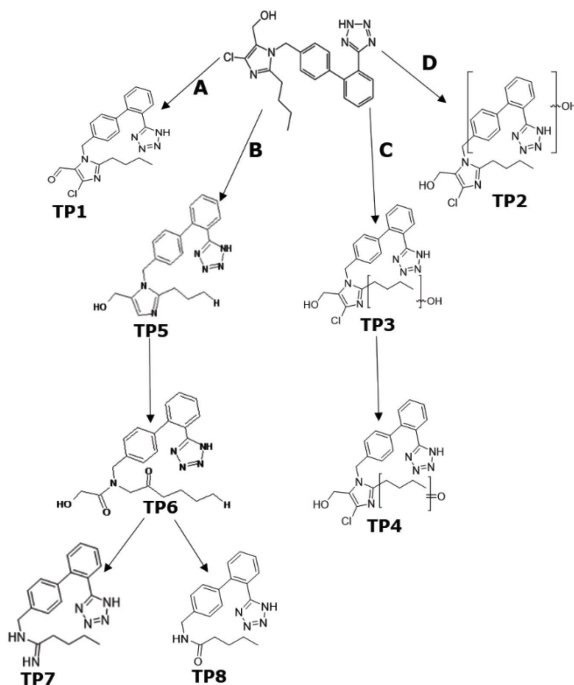
Figure 9. Proposed degradation pathway of LOR by studied UV-induced PS-based systems in UW

Conclusions

The application of UV-induced PS oxidation processes was studied for the effective elimination of ECs in water matrices. The novelty of the present study comprised the application of activated persulfate oxidation to degrade two β-lactam antibiotics under previously not studied treatment conditions, namely AMX in four different real water matrices by the UVC/PS and UVC/PS/Fe^{2+} systems and CTA by the UV-, UV/α-FeO(OH)- and UV/Fe$_3$O$_4$-activated PS systems in UW and GW. To widen the range of study, UVC- and UVC/Fe^{2+}-induced PS systems were investigated to degrade antihypertensive drug LOR in UW and GW for the first time. The application of UVC- and UVC/Fe^{2+}-induced PS/H$_2$O$_2$ systems to degrade endocrine disruptor NP in UW and GW was firstly investigated.

Overall, the use of the UV/PS system improved the degradation efficiency of the studied ECs compared with direct UV photolysis oxidation. The addition of Fe^{2+} or α-FeO(OH) into the UV/PS system demonstrated a further increase in the efficiency of the studied micropollutants decomposition under optimized treatment conditions. Irrespective of the studied UV-induced PS-based system, the mineralization of the target compounds was lower than their degradation. The composition of the real aqueous matrix markedly inhibited the decomposition rate of the target compounds in the UV-activated PS-based systems. The results of radical purification studies showed that the predominance of SO$_4^{\bullet-}$ or HO$^\bullet$ radicals strongly depends on the structure of the target compound as well as on the PS activation technique used. The oxidation pathways of AMX and LOR were proposed based on the transformation products identified. In the case of LOR, the ecotoxicity of the formed transformation products was assessed by a *Vibrio fischeri* bioluminescence inhibition assay.

The findings of this study enlarge the existing knowledge on the effectiveness of UV-induced PS-based systems and, thus, increase the potential for practical application of these methods for the advanced purification of contaminated water.

References

Abu Jafar Khan, & Watts, R. J. (1996). Mineral-catalyzed peroxidation of tetrachloroethylene. *Water, Air, and Soil Pollution*, *88*(3–4), 247–260. doi: 10.1007/BF00294104

Akbari, A., Remigy, J. C., & Aptel, P. (2002). Treatment of textile dye effluent using a polyamide-based nanofiltration membrane. *Chemical Engineering and Processing: Process Intensification*, *41*(7), 601–609. doi: 10.1016/S0255-2701(01)00181-7

Aksu Demirezen, D., Yıldız, Y. Ş., & Demirezen Yılmaz, D. (2019). Amoxicillin degradation using green synthesized iron oxide nanoparticles: Kinetics and mechanism analysis. *Environmental Nanotechnology, Monitoring & Management*, *11*, article id-100219. doi: 10.1016/j.enmm.2019.100219

Al-Ahmari, S. D., Watson, K., Fong, B. N., Ruyonga, R. M., & Ali, H. (2018). Adsorption kinetics of 4-n-nonylphenol on hematite and goethite. *Journal of Environmental Chemical Engineering*, *6*(4), 4030–4036. doi: 10.1016/j.jece.2018.05.052

Al-Shamsi, M. A., Thomson, N. R., & Forsey, S. P. (2013). Iron based bimetallic nanoparticles to activate peroxygens. *Chemical Engineering Journal*, *232*, 555–563. doi: 10.1016/j.cej.2013.07.109

An, J., Zhu, L., Zhang, Y., & Tang, H. (2013). Efficient visible light photo-Fenton-like degradation of organic pollutants using in situ surface-modified $BiFeO_3$ as a catalyst. *Journal of Environmental Sciences*, *25*(6), 1213–1225. doi: 10.1016/S1001-0742(12)60172-7

Anipsitakis, G. P., & Dionysiou, D. D. (2004). Radical Generation by the Interaction of Transition Metals with Common Oxidants. *Environmental Science & Technology*, *38*(13), 3705–3712. doi: 10.1021/es035121o

Aredes, S., Klein, B., & Pawlik, M. (2012). The removal of arsenic from water using natural iron oxide minerals. *Journal of Cleaner Production*, *29–30*, 208–213. doi: 10.1016/j.jclepro.2012.01.029

Asghar, A., Abdul Raman, A. A., & Wan Daud, W. M. A. (2015). Advanced oxidation processes for in-situ production of hydrogen peroxide/hydroxyl radical for textile wastewater treatment: a review. *Journal of Cleaner Production*, *87*, 826–838. doi: 10.1016/j.jclepro.2014.09.010

Ashfaq, M., Li, Y., Wang, Y., Chen, W., Wang, H., Chen, X., Wu, W., Huang, Z., Yu, C.-P., & Sun, Q. (2017). Occurrence, fate, and mass balance of different classes of pharmaceuticals and personal care products in an anaerobic-anoxic-oxic wastewater treatment plant in Xiamen, China. *Water Research*, *123*, 655–667. doi: 10.1016/j.watres.2017.07.014

Barrera-Díaz, C. E., Frontana-Uribe, B. A., Rodríguez-Peña, M., Gomez-Palma, J. C., & Bilyeu, B. (2018). Integrated advanced oxidation process, ozonation-electrodegradation treatments, for nonylphenol removal in batch and continuous reactor. *Catalysis Today*, *305*, 108–116. doi: 10.1016/j.cattod.2017.09.003

Beier, S., Köster, S., Veltmann, K., Schröder, H., & Pinnekamp, J. (2010). Treatment of hospital wastewater effluent by nanofiltration and reverse osmosis. *Water Science and Technology*, *61*(7), 1691–1698. doi: 10.2166/wst.2010.119

Bennedsen, L. R., Muff, J., & Søgaard, E. G. (2012). Influence of chloride and carbonates on the reactivity of activated persulfate. *Chemosphere*, *86*(11), 1092–1097. doi: 10.1016/j.chemosphere.2011.12.011

Bennett, R. A., Etman, H. A., Hicks, H., Richards, L., Wu, C., Castell, M. R., Dhesi, S. S., & Maccherozzi, F. (2018). Magnetic iron oxide nanowires formed by reactive dewetting. *Nano Letters*, *18*(4), 2365–2372. doi: 10.1021/acs.nanolett.7b05310

Besha, A. T., Gebreyohannes, A. Y., Tufa, R. A., Bekele, D. N., Curcio, E., & Giorno, L. (2017). Removal of emerging micropollutants by activated sludge process and membrane bioreactors and the effects of micropollutants on membrane fouling: A review. *Journal of Environmental Chemical Engineering*, *5*(3), 2395–2414. doi: 10.1016/j.jece.2017.04.027

Boslaugh, S. E. (2016). WHO Model Lists of Essential Medicines. In The SAGE Encyclopedia of Pharmacology and Society. 2455 Teller Road, Thousand Oaks, California 91320: SAGE Publications, Inc. doi: 10.4135/9781483349985.n433

Botero-Coy, A. M., Martínez-Pachón, D., Boix, C., Rincón, R. J., Castillo, N., Arias-Marín, L. P., Manrique-Losada, L., Torres-Palma, R., Moncayo-Lasso, A., & Hernández, F. (2018). An investigation into the occurrence and removal of pharmaceuticals in Colombian wastewater. *Science of The Total Environment*, *642*, 842–853. doi: 10.1016/j.scitotenv.2018.06.088

Brix, R., Hvidt, S., & Carlsen, L. (2001). Solubility of nonylphenol and nonylphenol ethoxylates. On the possible role of micelles. *Chemosphere*, *44*(4), 759–763. doi: 10.1016/S0045-6535(00)00366-0

Bu, L., Shi, Z., & Zhou, S. (2016). Modeling of Fe(II)-activated persulfate oxidation using atrazine as a target contaminant. *Separation and Purification Technology*, *169*, 59–65. doi: 10.1016/j.seppur.2016.05.037

Bush, K., & Jacoby, G. A. (2010). Updated Functional Classification of β-Lactamases. *Antimicrobial Agents and Chemotherapy*, *54*(3), 969–976. doi: 10.1128/AAC.01009-09

Carpinteiro, I., Castro, G., Rodríguez, I., & Cela, R. (2019). Free chlorine reactions of angiotensin II receptor antagonists: Kinetics study, transformation products elucidation and in-silico ecotoxicity assessment. *Science of The Total Environment*, *647*, 1000–1010. doi: 10.1016/j.scitotenv.2018.08.082

Casado, J., Rodríguez, I., Ramil, M., & Cela, R. (2014). Selective determination of antimycotic drugs in environmental water samples by mixed-mode solid-phase extraction and liquid chromatography quadrupole time-of-flight mass spectrometry. *Journal of Chromatography A*, *1339*, 42–49. doi: 10.1016/j.chroma.2014.02.087

Castiglioni, S., Bagnati, R., Calamari, D., Fanelli, R., & Zuccato, E. (2005). A multiresidue analytical method using solid-phase extraction and high-pressure liquid chromatography tandem mass spectrometry to measure pharmaceuticals of different therapeutic classes in urban wastewaters. *Journal of Chromatography A*, *1092*(2), 206–215. doi: 10.1016/j.chroma.2005.07.012

Cheng, D. L., Ngo, H. H., Guo, W. S., Liu, Y. W., Zhou, J. L., Chang, S. W., Nguyen, D. D., Bui, X. T., & Zhang, X. B. (2018). Bioprocessing for elimination antibiotics and hormones from swine wastewater. *Science of The Total Environment*, *621*, 1664–1682. doi: 10.1016/j.scitotenv.2017.10.059

Choi, K.-J., Kim, S.-G., & Kim, S.-H. (2008). Removal of antibiotics by coagulation and granular activated carbon filtration. *Journal of Hazardous Materials*, *151*(1), 38–43. doi: 10.1016/j.jhazmat.2007.05.059

Cortez, F. S., Souza, L. da S., Guimarães, L. L., Almeida, J. E., Pusceddu, F. H., Maranho, L. A., Mota, L. G., Nobre, C. R., Moreno, B. B., Abessa, D. M. de S., Cesar, A., Santos, A. R., & Pereira, C. D. S. (2018). Ecotoxicological effects of losartan on the brown mussel Perna perna and its occurrence in seawater from Santos Bay (Brazil). *Science of The Total Environment*, *637–638*, 1363–1371. doi: 10.1016/j.scitotenv.2018.05.069

De Andrade, J. R., Vieira, M. G. A., da Silva, M. G. C., & Wang, S. (2020). Oxidative degradation of pharmaceutical losartan potassium with N-doped hierarchical porous carbon and peroxymonosulfate. *Chemical Engineering Journal*, *382*, Article id-122971. doi: 10.1016/j.cej.2019.122971

Devi, P., Das, U., & Dalai, A. K. (2016). In-situ chemical oxidation: Principle and applications of peroxide and persulfate treatments in wastewater systems. *Science of The Total Environment*, *571*, 643–657. doi: 10.1016/j.scitotenv.2016.07.032

Diwan, V., Tamhankar, A. J., Khandal, R. K., Sen, S., Aggarwal, M., Marothi, Y., Iyer, R. V., Sundblad-Tonderski, K., & Stålsby- Lundborg, C. (2010). Antibiotics and antibiotic-resistant bacteria in waters associated with a hospital in Ujjain, India. *BMC Public Health*, *10*(1), 414. doi: 10.1186/1471-2458-10-414

Dong, H., Qiang, Z., Hu, J., & Sans, C. (2017). Accelerated degradation of iopamidol in iron activated persulfate systems: Roles of complexing agents. *Chemical Engineering Journal*, *316*, 288–295. doi: 10.1016/j.cej.2017.01.099

Eisenberg, G. (1943). Colorimetric Determination of Hydrogen Peroxide. *Industrial & Engineering Chemistry Analytical Edition*, *15*(5), 327–328. doi: 10.1021/i560117a011

Fatta-Kassinos, D., Meric, S., & Nikolaou, A. (2011). Pharmaceutical residues in environmental waters and wastewater: current state of knowledge and future research. *Analytical and Bioanalytical Chemistry*, *399*(1), 251–275. doi: 10.1007/s00216-010-4300-9

Flanagan, J., Griffith, W. P., & Skapski, A. C. (1984). The active principle of Caro's acid, HSO_5^-: X-ray crystal structure of $KHSO_5 \cdot H_2O$. *J. Chem. Soc., Chem. Commun.*, *23*, 1574–1575. doi: 10.1039/C39840001574

Furman, O. S., Teel, A. L., & Watts, R. J. (2010). Mechanism of Base Activation of Persulfate. *Environmental Science & Technology*, *44*(16), 6423–6428. doi: 10.1021/es1013714

Gao, F., Li, Y., & Xiang, B. (2018). Degradation of bisphenol A through transition metals activating persulfate process. *Ecotoxicology and Environmental Safety*, *158*, 239–247. doi: 10.1016/j.ecoenv.2018.03.035

Gao, Y., Ji, Y., Li, G., & An, T. (2016). Theoretical investigation on the kinetics and mechanisms of hydroxyl radical-induced transformation of parabens and its consequences for toxicity: Influence of alkyl-chain length. *Water Research*, *91*, 77–85. doi: 10.1016/j.watres.2015.12.056

Godoy, A. A., Kummrow, F., & Pamplin, P. A. Z. (2015). Ecotoxicological evaluation of propranolol hydrochloride and losartan potassium to *Lemna minor* L. (1753) individually and in binary mixtures. *Ecotoxicology*, *24*(5), 1112–1123. doi: 10.1007/s10646-015-1455-3

González, S., Müller, J., Petrovic, M., Barceló, D., & Knepper, T. P. (2006). Biodegradation studies of selected priority acidic pesticides and diclofenac in different bioreactors. *Environmental Pollution*, *144*(3), 926–932. doi: 10.1016/j.envpol.2006.02.021

Graham, D. Y., & Fischbach, L. (2010). Helicobacter pylori treatment in the era of increasing antibiotic resistance. *Gut*, *59*(8), 1143–1153. doi: 10.1136/gut.2009.192757

Guenther, K., Heinke, V., Thiele, B., Kleist, E., Prast, H., & Raecker, T. (2002). Endocrine Disrupting Nonylphenols Are Ubiquitous in Food. *Environmental Science & Technology*, *36*(8), 1676–1680. doi: 10.1021/es010199v

Herrmann, H. (2007). On the photolysis of simple anions and neutral molecules as sources of O$^-$/OH, SO$_x^-$ and Cl in aqueous solution. *Phys. Chem. Chem. Phys.*, *9*(30), 3935–3964. doi: 10.1039/B618565G

Huang, B., Wang, H.-C., Cui, D., Zhang, B., Chen, Z.-B., & Wang, A.-J. (2018). Treatment of pharmaceutical wastewater containing β-lactams antibiotics by a pilot-scale anaerobic membrane bioreactor (AnMBR). *Chemical Engineering Journal*, *341*, 238–247. doi: 10.1016/j.cej.2018.01.149

Ince, N. H., Gültekin, I., & Tezcanli-Güyer, G. (2009). Sonochemical destruction of nonylphenol: Effects of pH and hydroxyl radical scavengers. *Journal of Hazardous Materials*, *172*(2–3), 739–743. doi: 10.1016/j.jhazmat.2009.07.058

ISO (International Organization for Standardization). (2007). Water quality-Determination of the inhibitory effect of water samples on te light emission of vibrio fischeri (Luminescent bacteria test)- Part 3: Method using freeze-dried bacteria. *ISO 11348-3:2007*.

Ji, Y., Ferronato, C., Salvador, A., Yang, X., & Chovelon, J.-M. (2014). Degradation of ciprofloxacin and sulfamethoxazole by ferrous-activated persulfate: Implications for remediation of groundwater contaminated by antibiotics. *Science of The Total Environment*, *472*, 800–808. doi: 10.1016/j.scitotenv.2013.11.008

Jobling, S., & Sumpter, J. P. (1993). Detergent components in sewage effluent are weakly oestrogenic to fish: An in vitro study using rainbow trout (Oncorhynchus mykiss) hepatocytes. *Aquatic Toxicology*, *27*(3–4), 361–372. doi: 10.1016/0166-445X(93)90064-8

Joss, A., Andersen, H., Ternes, T., Richle, P. R., & Siegrist, H. (2004). Removal of Estrogens in Municipal Wastewater Treatment under Aerobic and Anaerobic Conditions: Consequences for Plant Optimization. *Environmental Science & Technology*, *38*(11), 3047–3055. doi: 10.1021/es0351488

Kanaujiya, D. K., Paul, T., Sinharoy, A., & Pakshirajan, K. (2019). Biological Treatment Processes for the Removal of Organic Micropollutants from Wastewater: a Review. *Current Pollution Reports*, *5*(3), 112–128. doi: 10.1007/s40726-019-00110-x

Kanwal, T., Kawish, M., Maharjan, R., Ghaffar, I., Ali, H. S., Imran, M., Perveen, S., Saifullah, S., Simjee, S. U., & Shah, M. R. (2019). Design and development of permeation enhancer containing self-nanoemulsifying drug delivery system (SNEDDS) for ceftriaxone sodium improved oral pharmacokinetics. *Journal of Molecular Liquids*, *289*, article id-111098. doi: 10.1016/j.molliq.2019.111098

Karci, A., Arslan-Alaton, I., & Bekbolet, M. (2013). Oxidation of nonylphenol ethoxylates in aqueous solution by UV-C photolysis, H$_2$O$_2$/UV-C, Fenton and photo-Fenton processes: are these processes toxicologically safe? *Water Science and Technology*, *68*(8), 1801–1809. doi: 10.2166/wst.2013.422

Kasprzyk-Hordern, B., Dinsdale, R. M., & Guwy, A. J. (2008). Multiresidue methods for the analysis of pharmaceuticals, personal care products and illicit drugs in surface water and wastewater by solid-phase extraction and ultra performance liquid chromatography–electrospray tandem mass spectrometry. *Analytical and Bioanalytical Chemistry*, *391*(4), 1293–1308. doi: 10.1007/s00216-008-1854-x

Kent, J., & Tay, J. H. (2019). Treatment of 17α-ethinylestradiol, 4-nonylphenol, and carbamazepine in wastewater using an aerobic granular sludge sequencing batch reactor. *Science of The Total Environment*, *652*, 1270–1278. doi: 10.1016/j.scitotenv.2018.10.301

Kim, D., Kwak, J. Il, & An, Y.-J. (2019). Physiological response of crop plants to the endocrine-disrupting chemical nonylphenol in the soil environment. *Environmental Pollution*, *251*, 573–580. doi: 10.1016/j.envpol.2019.04.101

Kim, S., Eichhorn, P., Jensen, J. N., Weber, A. S., & Aga, D. S. (2005). Removal of Antibiotics in Wastewater: Effect of Hydraulic and Solid Retention Times on the Fate of Tetracycline in the Activated Sludge Process. *Environmental Science & Technology*, *39*(15), 5816–5823. doi: 10.1021/es050006u

Klečka, G. M., Naylor, C. G., Staples, C. A., & Losey, B. (2010). Occurrence of Nonylphenol Ethoxylates and Their Metabolites in Municipal Wastewater Treatment Plants and Receiving Waters. *Water Environment Research*, *82*(5), 447–454. doi: 10.2175/106143009X12529484815674

Kolthoff, I. M., & Miller, I. K. (1951). The Chemistry of Persulfate. I. The Kinetics and Mechanism of the Decomposition of the Persulfate Ion in Aqueous Medium 1. *Journal of the American Chemical Society*, *73*(7), 3055–3059. doi: 10.1021/ja01151a024

Křesinová, Z., Linhartová, L., Filipová, A., Ezechiáš, M., Mašín, P., & Cajthaml, T. (2018). Biodegradation of endocrine disruptors in urban wastewater using Pleurotus ostreatus bioreactor. *New Biotechnology*, *43*, 53–61. doi: 10.1016/j.nbt.2017.05.004

Kümmerer, K. (2001). Drugs in the environment: emission of drugs, diagnostic aids and disinfectants into wastewater by hospitals in relation to other sources – a review. *Chemosphere*, *45*(6–7), 957–969. doi: 10.1016/S0045-6535(01)00144-8

Kümmerer, K. (2009). The presence of pharmaceuticals in the environment due to human use – present knowledge and future challenges. *Journal of Environmental Management*, *90*(8), 2354–2366. doi: 10.1016/j.jenvman.2009.01.023

Li, J., Mailhot, G., Wu, F., & Deng, N. (2010). Photochemical efficiency of Fe(III)-EDDS complex: OH radical production and 17β-estradiol degradation. *Journal of Photochemistry and Photobiology A: Chemistry*, *212*(1), 1–7. doi: 10.1016/j.jphotochem.2010.03.001

Li, X., Ying, G.-G., Su, H.-C., Yang, X.-B., & Wang, L. (2010). Simultaneous determination and assessment of 4-nonylphenol, bisphenol A and triclosan in tap water, bottled water and baby bottles. *Environment International*, *36*(6), 557–562. doi: 10.1016/j.envint.2010.04.009

Liang, C., Huang, C.-F., Mohanty, N., & Kurakalva, R. M. (2008). A rapid spectrophotometric determination of persulfate anion in ISCO. *Chemosphere*, *73*(9), 1540–1543. doi: 10.1016/j.chemosphere.2008.08.043

Liang, C. J., Bruell, C. J., Marley, M. C., & Sperry, K. L. (2003). Thermally Activated Persulfate Oxidation of Trichloroethylene (TCE) and 1,1,1-Trichloroethane (TCA) in Aqueous Systems and Soil Slurries. *Soil and Sediment Contamination: An International Journal*, *12*(2), 207–228. doi: 10.1080/713610970

Loyo-Rosales, J. E., Rice, C. P., & Torrents, A. (2010). Fate and distribution of the octyl- and nonylphenol ethoxylates and some carboxylated transformation products in the Back River, Maryland. *J. Environ. Monit.*, *12*(3), 614–621. doi: 10.1039/B913229E

Lutze, H. V., Kerlin, N., & Schmidt, T. C. (2015). Sulfate radical-based water treatment in presence of chloride: Formation of chlorate, inter-conversion of sulfate radicals into hydroxyl radicals and influence of bicarbonate. *Water Research*, *72*, 349–360. doi: 10.1016/j.watres.2014.10.006

Martín-Pozo, L., de Alarcón-Gómez, B., Rodríguez-Gómez, R., García-Córcoles, M. T., Çipa, M., & Zafra-Gómez, A. (2019). Analytical methods for the determination of emerging contaminants in sewage sludge samples. A review. *Talanta*, *192*, 508–533. doi: 10.1016/j.talanta.2018.09.056

Matsuo, H., Sakamoto, H., Arizono, K., & Shinohara, R. (2011). Behavior of Pharmaceuticals in Waste Water Treatment Plant in Japan. *Bulletin of Environmental Contamination and Toxicology*, *87*(1), 31–35. doi: 10.1007/s00128-011-0299-7

Matzek, L. W., & Carter, K. E. (2016). Activated persulfate for organic chemical degradation: A review. *Chemosphere*, *151*, 178–188. doi: 10.1016/j.chemosphere.2016.02.055

Miklos, D. B., Remy, C., Jekel, M., Linden, K. G., Drewes, J. E., & Hübner, U. (2018). Evaluation of advanced oxidation processes for water and wastewater treatment – A critical review. *Water Research*, *139*, 118–131. doi: 10.1016/j.watres.2018.03.042

Moreira, F. C., Boaventura, R. A. R., Brillas, E., & Vilar, V. J. P. (2017). Electrochemical advanced oxidation processes: A review on their application to synthetic and real wastewaters. *Applied Catalysis B: Environmental*, *202*, 217–261. doi: 10.1016/j.apcatb.2016.08.037

Moreno-Andrés, J., Farinango, G., Romero-Martínez, L., Acevedo-Merino, A., & Nebot, E. (2019). Application of persulfate salts for enhancing UV disinfection in marine waters. *Water Research*, *163*, article id-114866. doi: 10.1016/j.watres.2019.114866

Niu, C.-G., Wang, Y., Zhang, X.-G., Zeng, G.-M., Huang, D.-W., Ruan, M., & Li, X.-W. (2012). Decolorization of an azo dye Orange G in microbial fuel cells using Fe(II)-EDTA catalyzed persulfate. *Bioresource Technology*, *126*, 101–106. doi: 10.1016/j.biortech.2012.09.001

Niu, Y., Zhang, J., Duan, H., Wu, Y., & Shao, B. (2015). Bisphenol A and nonylphenol in foodstuffs: Chinese dietary exposure from the 2007 total diet study and infant health risk from formulas. *Food Chemistry*, *167*, 320–325. doi: 10.1016/j.foodchem.2014.06.115

Opriş, O., Copaciu, F., Loredana Soran, M., Ristoiu, D., Niinemets, Ü., & Copolovici, L. (2013). Influence of nine antibiotics on key secondary metabolites and physiological characteristics in Triticum aestivum: Leaf volatiles as a promising new tool to assess toxicity. *Ecotoxicology and Environmental Safety*, *87*, 70–79. doi: 10.1016/j.ecoenv.2012.09.019

Pan, X., Deng, C., Zhang, D., Wang, J., Mu, G., & Chen, Y. (2008). Toxic effects of amoxicillin on the photosystem II of Synechocystis sp. characterized by a variety of in vivo chlorophyll fluorescence tests. *Aquatic Toxicology*, *89*(4), 207–213. doi: 10.1016/j.aquatox.2008.06.018

Pulicharla, R., Drouinaud, R., Brar, S. K., Drogui, P., Proulx, F., Verma, M., & Surampalli, R. Y. (2018). Activation of persulfate by homogeneous and heterogeneous iron catalyst to degrade chlortetracycline in aqueous solution. *Chemosphere*, *207*, 543–551. doi: 10.1016/j.chemosphere.2018.05.134

Qian, Y., Liu, X., Li, K., Gao, P., Chen, J., Liu, Z., Zhou, X., Zhang, Y., Chen, H., Li, X., & Xue, G. (2020). Enhanced degradation of cephalosporin antibiotics by matrix components during thermally activated persulfate oxidation process. *Chemical Engineering Journal*, *384*, artcile id-123332. doi: 10.1016/j.cej.2019.123332

Rahmati, M. B., Sabouri, S., & Sabouri, F. (2017). The efficacy of montelukast in adjunct with amoxicillin in treatment of Acute Otitis Media (AOM) in children. *International Journal of Pediatrics*, *5*(1), 4257–4262. doi: 10.22038/IJP.2016.7803

Rao, Y. F., Qu, L., Yang, H., & Chu, W. (2014). Degradation of carbamazepine by Fe(II)-activated persulfate process. *Journal of Hazardous Materials*, *268*, 23–32. doi: 10.1016/j.jhazmat.2014.01.010

Rastogi, A., Al-Abed, S. R., & Dionysiou, D. D. (2009). Sulfate radical-based ferrous–peroxymonosulfate oxidative system for PCBs degradation in aqueous and sediment systems. *Applied Catalysis B: Environmental*, *85*(3–4), 171–179. doi: 10.1016/j.apcatb.2008.07.010

Roberts, P., Roberts, J. P., & Jones, D. L. (2006). Behaviour of the endocrine disrupting chemical nonylphenol in soil: Assessing the risk associated with spreading contaminated waste to land. *Soil Biology and Biochemistry*, *38*(7), 1812–1822. doi: 10.1016/j.soilbio.2005.12.006

Rodriguez, S., Santos, A., & Romero, A. (2017). Oxidation of priority and emerging pollutants with persulfate activated by iron: Effect of iron valence and particle size. *Chemical Engineering Journal*, *318*, 197–205. doi: 10.1016/j.cej.2016.06.057

Romero, A., Santos, A., Vicente, F., & González, C. (2010). Diuron abatement using activated persulphate: Effect of pH, Fe(II) and oxidant dosage. *Chemical Engineering Journal*, *162*(1), 257–265. doi: 10.1016/j.cej.2010.05.044

Ruzza, P., Vitale, R. M., Hussain, R., Montini, A., Honisch, C., Pozzebon, A., Hughes, C. S., Biondi, B., Amodeo, P., Sechi, G., & Siligardi, G. (2018). Chaperone-like effect of ceftriaxone on HEWL aggregation: A spectroscopic and computational study. *Biochimica et Biophysica Acta (BBA) - General Subjects*, *1862*(6), 1317–1326. doi: 10.1016/j.bbagen.2018.02.014

Salazar, C., Contreras, N., Mansilla, H. D., Yáñez, J., & Salazar, R. (2016). Electrochemical degradation of the antihypertensive losartan in aqueous medium by electro-oxidation with boron-doped diamond electrode. *Journal of Hazardous Materials*, *319*, 84–92. doi: 10.1016/j.jhazmat.2016.04.009

Serna-Galvis, E. A., Botero-Coy, A. M., Martínez-Pachón, D., Moncayo-Lasso, A., Ibáñez, M., Hernández, F., & Torres-Palma, R. A. (2019). Degradation of seventeen contaminants of emerging concern in municipal wastewater effluents by sonochemical advanced oxidation processes. *Water Research*, *154*, 349–360. doi: 10.1016/j.watres.2019.01.045

Shao, B., Hu, J., Yang, M., An, W., & Tao, S. (2005). Nonylphenol and Nonylphenol Ethoxylates in River Water, Drinking Water,and Fish Tissues in the Area of Chongqing, China. *Archives of Environmental Contamination and Toxicology*, *48*(4), 467–473. doi: 10.1007/s00244-003-0266-3

Shi, H., Ni, J., Zheng, T., Wang, X., Wu, C., & Wang, Q. (2020). Remediation of wastewater contaminated by antibiotics. A review. *Environmental Chemistry Letters*, *18*(2), 345–360. doi: 10.1007/s10311-019-00945-2

Silva-Oliveira, R. G., Orsolin, P. C., & Nepomuceno, J. C. (2016). Modulating effect of losartan potassium on the mutagenicity and recombinogenicity of doxorubicin in somatic cells of Drosophila melanogaster. *Food and Chemical Toxicology*, *95*, 211–218. doi: 10.1016/j.fct.2016.07.003

Singh, V., Pandey, B., & Suthar, S. (2018). Phytotoxicity of amoxicillin to the duckweed Spirodela polyrhiza: Growth, oxidative stress, biochemical traits and antibiotic degradation. *Chemosphere*, *201*, 492–502. doi: 10.1016/j.chemosphere.2018.03.010

Snyder, S. A., Adham, S., Redding, A. M., Cannon, F. S., DeCarolis, J., Oppenheimer, J., Wert, E. C., & Yoon, Y. (2007). Role of membranes and activated carbon in the removal of endocrine disruptors and pharmaceuticals. *Desalination*, *202*(1–3), 156–181. doi: 10.1016/j.desal.2005.12.052

Song, X., Liu, R., Chen, L., & Kawagishi, T. (2017). Comparative experiment on treating digested piggery wastewater with a biofilm MBR and conventional MBR: simultaneous removal of nitrogen and antibiotics. *Frontiers of Environmental Science & Engineering*, *11*(2), 11. doi: 10.1007/s11783-017-0919-5

Stackelberg, P. E., Gibs, J., Furlong, E. T., Meyer, M. T., Zaugg, S. D., & Lippincott, R. L. (2007). Efficiency of conventional drinking-water-treatment processes in removal of pharmaceuticals and other organic compounds. *Science of The Total Environment*, *377*(2–3), 255–272. doi: 10.1016/j.scitotenv.2007.01.095

Stefaniuk, M., Oleszczuk, P., & Ok, Y. S. (2016). Review on nano zerovalent iron (nZVI): From synthesis to environmental applications. *Chemical Engineering Journal*, *287*, 618–632. doi: 10.1016/j.cej.2015.11.046

Vazouras, K., Velali, K., Tassiou, I., Anastasiou-Katsiardani, A., Athanasopoulou, K., Barbouni, A., Jackson, C., Folgori, L., Zaoutis, T., Basmaci, R., & Hsia, Y. (2020). Antibiotic treatment and antimicrobial resistance in children with urinary tract infections. *Journal of Global Antimicrobial Resistance*, *20*, 4–10. doi: 10.1016/j.jgar.2019.06.016

Vicente, F., Santos, A., Romero, A., & Rodriguez, S. (2011). Kinetic study of diuron oxidation and mineralization by persulphate: Effects of temperature, oxidant concentration and iron dosage method. *Chemical Engineering Journal*, *170*(1), 127–135. doi: 10.1016/j.cej.2011.03.042

Vieno, N. M., Härkki, H., Tuhkanen, T., & Kronberg, L. (2007). Occurrence of Pharmaceuticals in River Water and Their Elimination in a Pilot-Scale Drinking Water Treatment Plant. *Environmental Science & Technology*, *41*(14), 5077–5084. doi: 10.1021/es062720x

Wang, J., & Wang, S. (2018). Activation of persulfate (PS) and peroxymonosulfate (PMS) and application for the degradation of emerging contaminants. *Chemical Engineering Journal*, *334*, 1502–1517. doi: 10.1016/j.cej.2017.11.059

Wang, Shizong, & Wang, J. (2017). Comparative study on sulfamethoxazole degradation by Fenton and Fe(II)-activated persulfate process. *RSC Adv.*, *7*(77), 48670–48677. doi: 10.1039/C7RA09325J

Wang, Shizong, & Wang, J. (2018). Trimethoprim degradation by Fenton and Fe(II)-activated persulfate processes. *Chemosphere*, *191*, 97–105. doi: 10.1016/j.chemosphere.2017.10.040

Wang, Shizong, Wang, J., & Sun, Y. (2017). Degradation of chlorinated paraben by integrated irradiation and biological treatment process. *Journal of Environmental Management*, *189*, 29–35. doi: 10.1016/j.jenvman.2016.11.067

Wang, Songlin, Wu, J., Lu, X., Xu, W., Gong, Q., Ding, J., Dan, B., & Xie, P. (2019). Removal of acetaminophen in the Fe^{2+}/persulfate system: Kinetic model and degradation pathways. *Chemical Engineering Journal*, *358*, 1091–1100. doi: 10.1016/j.cej.2018.09.145

Wang, Yan, Zhang, H., & Chen, L. (2011). Ultrasound enhanced catalytic ozonation of tetracycline in a rectangular air-lift reactor. *Catalysis Today*, *175*(1), 283–292. doi: 10.1016/j.cattod.2011.06.001

Wang, Yuwen, Li, Y., Hu, A., Rashid, A., Ashfaq, M., Wang, Y., Wang, H., Luo, H., Yu, C.-P., & Sun, Q. (2018). Monitoring, mass balance and fate of pharmaceuticals and personal care products in seven wastewater treatment plants in Xiamen City, China. *Journal of Hazardous Materials*, *354*, 81–90. doi: 10.1016/j.jhazmat.2018.04.064

Wen, Q., Kong, F., Zheng, H., Yin, J., Cao, D., Ren, Y., & Wang, G. (2011). Simultaneous processes of electricity generation and ceftriaxone sodium degradation in an air-cathode single chamber microbial fuel cell. *Journal of Power Sources*, *196*(5), 2567–2572. doi: 10.1016/j.jpowsour.2010.10.085

Westerhoff, P., Yoon, Y., Snyder, S., & Wert, E. (2005). Fate of Endocrine-Disruptor, Pharmaceutical, and Personal Care Product Chemicals during Simulated Drinking Water Treatment Processes. *Environmental Science & Technology*, *39*(17), 6649–6663. doi: 10.1021/es0484799

Wu, X., Gu, X., Lu, S., Xu, M., Zang, X., Miao, Z., Qiu, Z., & Sui, Q. (2014). Degradation of trichloroethylene in aqueous solution by persulfate activated with citric acid chelated ferrous ion. *Chemical Engineering Journal*, *255*, 585–592. doi: 10.1016/j.cej.2014.06.085

Xiao, S., Cheng, M., Zhong, H., Liu, Z., Liu, Y., Yang, X., & Liang, Q. (2020). Iron-mediated activation of persulfate and peroxymonosulfate in both homogeneous and heterogeneous ways: A review. *Chemical Engineering Journal*, *384*, article id-123265. doi: 10.1016/j.cej.2019.123265

Yang, H., Zhuang, S., Hu, Q., Hu, L., Yang, L., Au, C., & Yi, B. (2018). Competitive reactions of hydroxyl and sulfate radicals with sulfonamides in $Fe^{2+}/S_2O_8^{2-}$ system: Reaction kinetics, degradation mechanism and acute toxicity. *Chemical Engineering Journal*, *339*, 32–41. doi: 10.1016/j.cej.2018.01.106

Yang, L., Xue, J., He, L., Wu, L., Ma, Y., Chen, H., Li, H., Peng, P., & Zhang, Z. (2019). Review on ultrasound assisted persulfate degradation of organic contaminants in wastewater: Influences, mechanisms and prospective. *Chemical Engineering Journal*, *378*, article id-122146. doi: 10.1016/j.cej.2019.122146

Yang, Q., Ma, Y., Chen, F., Yao, F., Sun, J., Wang, S., Yi, K., Hou, L., Li, X., & Wang, D. (2019). Recent advances in photo-activated sulfate radical-advanced oxidation process (SR-AOP) for refractory organic pollutants removal in water. *Chemical Engineering Journal*, *378*, article id-122149. doi: 10.1016/j.cej.2019.122149

Yang, S.-F., Lin, C.-F., Wu, C.-J., Ng, K.-K., Yu-Chen Lin, A., & Andy Hong, P.-K. (2012). Fate of sulfonamide antibiotics in contact with activated sludge – Sorption and biodegradation. *Water Research*, *46*(4), 1301–1308. doi: 10.1016/j.watres.2011.12.035

Yasser, E.-N., & El-Dahdouh, N. (2015). Toxicity of Amoxicillin and Erythromycin to Fish and Mosquitoes. *Ecotoxicology and Environmental Contamination*, *10*(1), 13–21. doi: 10.5132/eec.2015.01.03

Yirsaw, B. D., Megharaj, M., Chen, Z., & Naidu, R. (2016). Environmental application and ecological significance of nano-zero valent iron. *Journal of Environmental Sciences*, *44*, 88–98. doi: 10.1016/j.jes.2015.07.016

Yu, X., Tang, X., Zuo, J., Zhang, M., Chen, L., & Li, Z. (2016). Distribution and persistence of cephalosporins in cephalosporin producing wastewater using SPE and UPLC–MS/MS method. *Science of The Total Environment*, *569–570*, 23–30. doi: 10.1016/j.scitotenv.2016.06.113

Yu, Z., Wang, Y., Chen, Y., Huang, M., Wang, Y., Shen, Z., Xia, Z., & Li, G. (2020). Antimicrobial resistance of bacterial pathogens isolated from canine urinary tract infections. *Veterinary Microbiology*, *241*, article id-108540. doi: 10.1016/j.vetmic.2019.108540

Zhang, Y., Xu, X., Pan, Y., Xu, L., & Zhou, M. (2019). Pre-magnetized Fe^0 activated persulphate for the degradation of nitrobenzene in groundwater. *Separation and Purification Technology*, *212*, 555–562. doi: 10.1016/j.seppur.2018.11.074

Zhen, G., Lu, X., Su, L., Kobayashi, T., Kumar, G., Zhou, T., Xu, K., Li, Y.-Y., Zhu, X., & Zhao, Y. (2018). Unraveling the catalyzing behaviors of different iron species (Fe^{2+} vs. Fe^0) in activating persulfate-based oxidation process with implications to waste activated sludge dewaterability. *Water Research*, *134*, 101–114. doi: 10.1016/j.watres.2018.01.072

Zhong, H., Brusseau, M. L., Wang, Y., Yan, N., Quig, L., & Johnson, G. R. (2015). In-situ activation of persulfate by iron filings and degradation of 1,4-dioxane. *Water Research*, *83*, 104–111. doi: 10.1016/j.watres.2015.06.025

Zhou, P., Su, C., Li, B., & Qian, Y. (2006). Treatment of High-Strength Pharmaceutical Wastewater and Removal of Antibiotics in Anaerobic and Aerobic Biological Treatment Processes. *Journal of Environmental Engineering*, *132*(1), 129–136. doi: 10.1061/(ASCE)0733-9372(2006)132:1(129)

Acknowledgements

It fills my heart with unspeakable joy to convey my gratitude to all colleagues at the Department of Materials and Environmental Technology for their support to make this work possible. ASTRA "TUT Institutional Development Programme for 2016-2022" Graduate School of Functional Materials and Technologies (2014-2020.4.01.16-0032), from EU Regional Development Fund, and the Estonian Research Council (PRG776), Estonian Ministry of Education and Research (IUT1-7), EU Regional Development Fund (Dora Plus Programme), European PhD School on Advanced Oxidation Processes (AOPs PhD school), Association for Chemistry and the Environment (ACE) are truly appreciated for their support and funding that helped this work reach the goal.

I express the deepest appreciation to Dr. Niina Dulova and Prof. Marina Trapido for continuous support and guidance. Profound gratitude is extended towards my teacher, patient supervisor, mentor, and guide of 5 years, Dr. Dulova for welcoming me to the group and her immense knowledge. Apart from being a rare blend of scientific caliber, Dr. Dulova is an extraordinary human being who continuously motivated and provided constructive criticism that helped my personal and professional growth. I am grateful to former research advisor Dr. Eneliis Kattel for her efforts in building the foundation of research and assistance in the laboratory work.

For all these years, the support of PhD students Liina Onga, Maarja Kask, and Priit Tikker is truly acknowledged. I appreciate Maarja Kask for her gratefulness and support. The wonderful and generous friend Liina Onga is deeply cherished for her encouragement and positive outlook. Everyone who contributed to the successful accomplishment of this PhD work is appreciated.

The cordial gratitude belongs to my parents and extended family for their patience and understanding. Loving sisters (Dr. Divya, Harsimran, Mohanpreet, Monica, Susmita, and Kiran), as well as brothers (Manoj, Mohandeep, Dr. Mukesh, and Rahul), are appreciated for providing unconditional love and I could always count on them when the times were rough. I consider myself the luckiest in the world to have such a lovely and caring family, standing beside me with their affection and support.

This thesis is dedicated to the utmost affectionate, endlessly supportive friend and husband Nikhil, who saw the best as well as worst of me during all these years. You have been my supporting pillar and I am truly obliged for your practical and emotional support.

I shall remain forever indebted for the support, guidance, and efforts of my colleagues at Tallinn University of Technology.

ABSTRACT

Development of photo-induced persulfate-based processes for efficient application in water treatment

The industrialization and urbanization result in release of a considerable amount of highly toxic contaminants into the ecosystem. This unregulated discharge of emerging contaminants (ECs) such as pharmaceuticals and personal care products, endocrine-disrupting chemicals, and other recalcitrant organic compounds, into the environment via municipal and industrial wastewater as well as runoffs from agricultural sites have a negative impact on the human health and the aquatic faunas. The traditional wastewater treatment facilities are facing complications such as a high organic load (g L^{-1}) or a low detection level of organic micropollutants (ng L^{-1}-µg L^{-1}) in the influent.

The removal of ECs from water and wastewater is of significant importance. Physical, biological, and chemical techniques can be practicable application to eliminate the organic contaminants in water. However, the application of physical methods, which are mainly separation techniques, generates smaller, but more concentrated waste streams that require further processing. Biological treatment, in turn, is a time-consuming process requiring sophisticated equipment. Moreover, biological processes are frequently not able to effectively eliminate persistent and toxic contaminants from wastewater. Finally, chemical oxidation technologies have demonstrated to be effective in removing noxious and non-biodegradable organic pollutants from various water matrices.

These methods, namely advanced oxidation technologies (AOTs), are highly effective for the decomposition of micropollutants, with the formation of more polar and less toxic products, or, if necessary, for the complete mineralization of ECs to CO_2 and H_2O. The effectiveness of AOTs in the decomposition of various organic micropollutants is based on the generation of highly reactive free radicals such as hydroxyl and sulfate radicals. Lately, sulfate radicals-based technology has received increasing attention. Owing to the high oxidation potential and performance of sulfate radicals at a wide pH range, the application of sulfate radicals-based AOTs is a promising solution for the removal of ECs in various aqueous matrices.

This thesis aimed at studying the applicability of UV-induced persulfate (PS) based systems for the treatment of water contaminated by widely consumed β-lactam antibiotics, amoxicillin (AMX) and ceftriaxone (CTA), which belongs to the World Health Organization's list of essential medicines, endocrine disruptor nonylphenol (NP) and angiotensin receptor blocker losartan (LOR). Accordingly, the degradation and mineralization of AMX and LOR by UVC- and UVC/Fe^{2+}-activated PS systems was studied. In the case of CTA oxidation, the efficacy of UVA- and UVC-induced persulfate systems in combination with heterogeneous activators, α-FeO(OH) and Fe_3O_4, was assessed and compared. Finally, the efficiency of UVC-activated PS and dual oxidant (PS/H_2O_2) system along with the optimized application of an iron activator was evaluated for the degradation of NP.

The effects of operating parameters including pH value, reaction time, and concentration of oxidant and activator on the efficacy of the studied systems were evaluated. The optimized results of the studied systems obtained in ultrapure water were subsequently used in real water samples, mainly in groundwater, but also in drinking water and secondary treated wastewater, to assess the efficacy of target compounds decomposition in a more complex natural or processed water matrix.

The application of the UV/PS system improved the degradation efficiency of all the studied ECs compared with direct UV photolysis and non-activated persulfate oxidation. Accordingly, the UVC-assisted PS oxidation resulted in >90% of the target compounds decomposition in UW. The addition of Fe^{2+} or α-FeO(OH) into the UV/PS system demonstrated a further increase in the efficiency of the studied ECs decomposition using an optimized amount of activator and oxidant. Regardless of the applied studied system, the mineralization of the target compound was lower than its degradation. The composition of the real aqueous matrix markedly inhibited the degradation rate of the target compounds in all UV-activated PS-based systems. Based on the results of radicals scavenging studies, the assessment of mineralization, the identification of transformation products, and the measurement of ecotoxicity for the selected target compounds, possible transformation pathways and oxidation mechanisms for the studied ECs were proposed.

The findings of this study enlarge the existing knowledge on the effectiveness of UV-induced PS-based systems and, thus, increase the potential for practical application of these methods for the advanced purification of contaminated water.

LÜHIKOKKUVÕTE

Foto-indutseeritud persulfaadi-põhiste protsesside väljatöötamine efektiivseks rakendamiseks vee puhastamisel

Tööstuse kasvu ning linnastumise tulemusel eraldub ökosüsteemi märkimisväärne kogus väga toksilisi saasteaineid. Esilekerkivate saasteainete nagu ravimid, hügieenitooted, endokriinseid häireid põhjustavad kemikaalid ning teised püsivad orgaanilised ühendid, reguleerimata väljavool keskkonda nii olme- ning tööstusreovee kui ka põllumajandusest tuleneva äravooluga, mõjutab negatiivselt inimese tervist ning veefaunat. Traditsioonilised veepuhastusjaamad seisavad silmitsi probleemidega nagu kõrge orgaaniliste ainete koormus (g L^{-1}) ning orgaaniliste mikrosaasteainete madal avastamispiir (ng L^{-1}-µg L^{-1}) sissevoolus.

Raskesti lagundatavate ainete eemaldamine veest ning reoveest on märkimisväärse tähtsusega. Orgaaniliste saasteainete eemaldamiseks veest saab rakendada füüsikalisi, bioloogilisi ning keemilisi meetodeid. Samas põhinevad füüsikalised meetodid peamiselt eraldamisel, mille tulemusel tekib väiksem, kuid palju kontsentreeritum jäätmevoog, mis vajab edasist puhastamist. Bioloogiline töötlus on aga aeganõudev protsess ning nõuab keerulisi seadmeid. Lisaks ei suuda bioloogilised protsessid tihtipeale efektiivselt eraldada reoveest püsivaid ning toksilisi saasteaineid. Keemilised oksüdeerimismeetodid on näidanud võimet efektiivselt eemaldada kahjulikke ning bioloogiliselt mitte lagunevaid orgaanilisi saasteaineid erinevate saastusastmetega vetest.

Antud meetodid, täpsemalt süvaoksüdatsioonitehnoloogiad, on mikrosaasteainete lagundamisel väga efektiivsed, moodustades polaarsemaid ning vähem toksilisi produkte või vajadusel mineraliseerides raskesti lagundatavaid aineid täielikult süsihappegaasiks ja veeks. Süvaoksüdatsioonitehnoloogiate efektiivsus erinevate orgaaniliste mikrosaasteainete lagundamisel põhineb reaktiivsete vabade radikaalide, nagu hüdroksüül- ning sulfaatradikaalide, tekkel. Viimasel ajal on hakatud rohkem tähelepanu pöörama sulfaatradikaalidel põhinevatele tehnoloogiatele. Tänu kõrgele oksüdatsioonipotentsiaalile ning sulfaatradikaalide võimele töötada laias pH vahemikus, on sulfaatradikaalidel põhinevate süvaoksüdatsioonitehnoloogiate rakendamine paljulubav lahendus mitmesuguste püsivate saasteainete eemaldamiseks erinevatest vesikeskkondadest.

Käesoleva doktoritöö eesmärk oli uurida UV-indutseeritud persulfaadil (PS) põhinevate süsteemide rakendatavust veele, mis sisaldab laialt kasutatavaid β-laktaamseid antibiootikume nagu amoksitsilliin (AMX) ja tseftriaksoon (CTA), mis kuuluvad Maailma Terviseorganisatsiooni (WHO) hädavajalike ravimite nimekirja, endokriinsüsteemi kahjustajat nonüülfenooli (NP) ning angiotensiini retseptorite blokaatorit losartaani (LOR). Sellest lähtudes uuriti AMX ning LOR lagunemist ning mineraliseerumist UVC- ja UVC/Fe^{2+}-aktiveeritud PS süsteemides. CTA puhul uuriti ja võrreldi UVA- ning UVC-indutseeritud PS süsteemide tõhusust, kombineerides neid heterogeensete aktivaatoritega α-FeO(OH) ja Fe₃O₄. NP lagundamise näitel uuriti optimeeritud raud-aktivaatori koguse kasutamist UVC-aktiveeritud PS ning kahe oksüdeerijaga (PS/H$_2$O$_2$) süsteemides.

Hinnati pH väärtuse, reaktsiooniaja, oksüdeerija ning aktivaatori kontsentratsioonide mõju uuritavatele süsteemidele. Optimeeritud parameetrid rakendati hiljem reaalsetele veeproovidele, peamiselt põhjaveele, kuid ka joogiveele ning sekundaarselt puhastatud

reoveele, et hinnata sihtühendite lagundamise efektiivsust keerulisemates või töödeldud vesikeskkondades.

UV/PS süsteemi rakendamine tõstis võrreldes UV fotolüüsi ning aktiveerimata PS-põhise oksüdatsiooniga lagundamise efektiivsust kõigi uuritud ainete puhul. UVC-aktiveeritud PS-põhine oksüdatsioon ülipuhtas vees andis kõigi sihtühendite puhul >90% lagunemise. Lisaks näitas optimeeritud koguses oksüdeerija ja aktivaatori, Fe^{2+} või α-FeO(OH), kasutamine UV/PS süsteemis edasist efektiivsuse suurenemist uuritud ainete lagundamisel. Sõltumata rakendatud süsteemist, oli mineraliseerumise määr madalam kui saasteaine lagunemine. Reaalse veeproovi koostis inhibeeris sihtaine lagunemise kiirust märkimisväärselt kõigis UV-aktiveeritud PS põhinevates süsteemides. Radikaalide püüdjate lisamisel uuritavatesse süsteemidesse hinnati valitud sihtainete mineraliseerumist, identifitseeriti nende laguprodukte ja määrati toksilisust ning pakuti saadud andmete põhjal välja sihtainete võimalikud lagunemise mehhanismid.

Antud töö tulemused laiendavad olemasolevaid teadmisi UV-indutseeritud persulfaadil põhinevate süsteemide efektiivsuse kohta ning seega tõstavad oluliselt nende meetodite praktilise rakendamise võimalikkust saastunud vee täiustatud puhastamiseks.

Appendix

Taylor & Francis
Taylor & Francis Group

Check for updates

Persulfate-based photodegradation of a beta-lactam antibiotic amoxicillin in various water matrices

Eneliis Kattel [ID], Balpreet Kaur, Marina Trapido [ID] and Niina Dulova [ID]

Department of Materials and Environmental Technology, Tallinn University of Technology, Tallinn, Estonia

ABSTRACT

Amoxicillin (AMX), a widely used beta-lactam antibiotic, belongs to the World Health Organization's list of essential medicines. This subsequently causes its long-term presence in the environment and therefore, affects different environmental compartments. In this research, the degradation and mineralisation of AMX by UVC-activated persulfate-based treatment in various aqueous media was assessed. The degradation of the target compound was in accordance with the pseudo-first-order reaction kinetics in all the UVC-induced systems. The results indicated that AMX degradation in any real water matrices is notably inhibited by the matrix properties. The trials with radical scavengers in ultrapure water proved the existence of SO_4^- and $HO^·$, but mainly SO_4^- contributed to the degradation of AMX in the $UVC/S_2O_8^{2-}$ and $UVC/S_2O_8^{2-}/Fe^{2+}$ systems. It was shown that the parent compound disappeared during the treatment, but the mineralisation extent referred to the formation of transformation products the main of which were identified. The findings of this study could provide valuable information about the elimination of beta-lactam antibiotics from various environmental and processed waters.
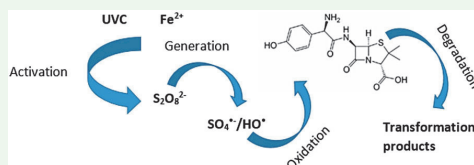
1. Introduction

Antibiotics are a large group of human and veterinary medicinal substances that in recent decades have been more extensively detected in different environmental compartments. The parent compounds and transformation products of antibiotics enter to the aqueous environment continuously through manufacturing, consumption and disposal [1]. This may pose an ecotoxic effect to aquatic and terrestrial organisms; the bacterial population may be disturbed and resistance against some antibiotics may be formed in pathogenic bacteria [2]. Conventional wastewater treatment processes only partially remove these substances and they generally occur in trace concentrations (ng L^{-1}) in treated effluent [1]. One of the most prescribed groups of antibiotics is beta-lactams that have a broad spectrum against infections caused by Gram-positive and Gram-negative bacteria [3]. A beta-lactam antibiotic amoxicillin

(AMX) is prevalently used to treat or prevent respiratory, gastrointestinal, urinary and skin bacterial infections regarding its pharmacological and pharmacokinetic properties [3]. Moreover, World Health Organization lists it as an essential medicine [4] that induces AMX lasting exposure to the environment, including aquatic systems.

Several researchers have reported promising treatment processes to degrade AMX in water. Accordingly, Andreozzi et al. [5] applied ozone for the degradation of 0.5 mM AMX in aqueous solution at pH 5.5; the results indicated more than 90% conversion of the target compound after 4 min, but moderate mineralisation (18%) after 20 min treatment. Elmolla and Chaudhuri [6] achieved the complete removal of 0.28 mM AMX in 2 min by the photo-Fenton process (H_2O_2/COD molar ratio of 1.5 and H_2O_2/Fe^{2+} molar ratio of 20) at pH 3.0. Klauson et al. [7] found that more than 80% of

🔗 Supplemental data for this article can be accessed at https://doi.org/10.1080/09593330.2018.1493149

AMX (initial concentration 68.4 μM) under solar radiation with iron-doped catalysts could be degraded with a 2-h treatment at pH 6.0. Su et al. [8] used ultrasound and cobalt activated oxone to eliminate 95 μM of AMX; the promising results were gained by the presence of highly active species – sulphate radicals ($SO_4^{\cdot-}$).

$SO_4^{\cdot-}$ are powerful oxidising agents usually derived from the activation of stable oxidant persulfate ($S_2O_8^{2-}$). Common activation methods are chemical [9], thermal [9,10] and UV-based [9,11]. Among these activator types, metal iron (Fe^{2+} or Fe^{3+}) is the most extensively used due to its non-toxic nature and relative abundance. Iron-activated $S_2O_8^{2-}$ application for *in situ* chemical oxidation (ISCO) of contaminated soil and groundwater (GW) has been successfully studied in several papers [12–14]. $S_2O_8^{2-}$ activation by UV light generates a pair of $SO_4^{\cdot-}$; such systems have indicated great potential in eliminating different organic contaminants from water [9,15]. Moreover, $S_2O_8^{2-}$ activation by pairing Fe^{2+} and UV light has shown enhanced degradation rate of several recalcitrant micropollutants in water [9,16,17].

The main advantages of using $SO_4^{\cdot-}$ to degrade organics are selectivity towards substances and scarce scavenging effect by dissolved organic matter in environmental waters [9,18]. Therefore, the present research focused on the degradation of a beta-lactam antibiotic AMX in environmental or processed aqueous matrices by UVC- and Fe^{2+}-activated $S_2O_8^{2-}$. The study includes the influence of $S_2O_8^{2-}$ and Fe^{2+} concentrations, pH value and water matrices (ultrapure water (UW), GW, drinking water (DW), secondary treated wastewater (STWW)). The efficacies of the treatment were evaluated and compared by the decrease in AMX concentration and total organic carbon (TOC) content. In addition, the radical species responsible for the degradation of AMX in the $UVC/S_2O_8^{2-}$ and $UVC/S_2O_8^{2-}/Fe^{2+}$ systems were identified. Based on the available literature, the degradation of AMX in various aqueous matrices is studied for the first time. The outcome of this paper could contribute to the knowledge of removing beta-lactam antibiotics under the natural conditions of aqueous matrices.

2. Experimental

2.1. Chemicals and materials

Amoxicillin trihydrate ($C_{16}H_{19}N_3O_5S \cdot 3H_2O$, ≥99%, molecular weight 419.4 g mol^{-1}) (Table 1), sodium persulfate ($Na_2S_2O_8$, ≥99%), ferrous sulphate heptahydrate ($FeSO_4 \cdot 7H_2O$, ≥99%), sulphuric acid (H_2SO_4, 95–98%) and sodium sulphite (Na_2SO_3, ≥98%) were purchased from Sigma-Aldrich. Acetonitrile (CH_3CN, LiChrosolv®), ethanol (C_2H_6O, EtOH, 99%), acetic acid (glacial) (CH_3CO_2H, 100%) and tertiary butanol (($CH_3)_3COH$, t-BuOH, ≥99%) were supplied from Merck KG. Stock solutions were prepared in UW (Millipore Simplicity® UV System, Merck, Germany).

DW from a local DW treatment plant (Tallinn, Estonia), GW without preceding purification (borehole depth 19 m, Harjumaa, Estonia) and STWW collected from the outlet of the secondary treatment of a local municipal wastewater treatment plant (Tallinn, Estonia) were used as natural and processed aqueous matrices for AMX degradation. The samples were collected in November 2016 and the main parameters are given in Table 2.
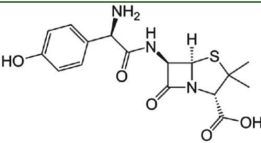
2.2. Experimental procedure

The experiments were conducted in a batch mode at ambient room temperature (22 ± 1 °C) with AMX initial concentration of 40 μM. UVC, $UVC/S_2O_8^{2-}$ and

Table 2. Chemical composition and main parameters of water samples.

Parameter	Unit	GW	DW	STWW
pH		8.10	7.40	7.40
Alkalinity	mgCaCO$_3$ L^{-1}	308	130	186
Conductivity	μS cm^{-1}	730	390	1275
TOC	mg L^{-1}	0.15	6.40	7.85
Fe^{2+}	mg L^{-1}	0.06	0.03	0.25
Total Fe	mg L^{-1}	0.17	0.05	0.57
F$^-$	mg L^{-1}	–[a]	3.5	2.4
Cl$^-$	mg L^{-1}	90.4	102.1	794.1
NO$_3^-$	mg L^{-1}	–	–	38.7
PO$_4^{3-}$	mg L^{-1}	–	–	–
SO$_4^{2-}$	mg L^{-1}	42.1	15.7	68.2

[a]Below detection limit.

Table 1. Physical properties of AMX [22].

Chemical formula	Chemical structure	Molecular weight, g mol^{-1}	Water solubility, mg L^{-1}	Density, g cm^{-3} (25 °C)	Melting point, °C	Log K_{OW}	pKa
C$_{16}$H$_{19}$N$_3$O$_5$S		365.4	3430	320	194	0.87	2.68 7.49 9.63

UVC/$S_2O_8^{2-}$/Fe^{2+} processes were carried out in a 1.0-L cylindrical glass reactor with a permanent agitation speed (300 rpm) for 2 h. The pH of the sample was not adjusted, if not stated otherwise. The Fe^{2+} source ($FeSO_4·7H_2O$) was added and after its complete dissolution, the reaction was initiated by adding $Na_2S_2O_8$ and simultaneous exposure to the UVC lamp that was turned on at least 5 min before the trial to provide a constant output. Mercury germicidal lamp (Philips TUV PL-S, 11 W) located in a quartz tube inside the reactor was used as a UVC source. UVC photolysis and UVC/$S_2O_8^{2-}$ processes were carried out according to a similar procedure. The average irradiance entering the solution in the reactor measured by a spectrometer (Ocean Optics USB2000+, USA) equipped with SpectraSuite software was 7.1 mW cm^{-2}. A water cooling jacket was used to keep the constant temperature in the reactor. Sample aliquots were taken at pre-determined time intervals from 0 to 120 min. The oxidation quenching was done by the addition of EtOH (sample/EtOH volume ratio of 10/1) or Na_2SO_3 at a [oxidant]$_0$/SO_3^{2-} molar ratio of 1/10 for HPLC-PDA-MS or TOC analysis, respectively. All experiments were duplicated; the final data show the results of at least three parallel replicates with an error less than 5% and are presented as mean.

2.3. Analytical methods

AMX concentration was quantified using high performance liquid chromatography combined with diode array detector and mass spectrometer (HPLC-PDA-MS, LC-MS 2020, Shimadzu, Japan) equipped with a Phenomenex Gemini (150 × 2.0 mm, 1.7 mm) NX-C18 (110 Å, 5 lm) column. The analysis was performed using an isocratic method with a mobile phase mixture of 10% acetonitrile (with 0.3% formic acid) and 90% formic acid (0.3%) aqueous solution. Samples (40 μL) were analysed at the flow rate of 200 μL min^{-1}. Mass spectrometry was applied in full-scan and in positive ionisation mode. Samples were scanned at 50–600 m/z. The concentration of AMX was determined by using the standard multipoint calibration.

TOC was measured by a TOC analyser multi N/C® 3100 (Analytik Jena, Germany) in 20 mL of samples with an injection volume of 500 μL for each replicate. The ion chromatography with chemical suppression of the eluent conductivity was used to measure the concentrations of anions in real water matrices (Table 2) (761 Compact IC, Metrohm Ltd., Switzerland). The pH was measured using a digital pH/ion meter (Mettler Toledo S220, Switzerland) and the electrical conductivity was measured using a digital EC meter (HQ 430d flexi, HACH Company, USA). The quantification of residual $S_2O_8^{2-}$ in the treated samples was done spectrophotometrically (Genesys 10S, Thermo Scientific, USA) at $\lambda = 352$ nm by an excess KI reaction with $S_2O_8^{2-}$ towards the formation of I_2 [19]. The alkalinity of GW and secondary effluent was measured by titration with hydrochloric acid (0.1 M) in the presence of methyl orange [20]. The final data shows the results of at least three parallel replicates with an error less than 5% and are presented as mean.

2.4. Identification of the main radical species

Radical scavengers were used to identify the radicals formed in the UVC/$S_2O_8^{2-}$ and UVC/$S_2O_8^{2-}$/Fe^{2+} processes. Radical probes, EtOH and t-BuOH, were employed to differentiate the role of $SO_4^{·-}$ and HO$^·$ in AMX oxidation by the studied systems. An excessive amount of scavenger was spiked into the reaction solutions before the Fe^{2+} and $S_2O_8^{2-}$ addition at an AMX/[scavenger]$_0$ molar ratio of 1/500 ([scavenger]$_0$ = 20 mM).

3. Results and discussion

3.1. Photolysis of AMX

Amoxicillin solution proved to absorb light mainly in the range of 190–290 nm with a maximum absorbance at 230 nm; therefore, the application of short-wave UVC radiation with the emittance maximum at 254 nm was predicted to undergo the photolysis of AMX.

AMX degradation under current experimental conditions followed a pseudo-first-order reaction kinetics ($r^2 \geq 0.99$) and can be described by the following rate law (Equation (1)):

$$\frac{dC_{AMX}}{dt} = -k_{obs} \times C_{AMX},\qquad(1)$$

where k_{obs} corresponds to the pseudo-first-order rate constant and C_{AMX} is AMX concentration. The $-k_{obs}$ constants were calculated from the slopes of the straight lines by plotting ln(C/C_0) as a function of time t, using linear regression. Uncertainties on k_{obs} were calculated based on the LINEST function in Excel.

UVC photolysis was carried out at unadjusted pH 6.40 ± 0.15 and at adjusted pH 3.0, 7.5 and 9.0. The results indicated that the pH value has a moderate influence on the degradation of AMX. The unadjusted pH and pH 9.0 favoured faster ($k_{obs} = 0.108 \pm 0.003$ min^{-1}) AMX degradation, whereas at pH 3.0 and 7.5 the target compound degradation was slightly slower with k_{obs} of 0.094 ± 0.001 and 0.076 ± 0.001 min^{-1}, respectively. A drop in the pH values after 2 h of UVC photolysis was noticed at pH 6.40 ± 0.15 (pH$_{120}$ 4.50) and at pH 7.50 (pH$_{120}$ 6), whereas at the strongly alkaline pH 9.0 the pH$_{120}$ was 6.20 (Table 3). No change was

Table 3. Final pH values and residual oxidant concentrations in different UVC-activated systems under various treatment conditions ($[AMX]_0 = 40$ μM; $t = 120$ min; limit of detection (LOD) for residual $S_2O_8^{2-} = 9.36$ μM).

Process	$[S_2O_8^{2-}]_0$, μM	$[Fe^{2+}]_0$, μM	pH_0	pH_{120}	$S_2O_8^{2-}$ remained, %
UVC photolysis	–	–	3.0	3.0	–
			6.3	4.55	–
			7.55	5.96	–
			9.02	6.20	–
UVC/$S_2O_8^{2-}$	40	–	6.55	4.11	24.2
	100		6.50	3.76	21.7
	200		6.48	3.48	10.3
	400		6.25	3.08	7.6
	800		6.48	2.96	2.1
UVC/$S_2O_8^{2-}$/ Fe^{2+}	400	10	6.46	3.18	3.6
		20	6.48	3.14	5.6
		40	6.43	3.09	4.0
		80	6.54	3.22	2.8

noticed at pH 3.0. Given the fact that AMX structure contains three active centres, carboxylic acid (pKa 2.68), amine (pKa 7.49) and phenolic hydroxyl (pKa 9.63) [21], the substance exists in an ionised form at all the pH values used in the trials. Therefore, at pH 3.0 the reaction is more pointed to amine and phenolic hydroxyl groups, whereas at pH 6.40 ± 0.15 the radical attack (if H_2O_2 is generated in photolysis) is directed to the amine group and at pH 9.0 towards the phenolic hydroxyl group [5]. These results are in good accordance with the study of Jung et al. [22], who conducted the UVC photolysis of AMX at pH 7.2.

Based on the results gained in our study, further experiments were performed at unadjusted pH.

3.2. Persulfate-based AMX degradation

The result of direct photolysis of AMX suggested that the target compound degradation could be improved. Thus, the effect of $S_2O_8^{2-}$ addition into the UVC system to the degradation efficacy of AMX in UW was studied. In such system, $SO_4^{•-}$ are formed according to Equation (2) [9]:

$$S_2O_8^{2-} + h\nu \rightarrow 2SO_4^{•-}. \qquad (2)$$

In this study, the UVC/$S_2O_8^{2-}$ trials with different $[S_2O_8^{2-}]_0$ (40, 100, 200, 400, 800 μM) were performed; the corresponding molar ratios of AMX/$S_2O_8^{2-}$ varied from 1/1 to 1/20. AMX degradation by this process also followed pseudo-first-order reaction kinetics. From Figure 1(a) appears that noticeable increase in the AMX degradation rate was achieved from the addition of $[S_2O_8^{2-}]_0 = 200$ μM ($k_{obs} = 0.131 \pm 0.008$ min^{-1}). Lower k_{obs} values at $[S_2O_8^{2-}]_0 = 40$ μM (0.092 ± 0.003 min^{-1}) and $[S_2O_8^{2-}]_0 = 100$ μM (0.095 ± 0.001 min^{-1}) could be explained by an insufficient amount of $S_2O_8^{2-}$ added
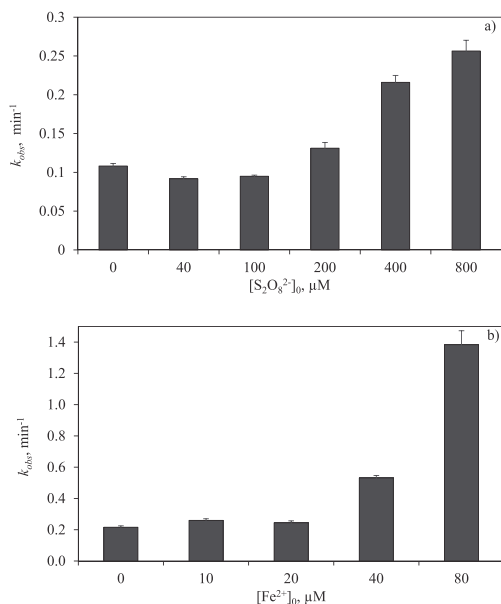

Figure 1. Pseudo-first-order rate constants (k_{obs}) by the UVC/$S_2O_8^{2-}$ process at different $[S_2O_8^{2-}]_0$ ($[AMX]_0 = 40$ μM) (a) and by the UVC/$S_2O_8^{2-}$/Fe^{2+} process at different $[Fe^{2+}]_0$ (b) at unadjusted pH ($[AMX]_0 = 40$ μM; $[S_2O_8^{2-}]_0 = 400$ μM).

which did not provide enough $SO_4^{•-}$ to attack AMX. Moreover, the k_{obs} at the lowest $[S_2O_8^{2-}]_0$ were slightly slower than for the UVC photolysis (0.108 ± 0.003 min^{-1}) of AMX. This could be explained by the formation of acidic transformation products and the addition of acidic $S_2O_8^{2-}$, which in turn with the low generated $SO_4^{•-}$ amount does not favour effective degradation of AMX. A further increase in the $[S_2O_8^{2-}]_0$ to 400 μM indicated a 2-fold higher k_{obs} (0.216 ± 0.009 min^{-1}) compared to the use of $[S_2O_8^{2-}]_0 = 200$ μM ($k_{obs} = 0.131 \pm 0.008$ min^{-1}). The highest $[S_2O_8^{2-}]_0 = 800$ μM used showed a moderate increase in k_{obs} (0.256 ± 0.012 min^{-1}) leading to a conclusion that $[S_2O_8^{2-}]_0 = 400$ μM added would be the most effective strategy for the degradation of AMX. The highest $[S_2O_8^{2-}]_0$, 800 μM, used was most likely near to excess amount of oxidant that could have led to scavenging of $SO_4^{•-}$, thus considering the decrease in degradation time and increase in the reaction rate, the most suitable concentration was selected as 400 μM. Ghauch et al. [11] also observed that the $S_2O_8^{2-}$ treatment ($[S_2O_8^{2-}]_0 = 0.25$ mM) coupled with UVC radiation significantly improved the degradation efficacy of chloramphenicol antibiotic with initial concentration of 31 μM.

The utilisation of $S_2O_8^{2-}$ in the UVC/$S_2O_8^{2-}$ system proved to enhance jointly with the increase of $[S_2O_8^{2-}]_0$

(Table 3). This pattern also explains the moderate reaction rates of AMX degradation at lower $[S_2O_8^{2-}]_0$. Regarding the pH change during the experiment (Table 3), it is probably actuated firstly by the increased addition of acidic $S_2O_8^{2-}$, secondly, by the degradation of the parent compound to acidic transformation products, and thirdly, by the formation of HSO_5^- [10].

In addition, a blank trial without UVC radiation was conducted to degrade AMX at similar experiment conditions. The results indicated more than 40% AMX degradation concurrently with its negligible mineralisation and high residual $S_2O_8^{2-}$ concentration (97%) in a 2-h treatment. The obtained results lead to a conclusion that it is necessary to use activating source (e.g. UVC radiation, Fe^{2+}) to incite the increased degradation and mineralisation of AMX as well the effective consumption of the added $S_2O_8^{2-}$.

Further trials were implemented with the simultaneous presence of $S_2O_8^{2-}$ and Fe^{2+} in the UVC-induced system to observe if the degradation rate of AMX will have the potential to increase. The experiments were performed at a fixed AMX/$S_2O_8^{2-}$ molar ratio of 1/10 ($[S_2O_8^{2-}]_0 = 400$ μM) and at initial pH 6.40 ± 0.15. The effect of Fe^{2+} addition was studied at a $[Fe^{2+}]_0$ of 10, 20, 40 and 80 μM at a constant $[S_2O_8^{2-}]_0 = 400$ μM that corresponds to an $S_2O_8^{2-}$/Fe^{2+} molar ratios of 10/0.25, 10/0.5, 10/1 and 10/2. The application of the UVC- and Fe^{2+}-activated $S_2O_8^{2-}$ treatment, that also followed pseudo-first-order reaction kinetics, indicated that Fe^{2+} addition to the oxidation system enhances the AMX degradation (Figure 1(b)). More significant improvement in AMX degradation was achieved at a $[Fe^{2+}]_0 = 40$ μM, where with $k_{obs} = 0.531 \pm 0.016$ min^{-1} the target compound degradation rate was approximately 2.5-fold faster compared to the UVC/$S_2O_8^{2-}$ system ($[S_2O_8^{2-}]_0 = 400$ μM, $k_{obs} = 0.216 \pm 0.009$ min^{-1}). The application of lower dosages $[Fe^{2+}]_0$ resulted in similar reaction rates of 0.260 ± 0.013 min^{-1} at 10 μM and 0.245 ± 0.012 min^{-1} at 20 μM, respectively. The use of $[Fe^{2+}]_0 = 80$ μM indicated the highest efficacy of AMX degradation ($k_{obs} = 1.383 \pm 0.090$ min^{-1}). Thus, the $[Fe^{2+}]_0 = 40$ μM was used in further trials of the study since the application of such concentration indicated reasonable efficacy of the AMX degradation. Furthermore, the addition of elevated amounts of Fe^{2+} can cause the formation of Fe^{3+}-sludge [9] at the studied pH values. All Fe^{2+} concentrations used in the current study did not cause any precipitation as the pH dropped below 4 in maximum 15 min of reaction time. In addition, a blank trial of $S_2O_8^{2-}$/Fe^{2+} ($[S_2O_8^{2-}]_0 = 400$ μM, $[Fe^{2+}]_0 = 40$ μM) was conducted to examine the target compound degradation without UVC radiation. It was observed that approximately 72.5% of AMX was degraded concurrently
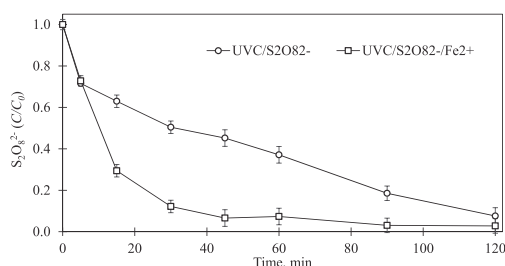

Figure 2. Residual $S_2O_8^{2-}$ of AMX degradation by the UVC/$S_2O_8^{2-}$ and UVC/$S_2O_8^{2-}$/Fe^{2+} processes at unadjusted pH ([AMX]$_0 =$ 40 μM; $[S_2O_8^{2-}]_0 = 400$ μM; $[Fe^{2+}]_0 = 40$ μM; LOD for residual $S_2O_8^{2-} = 9.36$ μM).

with negligible mineralisation and with 17.5% utilisation of $S_2O_8^{2-}$ in a 2-h treatment. This proves that UVC radiation is essential to activate the $S_2O_8^{2-}$/Fe^{2+} system for effective mineralisation of AMX. In our study, the UVC-activated H_2O_2-based treatment was also carried out for comparison (Supplemental Material).

The consumption of $S_2O_8^{2-}$ during AMX oxidation trial was expectedly higher under the dual activation by UVC and Fe^{2+}. However, the residual $S_2O_8^{2-}$ concentrations after a 2-h treatment at a $[S_2O_8^{2-}]_0 = 400$ μM were similar in both the UVC/$S_2O_8^{2-}$ (7.6%) and UVC/$S_2O_8^{2-}$/Fe^{2+} (2.8%) processes (Figure 2; Table 3). Also, the pH decrease in the trials was similar to the final value near 3 (Table 3) indicating the acidity of the added chemicals and the formed transformation products. This suggests that the amount of oxidant selected was suitable for the effective generation of radicals.

3.3. Identification of radical species

The radical species in the UVC-activated $S_2O_8^{2-}$ and $S_2O_8^{2-}$/Fe^{2+} systems were ascertained by the addition of radical scavengers. EtOH and t-BuOH as molecular probes were introduced to identify the proportion of SO_4^{-} or HO· in the oxidative system. EtOH is a well-studied scavenger for SO_4^{-} and HO· with similar reaction rates of $(1.6–7.7) \times 10^7$ L (mol s)$^{-1}$ and $(1.2–2.8) \times 10^9$ L (mol s)$^{-1}$, respectively [23]. t-BuOH is more effective scavenger for HO· $(3.8–7.6) \times 10^8$ L (mol·s)$^{-1}$ as compared to SO_4^{-} $(4–9.1) \times 10^5$ L (mol·s)$^{-1}$ [23].

Based on these characteristics, the prevalence of SO_4^{-} or HO· was estimated by adding excess EtOH or t-BuOH into the UVC/$S_2O_8^{2-}$ and UVC/$S_2O_8^{2-}$/Fe^{2+} systems. The assessment was done by estimating the degradation efficacy of AMX after adding the molecular probes; the results are presented in Table 4.

In both the UVC/$S_2O_8^{2-}$ and UVC/$S_2O_8^{2-}$/Fe^{2+} systems, the degradation of the studied compound was inhibited

Table 4. Degradation of AMX by the UVC/$S_2O_8^{2-}$ and UVC/$S_2O_8^{2-}$/Fe^{2+} processes at unadjusted pH ([AMX]$_0$ = 40 µM, [$S_2O_8^{2-}$]$_0$ = 400 µM, [Fe^{2+}]$_0$ = 40 µM; [t-BuOH]$_0$ = 20 mM; [EtOH]$_0$ = 20 mM; t = 5 min).

Process	Without scavenger	t-BuOH	EtOH
	[AMX]$_5$/[AMX]$_0$, %		
UVC/$S_2O_8^{2-}$	30.2	32.2	53.6
UVC/$S_2O_8^{2-}$/Fe^{2+}	5.8	12.6	43.1

in the presence of t-BuOH resulting in 2% and 6.8% additional residual AMX concentration, respectively. The presence of EtOH significantly affected both processes: the residual AMX concentration increased by 23.4% in the UVC/$S_2O_8^{2-}$ system and by 37.3% in the UVC/$S_2O_8^{2-}$/Fe^{2+} system. Such a tendency proposes that the SO_4^{-} were the prevalent oxidative species in the studied systems.

3.4. AMX degradation in environmental and processed waters

The chemical composition of water matrix can significantly influence the degradation efficacy of the pollutant. Therefore, the treatment of AMX was investigated in GW, DW and STWW by the UVC photolysis, UVC/$S_2O_8^{2-}$ and UVC/$S_2O_8^{2-}$/Fe^{2+} systems. The pH of the matrices was not adjusted to maintain initial conditions of the aqueous media. The studied matrices have pH value greater than 7, moderate alkalinity, and considerable concentrations of chloride (Cl^-) and sulphate (SO_4^{2-}) anions (Table 2).

The results of the trials to find out the k_{obs} are presented in Figure 3. In all matrices, the photolysis of AMX showed the slowest degradation efficacy with the following tendency according to k_{obs}: UW (0.108 ± 0.003 min^{-1}) > GW (0.096 ± 0.000 min^{-1}) > DW (0.076 ± 0.003 min^{-1} in) > STWW (0.056 ± 0.003 min^{-1}). The application of UVC/$S_2O_8^{2-}$ system resulted in enhanced
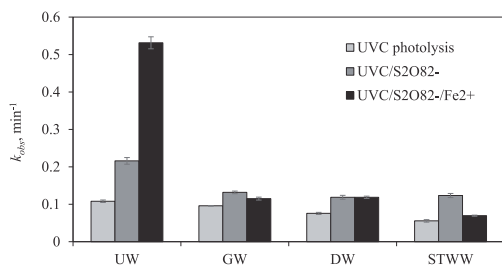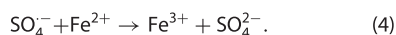

Figure 3. Pseudo-first-order rate constants (k_{obs}) of AMX degradation in different aqueous matrices at unadjusted pH ([AMX]$_0$ = 40 µM; [$S_2O_8^{2-}$]$_0$ = 400 µM; [Fe^{2+}]$_0$ = 40 µM).

k_{obs} with the highest value in UW (0.216 ± 0.009 min^{-1}) and lower rates in real matrices with 0.132 ± 0.004 min^{-1}, 0.119 ± 0.005 min^{-1} and 0.123 ± 0.005 min^{-1} in GW, DW and STWW, respectively. The application of the UVC/$S_2O_8^{2-}$/Fe^{2+} system indicated increased reaction rates only in UW (0.531 ± 0.016 min^{-1}); the reaction rates in other aqueous media decreased (0.115 ± 0.004 min^{-1} in GW; 0.069 ± 0.001 min^{-1} in STWW) or remained unchanged (0.119 ± 0.003 min^{-1} in DW). Regarding residual $S_2O_8^{2-}$, the dissociation extent was similar in all the studied environmental and processed waters, remaining at 22–36% from [$S_2O_8^{2-}$]$_0$ = 400 µM.

The reduced degradation efficacy of AMX in real aqueous matrices by the applied processes was predictable; however, the dual activation of $S_2O_8^{2-}$ by UVC and Fe^{2+} is suggested to improve the degradation efficacy of various organic micropollutants [9,16]. In our experimental conditions in GW, DW and STWW, such system showed lower efficacy. There could be several explanations that are mainly related to the matrix properties. Since the application of UVC to the AMX photolysis indicated moderate performance, it is likely influenced simultaneously by the reaction between UVC and natural organic matter (NOM) in the matrix. This derives a slower indirect photolysis of AMX, which in these matrices may result from the participation of NOM, bicarbonates (HCO_3^-) and NO_3^- (present in STWW), through what $HO^{\cdot}$ can be generated [24]. Due to amine nitrogen in the AMX structure, one of the pKa values for the studied beta-lactam is 7.49 [21] that could be a limiting factor for direct photolysis of AMX in DW and STWW. The application of the UVC/$S_2O_8^{2-}$ system in real matrices indicated increased treatment efficacy for AMX; these results are in accordance with the findings of Ji et al. [12] and Lutze et al. [18] that SO_4^{-} are more selective towards reactions with organic compounds and less influenced by the aqueous media constituents than $HO^{\cdot}$. The moderate results by the application of UVC/$S_2O_8^{2-}$/Fe^{2+} to degrade AMX could be derived from the reduction of a hydrated electron (e_{aq}^-) due to Fe^{2+} exposure to light (Equation (3)) [25]:

$$Fe^{2+} + h\nu \rightarrow Fe^{3+} + e_{aq}^-. \quad (3)$$
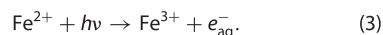
The formation of Fe^{3+} inhibits the SO_4^{-} oxidative efficacy as it does not react with $S_2O_8^{2-}$ and accumulates in the system [9]. The intensive UVC radiation induces the effective generation of SO_4^{-} via Eq. (2), that reacts intensively with Fe^{2+} towards the formation of Fe^{3+} (Equation (4)).

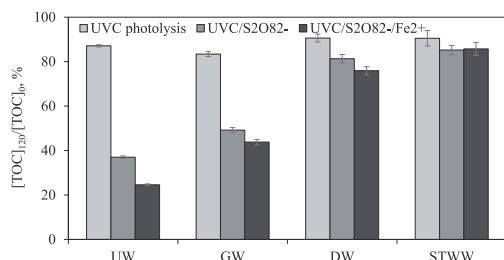$$SO_4^{-} + Fe^{2+} \rightarrow Fe^{3+} + SO_4^{2-}. \quad (4)$$

Figure 4. AMX mineralisation in different aqueous matrices at unadjusted pH ([AMX]$_0$ = 40 μM; [S$_2$O$_8^{2-}$]$_0$ = 400 μM; [Fe^{2+}]$_0$ = 40 μM; t = 120 min).

The intensive accumulation of Fe^{3+} in the oxidation system and the presence of various matrix constituents decrease the degradation efficacy of AMX.

Cl$^-$ are found to have a controversial influence on SO$_4^-$ derived oxidative systems. These anions can react with radicals (Equation (5)) and form less-reactive radicals that promote the decreased degradation efficacy of the target compound [26].

$$SO_4^- + Cl^- \rightarrow Cl^. + SO_4^{2-}. \qquad (5)$$
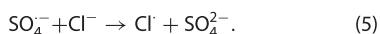
On the other hand, Monteagudo et al. [27] described the moderate influence of chloride ions to the degradation of carbamazepine. In general, the interference by Cl$^-$ is determined by its reactivity with the target compound.

Overall, the impact of matrix consists of several facts, including the target compound properties that should be considered before applying UVC-activated oxidative treatment.

3.5. AMX mineralisation in terms of TOC and detected transformation products

The main purpose of advanced oxidation techologies is to eliminate organic micropollutants; therefore, mineralisation of the organic compound is described in terms of the TOC content. Figure 4 shows the results of the applied processes for the TOC concentration changes. During the applied processes, the degradation of the target compound occurred, but the LC-MS analysis indicated the presence of transformation products, which refers that AMX was degraded, but not mineralised. The highest mineralisation was expectedly achieved in UW than compared to other matrices by all the applied processes. In environmental and processed water, the most promising results were gained in GW with the following performances: UVC/S$_2$O$_8^{2-}$/Fe^{2+} system (>56% of

TOC decrease) > UVC/S$_2$O$_8^{2-}$ system (>50%) > UVC photolysis (>16%). In DW and in STWW, the performance of the processes was similar with the following mineralisation extents: >24% > 18% > 9% (in DW) and >14% > 14% > 9% (in STWW). This indicates that the application of UVC- or UVC/Fe^{2+}-activated S$_2$O$_8^{2-}$ can be used for the elimination of beta-lactam antibiotics with careful further adjustment of the process conditions, especially when applying to environmental or processed waters.

The formation of several transformation products of AMX was verified by LC-MS analysis. The measured mass (m/z) for protonated AMX was 366. In UW, the most frequently detected m/z in the UVC/S$_2$O$_8^{2-}$/Fe^{2+} and UVC/S$_2$O$_8^{2-}$ systems were 122, 366, 382, that most likely correspond to penicilloic acid derivative (C$_7$H$_8$NO) [28], AMX-diketopiperazine-2′,5′ [29] and hydroxylated AMX, respectively. In GW, DW and STWW, the primary fragments were 208 and 366 of what the first could refer to AMX derivative C$_{10}$H$_{10}$NO$_2$S [28]. Primary proposed pathways of the transformation products are shown in Figure 5. Hydroxylation of AMX resulted in m/z of 382 (Figure 5 route A), opening of the unstable beta-lactam ring by hydrolysis yields in the intermediate product AMX-penicilloic acid which rapidly forms more stable AMX-diketopiperazine-2′,5′ (Figure 5 route B). Another possible final product of the AMX degradation could be C$_7$H$_8$NO that forms after opening of the beta-lactam ring followed by demethylation, decarboxylation, opening of the thiazole ring and loss of S atom (Figure 5 route C). Decarboxylation, demethylation and opening of the thiazole ring may result in the formation of AMX derivative C$_{10}$H$_{10}$NO$_2$S (Figure 5 route D).

4. Conclusions

This study was aimed to investigate the degradation of a beta-lactam antibiotic AMX by the UVC- or UVC/Fe^{2+}-activated S$_2$O$_8^{2-}$ processes. The findings indicated that the most effective conditions for the fast and complete degradation of AMX were at the S$_2$O$_8^{2-}$ concentration of 400 μM and Fe^{2+} concentration of 40 μM. All the UVC-activated treatment systems proved to follow pseudo-first-order reaction kinetics. The UVC/S$_2$O$_8^{2-}$ oxidation proved for effective degradation of AMX, but the application of UVC/S$_2$O$_8^{2-}$/Fe^{2+} system at different S$_2$O$_8^{2-}$ or Fe^{2+} concentrations significantly improved the treatment in UW. The identification of radical species in the UVC/S$_2$O$_8^{2-}$ and UVC/S$_2$O$_8^{2-}$/Fe^{2+} systems indicated that both radicals, SO$_4^-$ and HO$^.$, were present, but SO$_4^-$ were the predominant radicals. AMX removal was strongly influenced by the properties
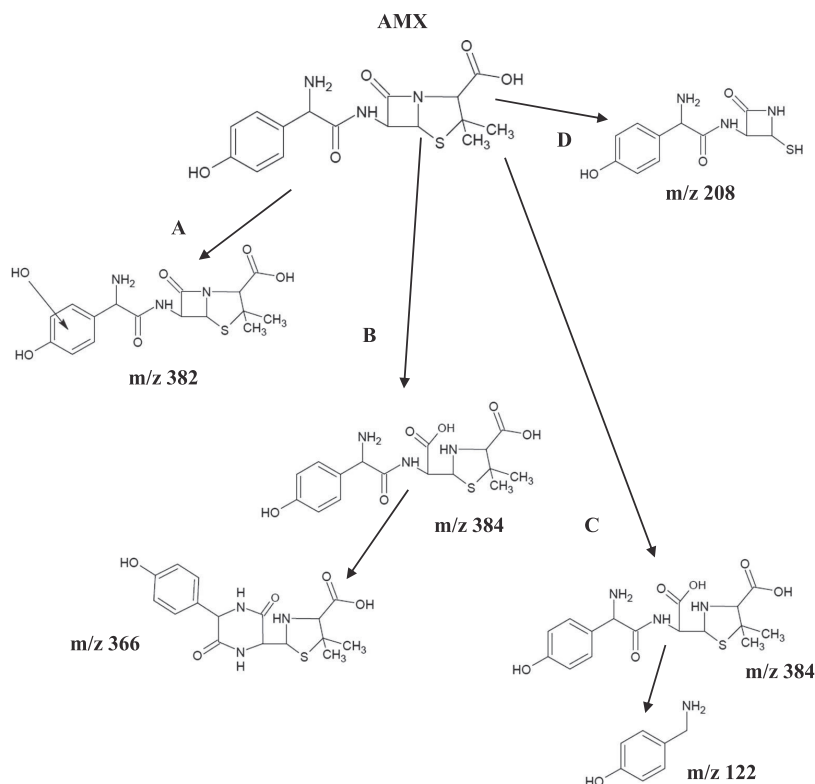
Figure 5. Proposed degradation pathways of the transformation of AMX by the studied systems in UW, GW, DW and STWW.

of the aqueous matrix, where the reaction rate constants were lower, but the > 99% AMX degradation still occurred in a 2-h treatment time. The proposed main transformation products of AMX were similar in all the studied water matrices. The results of this paper could provide important data for the removal of beta-lactam antibiotics from different environmental matrices and industrial effluents.

Acknowledgements

Disclosure statement

No potential conflict of interest was reported by the author(s).

Funding

ORCID

Eneliis Kattel http://orcid.org/0000-0001-6556-5617
Marina Trapido http://orcid.org/0000-0002-4033-5679
Niina Dulova http://orcid.org/0000-0001-5227-2401

References

[1] Homem V, Santos L. Degradation and removal methods of antibiotics from aqueous matrices – a review. J Environ Manage. 2011;92:2304–2347.
[2] Berendonk TU, Manaia CM, Merlin C, et al. Tackling antibiotic resistance: the environmental framework. Nat Rev Microbiol. 2015;13(5):310–317.
[3] Lara FJ, del Olmo-Iruela M, Cruces-Blanco C, et al. Advances in the determination of β-lactam antibiotics by liquid chromatography. Trends Anal Chem. 2012;38:52–66.
[4] World Health Organization. WHO model list of essential medicines. 20th ed. (March 2017) [Internet]. 2017 [4 February 2018]. Available from: http://www.who.int/medicines/publications/essentialmedicines/en/.
[5] Andreozzi R, Canterino M, Marotta R, et al. Antibiotic removal from wastewaters: The ozonation of amoxicillin. J Haz Mat. 2005;122(3):243–250.
[6] Elmolla E, Chaudhuri M. Degradation of the antibiotics amoxicillin, ampicillin and cloxacillin in aqueous solution

by the photo-fenton process. J Haz Mat. 2009;172(2–3): 1476–1481.

[7] Klauson D, Babkina J, Stepanova K, et al. Aqueous photocatalytic oxidation of amoxicillin. Catal Today. 2010;151(1–2):39–45.

[8] Su S, Guo W, Yi C, et al. Degradation of amoxicillin in aqueous solution using sulphate radicals under ultrasound irradiation. Ultrason Sonochem. 2012;19(3):469–474.

[9] Matzek LW, Carter KE. Activated persulfate for organic chemical degradation: a review. Chemosphere. 2016;151:178–188.

[10] Ghauch A, Tuqan AM. Oxidation of bisoprolol in heated persulfate/H_2O systems: kinetics and products. Chem Eng J. 2012;183:162–171.

[11] Ghauch A, Baalbaki A, Amasha M, et al. Contribution of persulfate in UV-254 nm activated systems for complete degradation of chloramphenicol antibiotic in water. Chem Eng J. 2017;317:1012–1025.

[12] Ji Y, Ferronato C, Salvador A, et al. Degradation of ciprofloxacin and sulfamethoxazole by ferrous-activated persulfate: implications for remediation of groundwater contaminated by antibiotics. Sci Total Environ. 2014;472:800–808.

[13] Peluffo M, Pardo F, Santos A, et al. Use of different kinds of persulfate activation with iron for the remediation of a PAH-contaminated soil. Sci Total Environ. 2016;563–564:649–656.

[14] Zhong H, Tian Y, Yang Q, et al. Degradation of landfill leachate compounds by persulfate for groundwater remediation. Chem Eng J. 2017;307:399–407.

[15] Yoon S-H, Jeong S, Lee S. Oxidation of bisphenol A by UV/$S_2O_8^{2-}$: comparison with UV/H_2O_2. Environ Technol. 2012;33(1):123–128.

[16] Shah NS, He X, Khan JA, et al. Comparative studies of various iron-mediated oxidative systems for the photochemical degradation of endosulfan in aqueous solution. J Photochem Photobiol A Chem. 2015;306:80–86.

[17] Kattel E, Trapido M, Dulova N. Oxidative degradation of emerging micropollutant acesulfame in aqueous matrices by UVA-induced H_2O_2/Fe^{2+} and $S_2O_8^{2-}/Fe^{2+}$ processes. Chemosphere. 2017;171:528–536.

[18] Lutze HV, Bircher S, Rapp I, et al. Degradation of chlorotriazine pesticides by sulfate radicals and the influence of organic matter. Environ Sci Technol. 2015; 49:1673–1680.

[19] Liang C, Huang C-F, Mohanty N, et al. A rapid spectrophotometric determination of persulfate anion in ISCO. Chemosphere. 2008;73(9):1540–1543.

[20] American Public Health Association. Standard methods for the examination of water and wastewater. 22nd ed. Washington (DC): American Water Works Association, Water Environment Federation; 2012.

[21] Goddard AF, Jessa MJ, Barrett DA, et al. Effect of omeprazole on the distribution of metronidazole, amoxicillin, and clarithromycin in human gastric juice. Gastroenterology. 1996;111(2):358–367.

[22] Jung YJ, Kim WG, Yoon Y, et al. Removal of amoxicillin by UV and UV/H_2O_2 processes. Sci Total Environ. 2012; 420:160–167.

[23] Anipsitakis G, Dionysiou DD. Radical generation by the interaction of transition metals with common oxidants. Environ Sci Technol. 2004;38:3705–3712.

[24] Wang X-H, Lin AY-C. Phototransformation of cephalosporin antibiotics in an aqueous environment results in higher toxicity. Environ Sci Technol. 2012;46:12417–12426.

[25] Dainton FS, Jones FT. Photo- and radiation-chemistry of low temperature aqueous glasses: part 1. – mineral acid glasses containing N_2O and Fe2+ ions. Trans Faraday Soc. 1965;61:1681–1700.

[26] Fang GD, Dionysiou DD, Wang Y, et al. Sulfate radical-based degradation of polychlorinated biphenyls: effects of chloride ion and reaction kinetics. J Haz Mat. 2012; 227–228:394–401.

[27] Monteagudo JM, Durán A, González R, et al. In situ chemical oxidation of carbamazepine solutions using persulfate simultaneously activated by heat energy, UV light, Fe2+ ions, and H2O2. Appl Catal B Environ. 2015;176–177:120–129.

[28] Trovo AG, Pupo Nogueira RF, Agüera A, et al. Degradation of the antibiotic amoxicillin by photo-fenton processes - chemical and toxicological assessment. Water Res. 2011;45:1394–1402.

[29] Lamm A, Gozlan I, Rotstein A, et al. Detection of amoxicillin-diketopiperazine-2′, 5′ in wastewater samples. Environ Sci Health A Tox Hazard Subst Environ Eng. 2009;44(14): 1512–1517.

# Photo-induced oxidation of ceftriaxone by persulfate in the presence of iron oxides

Balpreet Kaur *, Liina Kuntus, Priit Tikker, Eneliis Kattel, Marina Trapido, Niina Dulova

Tallinn University of Technology, Department of Materials and Environmental Technology, Ehitajate tee 5, 19086 Tallinn, Estonia

HIGHLIGHTS

- Degradation of ceftriaxone (CTA) by activated persulfate processes was investigated.
- CTA removal was higher in UVC-induced system compared to UVA-induced system.
- CTA degradation followed pseudo-first-order reaction kinetics.
- Results gained in the buffer solution reliably predict the efficacy in groundwater.
- Improved TOC removal and PS utilization was observed at acidic conditions (pH 3).

GRAPHICAL ABSTRACT
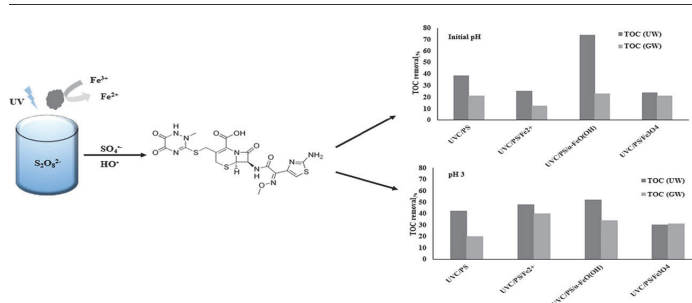
ARTICLE INFO

ABSTRACT

The present study focuses on degradation and mineralization of a third generation cephalosporin antibiotic ceftriaxone (CTA) in UVA- and UVC-induced persulfate (PS) system combined with heterogeneous (α-FeO(OH) and Fe_3O_4) activators. The CTA oxidation efficiency was investigated in buffered solution (pH 7.4) to stimulate the inhibitory properties of environmental and processed water matrices. Irrespective of the studied UV-induced persulfate system, the mineralization was less effective than CTA degradation. In turn, UVC-induced systems proved to be more effective than UVA-induced processes for decomposition of the target compound and removal of TOC. Accordingly, 2-h oxidation in UVA-induced systems resulted in partial decomposition and negligible mineralization of CTA. While the application of UVC-activated persulfate processes resulted in complete CTA degradation during the first 15 min of oxidation with the most efficient k_{obs} of 0.53 min^{-1} and 38.3% TOC removal obtained in the UVC/PS system at $[PS]_0 = 500$ μM. Groundwater (GW) trials results clearly indicated the inhibitory effect of the GW composition on the effectiveness of CTA degradation in the studied UV-induced PS-based systems, while the potential treatment efficacy in GW proved predictable based on the results obtained in the buffered UW trials. Adjusting the pH to 3 considerably improved the removal of TOC and the use of PS in both of the water matrices studied. The results of radicals scavenging experiments indicated that both $SO_4^{\bullet-}$ and $HO^\bullet$ contributed to the CTA decomposition efficacy in the UV-induced persulfate systems, but the former was the predominant radical in all studied processes. The findings of the study strongly suggest that the UV-induced PS systems are promising treatment technologies for the abatement of cephalosporin antibiotics pollution in natural aqueous matrices.

© 2019 Elsevier B.V. All rights reserved.

* Corresponding author.
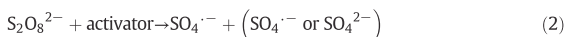   *E-mail address:* bakaur@ttu.ee (B. Kaur).

1. Introduction

Increasing population has led to elevated use of organic compounds such as pharmaceuticals and personal care products. Pharmaceuticals, above all the antibiotics, are micropollutants of the main concern. Intensive antibiotics use for humans and veterinary purposes allow partially metabolized antibiotics to escape into the aquatic environment. Moreover, the antibiotics are likely to pass without treatment from the conventional WWTPs that subsequently enter the drinking water system (Kümmerer, 2009; Wojcieszyńska et al., 2014). Elimination of such pharmaceuticals from the environment water and industrial effluents has been the focus of research for decades and thus to achieve the goal, efficient treatment technologies for degradation in aqueous matrices are required (Epold et al., 2012; Kattel et al., 2018; Owens and Dash, 2003).

The widely used class of β-lactam antibiotics, which contribute 50–70% of the worldwide consumption, demonstrate an antibacterial activity by inhibiting cell wall biosynthesis in bacterial organisms. Frequent use of the third-generation β-lactam antibiotics from the cephalosporin family, e.g. ceftriaxone (CTA), to treat various infections for instance, skin and abdominal infections has resulted in their occurrence in the wastewater and surface water (Dodd et al., 2010; Kümmerer, 2009). Low concentrations of antibiotics detected in drinking water in the range of ng L^{-1} to µg L^{-1} continuously entering human body can make the bacteria resistant and pass on through bacterial genetics (Hirsch et al., 1999). Moreover, the bioaccumulation of antibiotics in the environment followed by its entry into the food chain, proves to be a long-term risk to the ecosystem (Verlicchi et al., 2012).
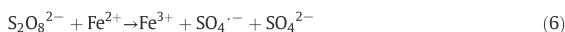
Advanced oxidation technologies (AOTs) are radical-based processes that have shown a great potential in degrading persistent and bio-refractory organic compounds present in various aqueous matrices. AOTs involve the generation of free radicals such as hydroxyl radicals (HO•) and sulfate radicals ($SO_4^{•-}$). The hydroxyl radicals ($E^0 = 2.80$ V) have a very short lifetime and are produced in situ through different methods, including a combination of oxidizing agents (such as H_2O_2 and O_3), irradiation (such as UV light or ultrasound), transition metal (such as Fe^{2+}), and other homogeneous and heterogeneous activators (Pignatello et al., 2006). High reaction rates and non-selective oxidation inherent to HO• allow simultaneous degradation of various contaminants and decline in secondary product formation (Hirsch et al., 1999; Pignatello et al., 2006). Sulfate radicals ($E_0 = 2.6$ V) are increasingly emerging as an oxidizing agent for pollutant degradation in water treatment and are generated by activated persulfate ion ($S_2O_8^{2-}$, PS) or peroxymonosulfate ion (HSO_5^-, PMS) (Golshan et al., 2018; Neta et al., 1977; Takdastan et al., 2018). $SO_4^{•-}$ have a longer lifetime than hydroxyl radicals therefore, these radicals are more likely to react with organic pollutants (Tsitonaki et al., 2010). Different from HO•, which decompose organic matter mainly by abstracting H from C—H bonds or adding itself to C=C bonds, $SO_4^{•-}$ preferably remove electrons from organic molecules that are subsequently transformed to organic radical cations (Neta et al., 1977). The promising parent compound to generate $SO_4^{•-}$ is persulfate ion ($S_2O_8^{2-}$, PS), that belongs to the peroxygen family, which itself is a strong oxidant ($E^0 = 2.10$ V) and is highly reactive. Accordingly, PS can react directly with many organic contaminants by exchanging electrons in a process known as direct oxidation. As a result, two sulfate anions are formed upon reduction of the persulfate anion (Tsitonaki et al., 2010).

$$S_2O_8^{2-} + 2e^- \rightarrow 2SO_4^{2-} \quad (1)$$

The most water soluble form of persulfate is sodium salt ($Na_2S_2O_8$), which under proper reaction conditions can generate free sulfate radicals via activation by heat, UV light or ultrasonic activation, peroxide or ozone activation, and alkaline activation (Kermani et al., 2018; Tsitonaki et al., 2010).
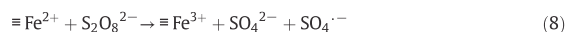
$$S_2O_8^{2-} + activator \rightarrow SO_4^{•-} + \left(SO_4^{•-} \text{ or } SO_4^{2-}\right) \quad (2)$$

$$S_2O_8^{2-} + heat \rightarrow 2SO_4^{•-} \quad (3)$$

$$S_2O_8^{2-} + h\nu \rightarrow 2SO_4^{•-} \quad (4)$$

Similar to hydrogen peroxide in the Fenton process (Eq. (5)), PS can be activated by transition metal ions (Fe^{2+}, Co^{2+}, etc.) to generate a considerable amount of $SO_4^{•-}$ (Eq. (6)). Ferrous iron (Fe^{2+}) the most widely studied metal activator is less expensive than other transition metals, relatively non-toxic and readily available (Liang and Su, 2009).

$$Fe^{2+} + H_2O_2 \rightarrow Fe^{3+} + OH^- + HO^• \quad (5)$$

$$S_2O_8^{2-} + Fe^{2+} \rightarrow Fe^{3+} + SO_4^{•-} + SO_4^{2-} \quad (6)$$

According to the literature, the Fe^{2+}-activated PS-based process results in the generation of both HO• and $SO_4^{•-}$ (Liang and Su, 2009; Takdastan et al., 2018). Notably, the Fe^{2+} activator is involved both in $SO_4^{•-}$ generation as well as scavenging. It was found that optimization of the iron dose is necessary for the effective activation of PS (Tsitonaki et al., 2010). Accordingly, lower concentration of the activator causes inefficient $SO_4^{•-}$ formation and at higher concentrations, excessive scavenging of radicals has been observed (Golshan et al., 2018; Takdastan et al., 2018).

Therefore, high efficacy and relatively low cost make soluble Fe^{2+}-activated PS oxidation a promising choice among the AOTs. Even more, the Fe^{2+} used to activate PS requires a relatively low activation energy of 12 kcal mol^{-1} (Kolthoff and Miller, 1951). For example, this is lower than the value of 33.5 kcal mol^{-1} required for thermal rupture of the O—O bond in the persulfate molecule. Thus it is considered that the Fe^{2+} activation of PS is highly efficient in generating $SO_4^{•-}$ and, therefore, in degrading pollutants. However, this homogenous process has limitations associated with precipitation of iron at neutral and alkaline pH values (Kolthoff and Miller, 1951; Rastogi et al., 2009).

To overcome this limitation, heterogeneous activators, such as ferrihydrite, hematite, goethite (α-FeO(OH)), lepidocrocite, magnetite (Fe_3O_4), pyrite, etc., could be used to activate PS for subsequent degradation of organic pollutants by generated radicals (Liang et al., 2004; Kamagate et al., 2018; Oh et al., 2011; Zhao et al., 2010). Heterogeneous activators such as goethite and magnetite are iron oxides commonly found in soil. The advantages of using iron oxides as activators are environmental friendliness, relatively low cost, applicability in a wide pH range and the possibility of their repeated use for the decomposition of pollutants. The degradation mechanism of organic contaminants by Fe^{3+}-containing minerals activated PS is proposed to comprise two steps (Lu, 2000). First, Fe^{3+} attached to the iron oxide surface (denoted as $\equiv Fe^{3+}$) is reduced by PS (Eq. (7)), which results in the formation of persulfate radical ($S_2O_8^{•-}$) and $\equiv Fe^{2+}$; the latter, in turn, activates PS to produce $SO_4^{•-}$ (Eq. (8)).

$$\equiv Fe^{3+} + S_2O_8^{2-} \rightarrow \equiv Fe^{2+} + S_2O_8^{•-} \quad (7)$$

$$\equiv Fe^{2+} + S_2O_8^{2-} \rightarrow \equiv Fe^{3+} + SO_4^{2-} + SO_4^{•-} \quad (8)$$

According to the available literature, the application of AOPs, including UV- and solar light-assisted catalytic oxidation (Kordestani et al., 2019; Sacco et al., 2019), ozonation (Norte et al., 2018), electrochemical (Li et al., 2018) and electro-catalytic (Guo et al., 2015) oxidation proved to be promising solution for CTA degradation in water matrices. However, it should be emphasized that at present there is a very scarce literature available regarding the performance of goethite- and magnetite-activated persulfate systems application for degradation and mineralization of micropollutants, particularly β-lactam antibiotics. For that reason, the main objective of the present study was to investigate and compare the efficiency of UV/PS, UV/PS/α-FeO(OH) and UV/PS/Fe₃O₄ systems towards CTA degradation and mineralization as well as PS

consumption. The effect of the operating parameters such as the pH value, activator dosage, oxidant concentration and initial concentration of the target compound was evaluated. The impact of matrix composition on the decomposition of CTA by the UV-induced PS-based systems was also studied.

2. Materials and methods

2.1. Chemicals and materials

Ceftriaxone ($C_{18}H_{18}N_8O_7S_3$, ≥99%, molecular weight 554.58 g mol^{-1}, Fig. 1), sodium persulfate ($Na_2S_2O_8$, ≥99%), ferrous sulfate heptahydrate ($FeSO_4 \cdot 7H_2O$, ≥99%), potassium iodide (KI, ≥99%), sodium hydrogen carbonate ($NaHCO_3$, 99%), sodium sulfite (Na_2SO_3, ≥98%), sodium hydroxide (NaOH, ≥98%), sulfuric acid (H_2SO_4, 95–98%) potassium phosphate dibasic (K_2HPO_4, ≥98%), potassium phosphate monobasic (KH_2PO_4, ≥98%), were purchased from Sigma-Aldrich. Acetonitrile (CH_3CN, LiChrosolv®), formic acid (CH_2O_2, 99%), ethanol (C_2H_6O, EtOH, 99%), were obtained from Merck KGaA.

Heterogeneous activators in the form of goethite (α-FeO(OH), 30–50 mesh), magnetite (Fe_3O_4, 98%, <5 μm) were purchased from Sigma-Aldrich. The specific surface area observed for goethite as well as magnetite was 112.5 and 7.5 m^2 g^{-1} respectively, measured by the multipoint N_2-BET analysis using a sorptometer KELVIN 1042 (COSTECH instruments).

All the chemicals were of analytical grade used without further purification. All stock solutions were prepared in ultrapure water (Millipore Simplicity®UV System, Merck) or in twice-distilled water (>18.2 MΩ cm).

2.2. Properties of groundwater

Groundwater (GW) collected from a borehole of 19 m depth (Harjumaa, Estonia) was used without preceding purification as real aqueous matrices for CTA degradation. The groundwater samples were stored at 4 °C. The main parameters of GW are presented in Table 1.

2.3. Experiment procedure

Unless otherwise specified, the laboratory scale experiments of the photo-chemical CTA oxidation were performed in batch mode at ambient room temperature (23 ± 1 °C). CTA solutions (50 μM, 0.8 L) were treated in 1.0-L cylindrical glass reactor for a period of 2-h along with permanent agitation at speed (400 rpm) sufficient for uniform distribution and full suspension of iron oxides particles or complete dissolution of iron activator. The treatment trials were carried out in 0.1 M potassium phosphate buffered solution at pH 7.4 ± 0.2 in UW as well as at initial pH 7.9 ± 0.1 in GW. To determine the effect of pH on degradation of CTA, several trials were conducted at adjusted pH 3 by the addition of H_2SO_4 aqueous solutions. The activator was added first and after it complete dissolution ($FeSO_4 \cdot 7H_2O$) or establishment of adsorption/desorption equilibrium between the CTA and the iron oxide (α-FeO(OH),
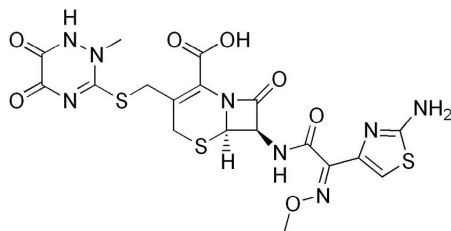
Table 1
Chemical composition and main parameters of water samples.

Parameter	Unit	Groundwater
pH		7.9
Alkalinity	mgCaCO$_3$ L^{-1}	366
Conductivity	μS cm^{-1}	763
Total organic carbon (TOC)	mg L^{-1}	16.91
Fe^{2+}	mg L^{-1}	0.01
Total Fe	mg L^{-1}	0.068
Cl$^-$	mg L^{-1}	128.2
NO$_3^-$	mg L^{-1}	2.25
PO$_4^{3-}$	mg L^{-1}	–[a]
SO$_4^{2-}$	mg L^{-1}	36

[a] Below detection limit.

Fe_3O_4) particles (~30 min of continuous stirring), the oxidation was initiated by adding $Na_2S_2O_8$ and exposure to the UV lamp. A low-pressure mercury germicidal lamp (11 W, Philips TUV PL-S) or a low-pressure mercury lamp (11 W OSRAM Dulux S BLUE) located in a quartz tube inside the reactor were used as an UVC and UVA source, respectively. The average irradiance entering the solution in the reactor measured by spectrometer (Ocean Optics USB2000+) equipped with SpectraSuite software was 2.68 mW cm^{-2} and 3.89 mW cm^{-2} for the UVC and UVA lamp, respectively. The lamps were turned on at least 5 min prior the trial to provide a constant output. A water cooling jacket was used to keep the constant temperature in the reactor. The molar ratio of PS/Fe^{2+} was kept constant at 10/1 in the UV/PS/Fe^{2+} systems. The UV/PS/α-FeO(OH) and UV/PS/Fe_3O_4 trials were conducted at goethite (concentrations range of 0.1–2.5 g L^{-1}) and magnetite (concentrations range of 0.01–0.5 g L^{-1}). Samples were withdrawn at pre-determined time intervals and filtered through a 0.45 μm pore size filter (CA, Millipore™). The oxidation quenching was done by the addition of EtOH (sample/EtOH volume ratio of 10/1) for HPLC and by the addition of Na_2SO_3 ([PS]$_0$/[SO$_3^{2-}$] molar ratio of 1/10) for TOC analysis. All experiments were duplicated. The results of the analysis are presented as the mean with a standard deviation of at least two parallel replicates <5% error.

2.4. Identification of the main radical species

Radical scavengers were used to identify the radicals formed during the UV/PS, UV/PS/α-FeO(OH) and UV/PS/Fe_3O_4 processes in buffered UW. To differentiate the role of SO$_4^{\bullet-}$ and HO• in CTA oxidation by the studied UV-induced PS-based systems two radical probes, ethanol (EtOH) and t-butanol (TBA), were employed. An excessive amount of scavenger was spiked into the reaction solutions before the activator and the oxidant addition at a CTA/[scavenger]$_0$ molar ratio of 1/500.

2.5. Analytical methods

CTA concentration was quantified using a high performance liquid chromatography combined with diode array detector (HPLC-PDA, Shimadzu, Japan) equipped with a Phenomenex Gemini (150 × 2.0 mm, 1.7 mm) NX-C18 (110 Å, 5 μm) column. The analysis was performed using an isocratic method with a mobile phase mixture of 15% acetonitrile (with 0.3% formic acid) and 85% formic acid (0.3%) aqueous solution. Samples (40 μL) were analyzed at the flow rate of 0.2 mL min^{-1}. The pH was measured using a digital pH/Ion meter (Mettler Toledo S220). The electrical conductivity was measured using a digital EC meter (HQ 430d flexi, HACH Company). The total organic carbon (TOC) was measured by a TOC analyzer multi N/C® 3100 (Analytik Jena). The concentration of anions was measured using ion chromatography with chemical suppression of the eluent conductivity (761 Compact IC, Metrohm Ltd.). The measurement of residual PS concentration in the treated samples (0.4 mL) was done spectrophotometrically (Genesys 10S, Thermo Scientific) at λ = 352 nm by an excess KI reaction with PS towards the formation of I$_2$ (Liang et al., 2008). The

Fig. 1. Molecular structure of ceftriaxone.

residual concentration of PS was determined by using the standard multipoint calibration. The alkalinity of groundwater was measured by titration with hydrochloric acid (0.1 M) in the presence of methyl orange.

3. Results and discussion

3.1. UVA versus UVC activation of PS for CTA oxidation

The performance of direct UVA and UVC photolysis in PS activation to degrade CTA was investigated in artificial buffered solution (pH 7.4). The dose of oxidant was optimized for further trials; since excess oxidant hinders the activation by competing between the oxidant and pollutant (Ding et al., 2017). The molar concentration of CTA was constant (50 μM), the different $[PS]_0$ (50, 250, 500, 1000, 2000 μM) corresponding to CTA/PS molar ratio of 1/1, 1/5, 1/10, 1/20, 1/40, respectively, were studied. The obtained results indicated that under studied experiment conditions, CTA degradation followed a pseudo-first order reaction kinetics ($r^2 ≥ 0.95$) in UVA- and UVC-induced systems and may be described with regard to the CTA concentration through Eq. (9).

$$\frac{dC_{CTA}}{dt} = -k_{obs} \times C_{CTA} \tag{9}$$

Where k_{obs} is the observed pseudo-first-order rate constant and C_{CTA} is the CTA concentration. The k_{obs} constants were calculated from the slopes of the straight lines by plotting ln (C_t/C_0) as a function of time t through linear regression.

The results of UVA photolysis and UVA/PS systems application for CTA degradation and mineralization within 2 h of treatment as presented in Fig. 2a.

The lowest $k_{obs} \times 10^2$ value of 0.17 min^{-1} was observed in the UVA/PS system at a CTA/PS molar ratio of 1/1 ($[PS]_0 = 50$ μM) with around 19% of CTA degraded and 8% PS utilized after 2-h of treatment. An increase in the initial concentration of oxidant used in UVA/PS systems led to an improvement in CTA degradation and PS utilization. Accordingly, about 72% of CTA was degraded and 14% of PS consumed at a $[PS]_0$ of 2000 μM. Similar trend was observed for TOC removal by the UVA/PS system, and thus 1% and 4% of CTA mineralization were observed at a $[PS]_0$ of 50 and 2000 μM, respectively.

In the case of studied UVC/PS systems, a fast degradation of CTA (≥99%) in first 15 min of treatment in all trials was observed resulting in much higher values of k_{obs} as compared to UVA-induced processes (Fig. 2b). Likewise, the TOC removal was considerably higher in the UVC-induced systems. Accordingly, at a $[PS]_0 = 50$ μM CTA mineralization of 20% was observed and further improved to 74% at a $[PS]_0 = 2000$ μM after 2-h of treatment.

The lowest applied $[PS]_0 = 50$ μM in the UVC/PS system resulted in k_{obs} of 0.47 min^{-1}. A 5-fold increase in $[PS]_0$ to 250 μM demonstrated faster decomposition of the target compound with k_{obs} of 0.54 min^{-1}.

However, a further increase in $[PS]_0$ beyond 500 μM showed a constant decrease in k_{obs} values corresponding to decline in CTA degradation efficacy probably due to the PS scavenging reactions (Eqs. (10)–(12)), the recombination of both $SO_4^{•−}$ and $HO^•$ radicals
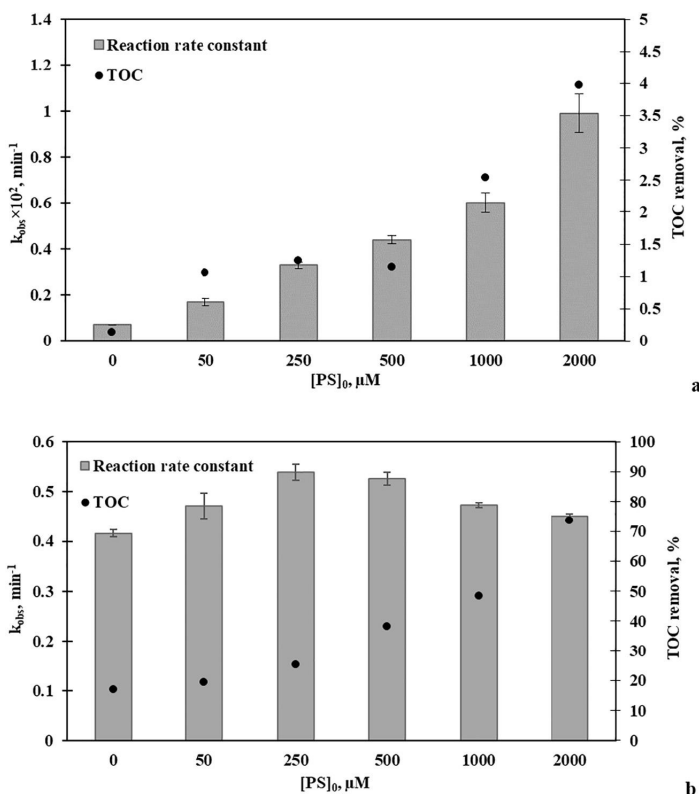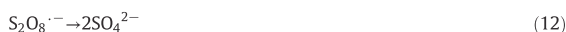

Fig. 2. CTA degradation observed reaction rate constants and TOC removal by UV photolysis and UV/PS process (a for UVA, b for UVC) at different PS concentrations ($[CTA]_0 = 50$ μM, $t = 2$ h).

(Eqs. (13), (14)), and the reactions between $SO_4^{\bullet-}$ and $HO^\bullet$ radicals (Eqs. (14)–(18)) (Wang and Zhou, 2016).

$$SO_4^{\cdot-} + S_2O_8^{2-} \rightarrow SO_4^{2-} + S_2O_8^{\cdot-} \tag{10}$$

$$HO^\cdot + S_2O_8^{2-} \rightarrow S_2O_8^{\cdot-} + OH^- \tag{11}$$

$$S_2O_8^{\cdot-} \rightarrow 2SO_4^{2-} \tag{12}$$

$$SO_4^{\cdot-} + SO_4^{\cdot-} \rightarrow S_2O_8^{2-} \tag{13}$$

$$HO^\cdot + HO^\cdot \rightarrow H_2O_2 \tag{14}$$

$$SO_4^{\cdot-} + HO^\cdot \rightarrow HSO_5^- \tag{15}$$

$$SO_4^{\cdot-} + HSO_5^- \rightarrow HSO_4^- + SO_5^{\cdot-} \tag{16}$$

$$HO^\cdot + HSO_5^- \rightarrow SO_5^{\cdot-} + H_2O \tag{17}$$

$$2SO_5^{\cdot-} \rightarrow S_2O_8^{2-} + O_2 \tag{18}$$

Similarly, the oxidant consumption in the UVC/PS systems proved to upsurge simultaneously with increase in applied $[PS]_0$. For instance, at the lowest studied $[PS]_0 = 50\,\mu M$, the observed consumption of oxidant after 2 h of treatment was 57%. The highest PS utilization, equal to 94%, was obtained at a $[PS]_0 = 1000\,\mu M$, while a further increase in $[PS]_0 = 2000\,\mu M$ led to decline in oxidant activation efficacy with around 20% of PS remained in solution. The latter observation can be explained by the limited activation capacity of the used source of UV irradiation in the case of elevated PS concentrations.

The effect of initial CTA concentrations on the performance of UV/PS system was investigated in the range of 30 to 70 μM. The trials were performed at the fixed $[PS]_0 = 500\,\mu M$ and at different UV irradiation sources. As shown in Fig. 3, irrespective of the used initial concentration of the target compound, the CTA degradation efficiency by the UVA/PS process was similar. Accordingly, 2-h oxidation in systems induced by UVA resulted in 64–67% residual concentration of CTA in solution.

In the case of UVC/PS trials, the increase in the initial CTA retarded the degradation efficiency of the target compound. Thus, the observed reaction rate constant decreased from 0.77 min^{-1} to 0.20 min^{-1} with increase in initial CTA concentration from 30 to 70 μM, respectively. The results were consistent with recent study conducted by Golshan et al. (2018) and Kordestani et al. (2019).

Notably, to prove the efficacy of UV activation of persulfate, a blank trial on non-activated persulfate oxidation was conducted at a $[PS]_0 = 500\,\mu M$. The results indicated 9.5% CTA degradation and 18.3%

persulfate consumption after 2 h of treatment in artificial buffered solution. The obtained results verified the promotion effect of UV activation for both used UV sources. Therefore, to maintain overall cost of the treatment process and to prevent $SO_4^{\bullet-}$ scavenging, $[PS]_0 = 500\,\mu M$ was selected as the most practicable concentration for the following trials.

3.2. Effect of goethite and magnetite addition on CTA oxidation by UVA/PS and UVC/PS systems

The heterogeneous reduction of organic xenobiotic by ferrous iron is considered to be a key process affecting the fate and transformation of pollutants in the environment (Do et al., 2010). In view of that, heterogeneous systems involving persulfate dual activation by UV radiation and iron oxides such as magnetite (Fe_3O_4) and goethite (α-FeO(OH)) were investigated for degradation and mineralization of CTA in buffered solution. The interaction of atoms, molecules and ions on the mineral-interface involves: surface reactions (surface hydrolysis, formation of coordinative bond with metal ions and with ligands), hydrophobic sorption (the adsorption of hydrocarbon substance on the mineral surface due to hydrophobic forces to reduce the mineral surface energy), and adsorption of surfactant molecules that contain both hydrophobic and hydrophilic end to reduce surface energy and become adsorbed at the mineral surface (Kakavandi et al., 2018; Zhang and Somasundaran, 2006).

Accordingly, as shown in Fig. 4, the persulfate in PS/iron-bearing mineral systems can be activated to generate sulfate radicals and subsequently hydroxyl radicals (Eq. (19)) either on the surface of iron-bearing activator (Eq. (8)) or in the bulk solution by Fe^{2+} leached from the surface of a heterogeneous activator (Eqs. (5), (6)) (Do et al., 2010). Thus, it is suggested that CTA molecule can be adsorbed on the surface of heterogeneous activator (α-FeO(OH) and Fe_3O_4) in the studied systems and/or is degraded by the in-situ generated $SO_4^{\bullet-}$ and $HO^\bullet$ by surface bound Fe^{2+} from activated persulfate (Eqs. (20)–(23)) (Khataee et al., 2015; Kordestani et al., 2019).

$$SO_4^{\cdot-} + H_2O \rightarrow HO^\cdot + HSO_4^- \tag{19}$$

$$CTA + SO_4^{\cdot-} \rightarrow CTA^{\cdot+} + SO_4^{2-} \tag{20}$$

$$CTA^{\cdot+} + H_2O \rightarrow (HO)CTA^\cdot + H^+ \tag{21}$$

$$CTA + HO^\cdot \rightarrow (HO)CTA^\cdot \tag{22}$$

$$(HO)CTA^\cdot \rightarrow \text{transformation products} \rightarrow CO_2 + H_2O \tag{23}$$

First, the UVA/PS/α-FeO(OH) system at the fixed CTA/PS m/m of 1/10 and different goethite dosage varying from 0.1 g L^{-1} to 2.5 g L^{-1}
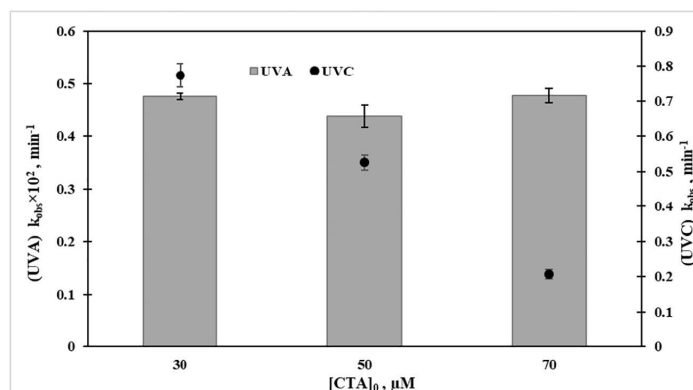

Fig. 3. CTA degradation observed reaction rate constants by UVA/PS and UVC/PS processes at different CTA concentrations ($[PS]_0 = 500\,\mu M$).

Fig. 4. Description of mineral-interface mechanism of heterogeneous activators.

was examined as presented in Fig. 5a. The highest $k_{obs} \times 10^2$ of 0.325 min^{-1} was obtained at a $[\alpha$-FeO(OH)$]_0 = 1$ g L^{-1}. However, a further increase in goethite concentration resulted in more than two-fold decrease in the observed rate of CTA degradation. Irrespective of the applied $[\alpha$-FeO(OH)$]_0$ dosage, the CTA degradation was considerably lower in the UVA/PS/α-FeO(OH) system as compared with the UVA/ PS oxidation at the same oxidant concentration. In contrast, PS utilization in the UVA/PS/α-FeO(OH) systems after 2-h treatment (10–17%) was comparable with the result obtained in the UVA/PS system (8–14%). Consequently, the observed reduction in the treatment

efficacy could be explained by the amplified impact of radicals scavenging reactions in the dually activated UVA/PS/α-FeO(OH) systems. To elucidate the type of persulfate activation (homogeneous and heterogeneous) caused by the presence of goethite, iron leaching in the studied systems was considered. Accordingly, the amount of the total dissolved iron in the bulk solution for all the UVA/PS/α-FeO(OH) systems was <4.3 μM after 2 h of oxidation, indicating the prevalence of heterogeneous activation reactions.

The UVC/PS/α-FeO(OH) system trials were also conducted at the same treatment conditions. As presented in Fig. 5b, the application of goethite concentration in the range of 0.1–2 g L^{-1} led to a substantial improvement in the efficacy of CTA degradation (as compared to the system without the addition of goethite) with k_{obs} values of around 0.60 min^{-1}. It should be noted that when using this dual activation, a slight improvement in PS consumption was also observed; thus around 34% and 38% of PS was utilized at a $[\alpha$-FeO(OH)$]_0$ of 0.1 g L^{-1} and 1 g L^{-1}, respectively, after 2-h of treatment. A further increase in the load of goethite to 2.5 g L^{-1} resulted in noticeable k_{obs} values drop (0.50 min^{-1}) along with slight reduction in PS utilization (36%). This observation can be explained by scavenging effect of the excessively generated sulfate radicals via reaction shown in Eq. (10). Similar results were obtained by Xue et al. (2009) during oxidation of pentachlorophenol; the authors suggested that excessive Fe-sites can act as $SO_4^{\bullet-}$ radical scavenger (Kolthoff and Miller, 1951). The results of the iron leaching measurements after 2 h of UVC/PS/α-FeO(OH) oxidation indicated a steady increase in total dissolved iron concentration from 2.1 μM to 4.5 μM in the bulk solution with upsurge of goethite amount from
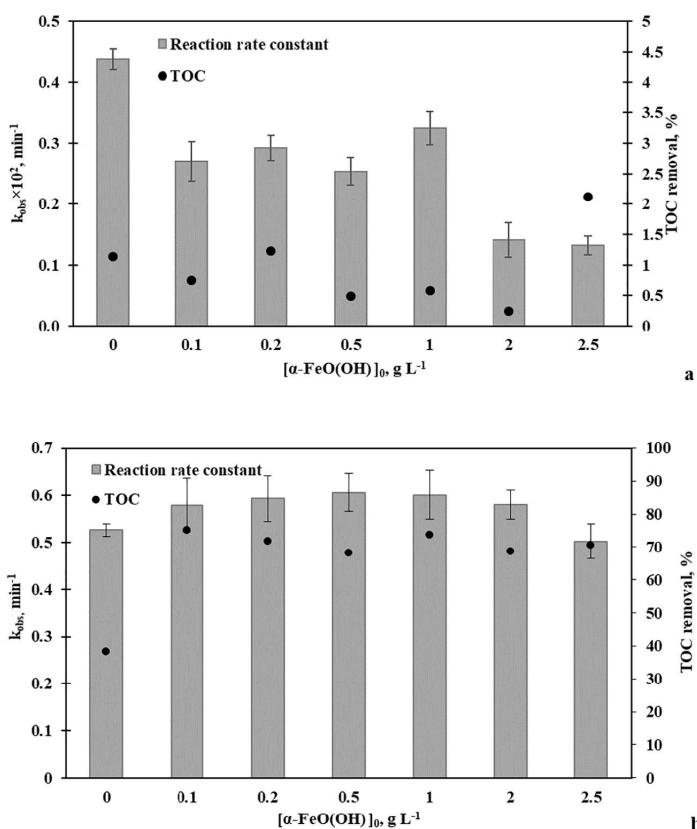

Fig. 5. CTA degradation observed reaction rate constants and TOC removal by UV/PS and UV/PS/α-FeO(OH) processes (a for UVA, b for UVC) at different goethite concentrations ($[CTA]_0 = 50$ μM, $[PS]_0 = 500$ μM, $t = 2$ h).

0.1 g L^{-1} to 2.5 g L^{-1}, respectively. However, due to the insignificant concentration of dissolved iron, regardless of the loading of goethite, the predominant PS activation reactions proved to occur on the surface of the heterogeneous activator (Khataee et al., 2015). Irrespective of the applied goethite dosages, TOC removal after a 2-h UVC/PS/α-FeO(OH) treatment was in the range 68–75%.

The efficacy of UV/PS/Fe$_3$O$_4$ system for CTA degradation and mineralization was studied at the same fixed CTA/PS molar ratio of 1/10 and at different Fe$_3$O$_4$ dosages in the range of 0.01–0.5 g L^{-1} (Fig. 6). As presented in Fig. 6a, an increase in the applied Fe$_3$O$_4$ concentration led to a drop in k$_{obs}$ values corresponding to a decrease in the efficacy of CTA degradation. The UVA/PS/Fe$_3$O$_4$ oxidation at a [Fe$_3$O$_4$]$_0$ = 0.01 g L^{-1} resulted in a k$_{obs}$ × 10^2 value of 0.2 min^{-1} with only 16% of CTA degradation after 2-h of treatment. A further increase in magnetite concentration up to 0.5 g L^{-1} led to a k$_{obs}$ × 10^2 value of 0.04 min^{-1}. In general, in all the studied UVA-induced PS/Fe$_3$O$_4$ systems persulfate consumption was lower (8–16%) that in the case of UVA/PS system (8–14%) with a negligible extent of CTA mineralization (0.14–0.22%).

A comparison of k$_{obs}$ values obtained in the UVA/PS/Fe$_3$O$_4$ and UVA/PS systems at a [PS]$_0$ = 500 μM suggests that an increase in the Fe$_3$O$_4$ dosage in fact hindered the CTA degradation. This observation can be explained by the low (up to 2.3 μM) concentration of the total dissolved iron detected in the bulk solution after 2 h of the UVA/PS/Fe$_3$O$_4$ oxidation and probably by the inadequate efficiency of heterogeneous catalysis on the surface of magnetite.

To understand the effect of homogeneous iron catalysis, the performance of CTA degradation in UVA/PS/Fe^{2+} system at a CTA/PS/Fe^{2+} molar ratio of 1/10/1 was also studied. The obtained results clearly

indicated that the application of UVA/PS/Fe^{2+} system result in higher (57%) CTA degradation, but similar PS consumption (10%) and TOC removal (2%), as in the case of UVA/iron oxide activated PS-based processes.

The results of CTA decomposition by the UVC/PS/Fe$_3$O$_4$ process indicated that this system can be applied for nearly complete CTA degradation (≥97%) with a 2-h treatment, but, as in the UVA-induces system, does not enhance the effectiveness of the UVC/PS system at the same concentration of oxidant. For instance, the application of [Fe$_3$O$_4$]$_0$ of 0.01 g L^{-1} and 0.5 g L^{-1} led to a k$_{obs}$ value of 0.41 min^{-1} and 0.32 min^{-1} along with ≥65% and ≥ 44% PS utilization, respectively. In the same way, the removal of TOC in all the studied UVC/PS/Fe$_3$O$_4$ systems was lower (up to 24%) compare to the UVC/PS (39%) process. As in the case of dual UVC and goethite activated PS-based process, the total dissolved iron concentration for the UVC/PS/Fe$_3$O$_4$ systems was low (up to 2.9 μM) after 2 h of treatment, indicating a negligible possibility of homogeneous activation of the oxidant.

Similar to UVA-induced trials, the efficacy of UVC/PS/Fe^{2+} system at a CTA/PS/Fe^{2+} molar ratio of 1/10/1 in CTA degradation and mineralization was studied. Accordingly, the k$_{obs}$ value of 0.38 min^{-1} with 68% PS consumption and 25% TOC removal was obtained after 2-h of treatment, indicating the predominance of a heterogeneous pathway of reaction in CTA degradation by UVC/PS/iron oxide systems.

It is noteworthy that the adsorption test conducted at a [Fe$_3$O$_4$]$_0$ = 0.2 g L^{-1} and [α-FeO(OH)]$_0$ = 2 g L^{-1} indicated a negligible decrease in CTA concentration (around 5 and 2%, respectively) indicating a low efficacy of adsorption/heterogeneous reduction in the target compound removal within 2.5 h of treatment.
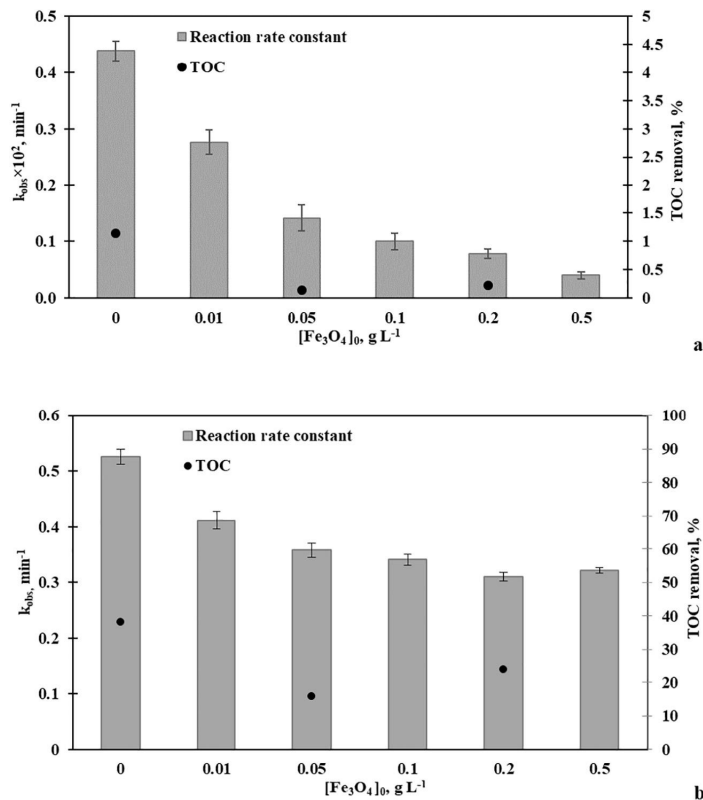

Fig. 6. CTA degradation observed reaction rate constants and TOC removal by UV/PS and UV/PS/Fe$_3$O$_4$ processes (a for UVA, b for UVC) at different magnetite concentrations ([CTA]$_0$ = 50 μM, [PS]$_0$ = 500 μM, t = 2 h).

Overall, the results of testing of UV-induced heterogeneous systems suggest that the use of UVC irradiation in combination with goethite is the most effective technology for removing CTA and efficiently using PS among the studied. In addition, it was observed that the CTA degradation efficiency by the combined UVC/PS/α-FeO(OH) system (Fig. 5b) was somewhat higher than those for all individual processes which proved the synergistic effect between the photochemical and catalytic decomposition of the target compound. The enhanced efficiency of goethite-based systems in buffered UW can be explained by the influence of pH as the solution pH (7.4 ± 0.2) was close to the point of zero charge (PZC) of goethite (6.2–7.4) (Zhao et al., 2017). The latter situation might raise the amount of positive surface charge, which probably enhanced the static interaction between α-FeO(OH) surface and $S_2O_8^{2-}$ and the adsorption of CTA (Barale et al., 2008; Herney-Ramirez et al., 2010). The obtained results were in correspondence with a previous study conducted on oxidation of diclofenac in the presence of goethite at similar pH by Zhao et al. (2017).

3.3. Effect of natural matrix composition on CTA oxidation by different UV-induced PS systems

To assess the reliability of using the results obtained in an artificially buffered solution to predict the efficiency of treatment in a real water matrix, all the systems studied were applied to decompose CTA in groundwater (Fig. 7). Typical composition of groundwater can affect the oxidation efficiency of organic pollutants, which often requires the addition of an increased dosage of in situ applied oxidants. Accordingly, highly reactive sulfate and hydroxyl radicals can react with natural

organic materials and inorganic anions presented in the matrix of groundwater as shown in Eqs. (24)–(29):

$$SO_4^{\cdot-} + Cl^- \rightarrow SO_4^{2-} + Cl^\cdot \tag{24}$$

$$SO_4^{\cdot-} + Br^- \rightarrow SO_4^{2-} + Br^\cdot \tag{25}$$

$$SO_4^{\cdot-} + NO_3^- \rightarrow SO_4^{2-} + NO_3^\cdot \tag{26}$$

$$HO^\cdot + NO_3^- \rightarrow NO_3^\cdot + HO^- \tag{27}$$

$$HO^\cdot + Br^- \rightarrow Br^\cdot + OH^- \tag{28}$$

$$HO^\cdot + Cl^- \rightarrow Cl^\cdot + OH^- \tag{29}$$

The results indicated that the direct UVA photolysis was responsible for approximately 35% CTA degradation ($k_{obs} \times 10^2$ of 0.3 min^{-1}) within 2-h of treatment (Fig. 7a). Addition of PS at a CTA/PS molar ratio of 1/10 ($[PS]_0 = 500$ μM) into the system improved the value of $k_{obs} \times 10^2$ (0.5 min^{-1}), corresponding to a decomposition of 48% CTA and utilization of 22% PS.

The performance of dual activated PS-based systems in the target compound oxidation was as follows: the UVA/PS/α-FeO(OH) system > the UVA/PS/Fe^{2+} system > the UVA/PS/Fe$_3$O$_4$ system. In the whole, the UVA/PS system proved to be the most efficient process for CTA degradation ($k_{obs} \times 10^2 = 0.5$ min^{-1}) and PS utilization (22%) in GW after 2-h of treatment. Irrespective of the applied treatment process, the TOC removal (up to 5.2%) was considerably less effective that CTA
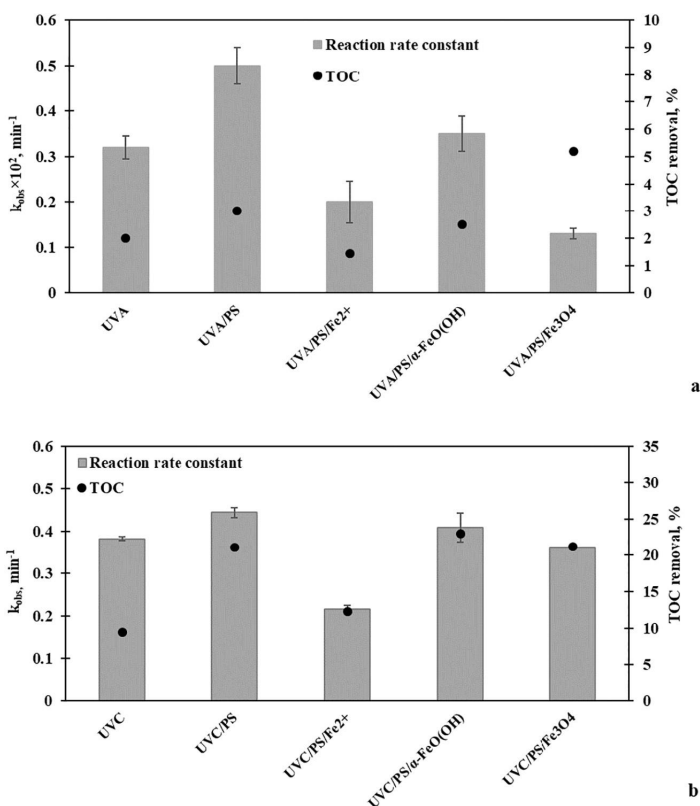

Fig. 7. CTA degradation observed reaction rate constants and TOC removal by different UV-induced systems (a for UVA, b for UVC) in groundwater ([CTA]$_0$ = [Fe^{2+}]$_0$ = 50 μM, [PS]$_0$ = 500 μM, [α-FeO(OH)]$_0$ = 1 g L^{-1}, [Fe$_3$O$_4$]$_0$ = 0.2 g L^{-1}, t = 2 h).

degradation. A comparison of the performance of UVA-induced PS-based systems in CTA degradation in the studied matrices indicated that the results obtained in buffered UW can be used to predict the treatment efficacy in GW.

The results of UVC-induced systems application for CTA degradation and TOC removal in GW are presented in Fig. 7b. Accordingly, the use of direct UVC photolysis and UVC-induced PS-based processes at a $[PS]_0 = 500 \mu M$ showed >95% CTA degradation within the first 15 min in GW. Moreover, the calculated k_{obs} values were in the range of 0.36–0.44 min^{-1} for all the studied processes, except the UVC/PS/Fe^{2+} system with the lowest k_{obs} of 0.21 min^{-1}.

The latter observation can be explained as the anions commonly present in GW (Table 1) have ability to scavenge free radicals (Eqs. (24)–(29)), thus affecting the rate of the target compound degradation and competing for $SO_4^{\bullet-}$ effectively produced by the ferrous ion activation of PS (Anipsitakis and Dionysiou, 2004). In addition, the observed turbidity considerably impaired the penetration of ultraviolet light inhibiting the activation of PS caused by UV radiation and, as a result, reducing the overall degradation of the target compound. Irrespective of the applied UVC-induced process, the effective PS consumption (around 57%) and modest TOC removal (9–23%) was observed within 2-h of treatment. A comparative study of all UVC-induced systems trials conducted in UW and GW at the same treatment conditions showed that the results obtained in UW can be reliably used to predict the degradation efficiency of CTA in GW. For example, the UVC/PS system proved to be the most efficient technology for CTA degradation and TOC removal in both studied water matrices.

The findings of this study strongly suggested that the results obtained for activated PS processes in buffered UW trials can be used to predict the potential treatment efficacy in real environmental matrices, e.g. in groundwater.

3.4. Effect of pH on CTA oxidation

The pH value of the solution is known to be an important parameter affecting degradation of organic contaminants especially in the case of soluble iron containing systems. The latter is relatively insoluble at the pH > 5 of natural aquifer systems and tend to precipitate in the form of amorphous ferric oxyhydroxides (Zhao et al., 2010). From the point of view of the tagret compound structure, ceftriaxone has four ionization groups: carboxylic, hydroxytriazinone, aminothiazole and amide. In acid medium three overlapping acid–base processes coexist with pK_1 2.37 (COOH), pK_2 3.03 (aminothiazole) and pK_3 4.21 (hydroxytriazinone) (Aleksić et al., 2005). Protolysis of amide group is happening in the alkaline medium as completely separated process from those in acid medium. The acidity constant which corresponds to amide group is pK_4 10.74 (Aleksić et al., 2005). Therefore, the effect of acidic pH 3 on the removal of TOC and PS consumption in the UV/PS, UV/PS/α-FeO(OH), UV/PS/Fe_3O_4 and UV/PS/Fe^{2+} system was also evaluated and the results are presented in Fig. 8. It should be noted that the trials were carried out under optimized treatment conditions previously determined in this study.

The performance of the studied UVA-induced systems (pH 3) in TOC removal in UW was as follows: the UVA/PS/Fe^{2+} system > the UVA/PS/
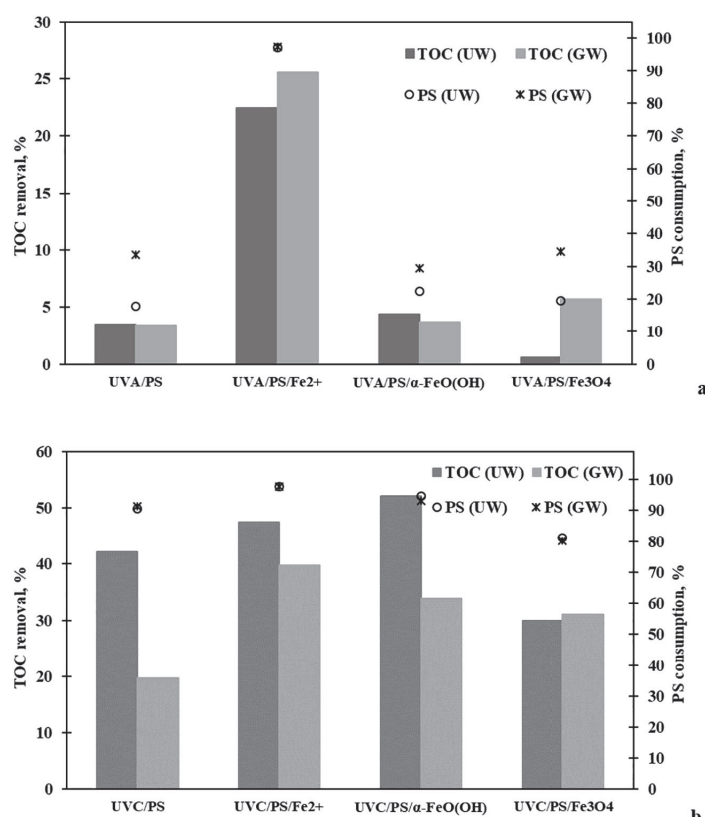

Fig. 8. TOC removal and PS utilization UV-induced PS-based system (a for UVA, b for UVC) in different aqueous matrices at adjusted pH = 3 ($[CTA]_0 = [Fe^{2+}]_0 = 50 \mu M$, $[PS]_0 = 500 \mu M$, $[α$-FeO(OH)]_0 = 1$ g L^{-1}, $[Fe_3O_4]_0 = 0.2$ g L^{-1}, $t = 2$ h).

α-FeO(OH) system > the UVA/PS system > the UVA/PS/Fe₃O₄ system (Fig. 8a). A similar tendency was observed for PS consumption, and thus the highest PS utilization after 2-h of treatment was observed in the UVA/PS/Fe^{2+} system (98%) followed by the UVA/PS/α-FeO(OH) system (29%). In the case of GW trials, the highest TOC removal and PS consumption was also obtained in the UVA/PS/Fe^{2+} system followed by the UVA/PS/Fe₃O₄ system; the lowest treatment efficacy was observed in the UVA/PS/α-FeO(OH) system. The increased effectiveness of the UVA/PS/Fe^{2+} system can be explained by higher solubility/stability and, consequently, availability of ferrous iron at acidic pH in both matrices. While in the PS-based systems activated by iron oxide, only a heterogeneous surface reaction occurred, because the amount of leached iron was insignificant in order to initiate a homogeneous activation.

The UVC-induced oxidation trials conducted at pH 3 in UW as shown in Fig. 8b indicated the highest TOC removal in the UVC/PS/α-FeO(OH) system followed by the UVC/PS/Fe^{2+} system and the lowest treatment efficacy in the UVC/PS/Fe₃O₄ system. Whereas in the case of GW samples the largest extent in the mineralization was observed in the UVC/PS/Fe^{2+} system followed by the UVC/PS/α-FeO(OH). It is noteworthy that the consumption of PS in both water matrices followed a similar trend.

Comparing the results of all the UV-induced systems studied conducted both at initial and acidic pH, it can be concluded that the removal of CTA and the use of PS improved in the latter conditions.

3.5. Identification of active radicals in the UV-induced persulfate systems

The radical scavenging experiments and/or the ESR spin-trap with DMPO technique are the principal methods used to identify the main active species in radical-based processes (Chen et al., 2017; Chen et al., 2018). Accordingly, to ascertain the predominant oxidative species involved in CTA oxidation by the UV/PS, UV/PS/α-FeO(OH) and UV/PS/Fe₃O₄ systems, scavenging studies with the addition of EtOH and TBA were carried out in buffered UW. EtOH is a well-studied scavenger for SO₄•$^{-}$ (1.6–7.7) × 10^7 M^{-1} s^{-1} and HO• (1.2–2.8) × 10^9 M^{-1} s^{-1}, whereas TBA is more effective scavenger for HO• (3.8–7.6) × 10^8 M^{-1} s^{-1} than for SO₄•$^{-}$ (4–9.1) × 10^5 M^{-1} s^{-1} (Anipsitakis and Dionysiou, 2004).

Based on these data, the presence of hydroxyl radicals was identified by adding an excess of TBA to the studied UV-induced systems. The effect of sulfate radicals was estimated by comparing the difference between the efficiency of CTA degradation after the addition of excess TBA and EtOH. The results presented in Table 2 showed that the addition of excess TBA inhibited the degradation of the target compound to some extent in all the UV-induced systems studied, suggesting that HO• was involved in all cases. Thus, the residual CTA concentration increased by about 3% and 6% in the UVA/PS and UVC/PS systems, respectively. The addition of excess EtOH resulted in a more noticeable inhibition of CTA decomposition in all studied systems; thus the residual CTA concentration increased by 10.5% in the UVA/PS system and by 8% in the UVC/PS system. The amount of CTA degradation that could not be eliminated by the addition of excess EtOH can be attributed to the

efficacy of direct UV photolysis. These findings suggested that both hydroxyl and sulfate radicals contribute to the degradation of CTA, whereas SO₄•$^{-}$ proved the predominant oxidative species in the UV-induced persulfate systems.

4. Conclusion

The present study focused on application of UVA- and UVC-induced PS-based processes for the CTA degradation and mineralization. In all studied UVA-induced systems the complete CTA degradation was not achieved in 2 h of treatment. The efficacy of the performance of studied UVA-induced systems in CTA degradation in artificially buffered UW was as follows: the UVA/PS system > the UVA/PS/Fe^{2+} system > the UVA/PS/α-FeO(OH) system > the UVA/PS/Fe₃O₄. The application of UVC-induced systems resulted in complete target compound degradation within the first 15 min of treatment with the most practicable k$_{obs}$ of 0.53 min^{-1} obtained in the UVC/PS system at a CTA/PS molar ratio of 1/10 ([PS]₀ = 500 μM). Irrespective of the applied UV-induced PS-based process, the CTA mineralization was less effective than the target compound degradation. The results of the scavenging studies suggested that both hydroxyl and sulfate radicals contributed to the degradation of CTA in the UV-induced persulfate systems, while SO₄•$^{-}$ proved the predominant radical in all studied systems. In general, the use of UVC-induced systems proved to be more effective in the degradation and mineralization of CTA as well as in the utilization of PS than PS-based systems induced by UVA both in buffered UW and in GW. The composition of GW undoubtedly reduced the effectiveness of CTA degradation in studied activated PS systems. Nevertheless, the results obtained in the buffered UW can be reliably used to predict the treatment efficacy of the studied processes in GW. The adjustment of pH to 3 showed a considerable improvement in the use of PS and the removal of TOC compared with trials conducted at initial pH. Irrespective of the studied water matrix, the UV/PS/Fe^{2+} system proved to be most feasible system at pH 3. While UVC/PS/α-FeO(OH) proved efficient both at unadjusted pH and pH 3. The findings of this study provide valuable information for the further practicable applications of UV-induced activated persulfate processes for the purification of CTA-contaminated water and groundwater with the most effective concentrations of reagents used.

Table 2
Degradation of CTA by the UV/PS, UV/PS/α-FeO(OH) and UV/PS/Fe₃O₄ systems ([CTA]₀ = 50 μM, [PS]₀ = 500 μM, [α-FeO(OH)]₀ = 1 g L^{-1}, [Fe₃O₄]₀ = 0.2 g L^{-1}, [EtOH]₀ = 25 mM, [TBA]₀ = 25 mM, t$_{UVA}$ = 60 min, t$_{UVC}$ = 5 min).

Process	[CTA]$_t$/[CTA]₀,%		
	Without scavenger	EtOH	TBA
UVA/PS	75.6	86.1	78.7
UVA/PS/α-FeO(OH)	78.9	90.4	88.4
UVA/PS/Fe₃O₄	92.8	100	99.3
UVC/PS	5.3	13.3	11.5
UVC/PS/α-FeO(OH)	10.1	13.5	12.3
UVC/PS/Fe₃O₄	14.3	19.5	14.9

References

Aleksić, M., Savić, V., Popović, G., Burić, N., Kapetanović, V., 2005. Acidity constants of cefetamet, cefotaxime and ceftriaxone; the effect of the substituent at C3 position. J. Pharm. Biomed. Anal. 39 (3–4), 752–756.

Anipsitakis, G.P., Dionysiou, D.D., 2004. Radical generation by the interaction of transition metals with common oxidants. Environ. Sci. Technol. 38 (13), 3705–3712.

Barale, M., Mansour, C., Carrette, F., Pavageau, E.M., Catalette, H., Lefèvre, G., ... Cote, G., 2008. Characterization of the surface charge of oxide particles of PWR primary water circuits from 5 to 320 C. J. Nucl. Mater. 381 (3), 302–308.

Chen, F., Yang, Q., Wang, S., Yao, F., Sun, J., Wang, Y., Zhang, C., Li, X., Niu, C., Wang, D., Zeng, G., 2017. Graphene oxide and carbon nitride nanosheets co-modified silver chromate nanoparticles with enhanced visible-light photoactivity and anti-photocorrosion properties towards multiple refractory pollutants degradation. Appl. Catal. B Environ. 209, 493–505.

Chen, F., Yang, Q., Wang, Y., Yao, F., Ma, Y., Huang, X., Li, X., Wang, D., Zeng, G., Yu, H., 2018. Efficient construction of bismuth vanadate-based Z-scheme photocatalyst for simultaneous Cr (VI) reduction and ciprofloxacin oxidation under visible light: Kinetics, degradation pathways and mechanism. Chem. Eng. J. 348, 157–170.

Ding, D., Liu, C., Ji, Y., Yang, Q., Chen, L., Jiang, C., Cai, T., 2017. Mechanism insight of degradation of norfloxacin by magnetite nanoparticles activated persulfate: identification of radicals and degradation pathway. Chem. Eng. J. 308, 330–339. https://doi.org/10.1016/j.cej.2016.09.077.

Do, S.H., Kwon, Y.J., Kong, S.H., 2010. Effect of metal oxides on the reactivity of persulfate/Fe(II) in the remediation of diesel-contaminated soil and sand. J. Hazard. Mater. 182, 933–936. https://doi.org/10.1016/j.jhazmat.2010.06.068.

Dodd, M.C., Rentsch, D., Singer, H.P., Kohler, H.P.E., von Gunten, U., 2010. Transformation of β-lactam antibacterial agents during aqueous ozonation: reaction pathways and quantitative bioassay of biologically-active oxidation products. Environ. Sci. Technol. 44 (15), 5940–5948.

Epold, I., Dulova, N., Veressinina, Y., Trapido, M., 2012. Application of ozonation, UV photolysis, Fenton treatment and other related processes for degradation of ibuprofen and sulfamethoxazole in different aqueous matrices. J. Adv. Oxid. Technol. 15 (2), 354–364.

Golshan, M., Kakavandi, B., Ahmadi, M., Azizi, M., 2018. Photocatalytic activation of peroxymonosulfate by TiO$_2$ anchored on cupper ferrite (TiO$_2$@CuFe$_2$O$_4$) into 2, 4-D degradation: Process feasibility, mechanism and pathway. J. Hazard. Mater. 359, 325–337.

Guo, X., Li, D., Wan, J., Yu, X., 2015. Preparation and electrochemical property of TiO2/Nano-graphite composite anode for electro-catalytic degradation of ceftriaxone sodium. Electrochim. Acta 180, 957–964.

Herney-Ramirez, J., Vicente, M.A., Madeira, L.M., 2010. Heterogeneous photo-Fenton oxidation with pillared clay-based catalysts for wastewater treatment: a review. Appl. Catal. B Environ. 98 (1-2), 10–26.

Hirsch, R., Ternes, T., Haberer, K., Kratz, K.L., 1999. Occurrence of antibiotics in the aquatic environment. Sci. Total Environ. 225, 109–118. https://doi.org/10.1016/S0048-9697(98)00337-4.

Kakavandi, B., Takdastan, A., Pourfadakari, S., Ahmadmoazzam, M., Jorfi, S., 2019. Heterogeneous catalytic degradation of organic compounds using nanoscale zero-valent iron supported on kaolinite: Mechanism, kinetic and feasibility studies. J. Taiwan Inst. Chem. Eng. 96, 329–340.

Kamagate, M., Amin Assadi, A., Kone, T., Coulibaly, L., Hanna, K., 2018. Activation of persulfate by irradiated laterite for removal of fluoroquinolones in multi-component systems. J. Hazard. Mater. 346, 159–166. https://doi.org/10.1016/j.jhazmat.2017.12.011.

Kattel, E., Kaur, B., Trapido, M., Dulova, N., 2018. Persulfate-based photodegradation of a beta-lactam antibiotic amoxicillin in various water matrices. Environ. Technol. https://doi.org/10.1080/09593330.2018.1493149

Kermani, M., Mohammadi, F., Kakavandi, B., Esrafili, A., Rostamifasih, Z., 2018. Simultaneous catalytic degradation of 2, 4-D and MCPA herbicides using sulfate radical-based heterogeneous oxidation over persulfate activated by natural hematite (α-Fe2O3/PS). J. Phys. Chem. Solids 117, 49–59.

Khataee, A., Salahpour, F., Fathinia, M., Seyyedi, B., Vahid, B., 2015. Iron rich laterite soil with mesoporous structure for heterogeneous Fenton-like degradation of an azo dye under visible light. J. Ind. Eng. Chem. 26, 129–135. https://doi.org/10.1016/j.jiec.2014.11.024.

Kolthoff, I.M., Miller, I.K., 1951. The chemistry of persulfate. I. the kinetics and mechanism of the decomposition of the persulfate ion in aqueous medium. J. Am. Chem. Soc. 73, 3055–3059. https://doi.org/10.1021/ja01151a024.

Kordestani, B., Yengejeh, R.J., Takdastan, A., Neisi, A.K., 2019. A new study on photocatalytic degradation of meropenem and ceftriaxone antibiotics based on sulfate radicals: Influential factors, biodegradability, mineralization approach. Microchem. J. 146, 286–292.

Kümmerer, K., 2009. Antibiotics in the aquatic environment–a review–part II. Chemosphere 75 (4), 435–441.

Li, D., Guo, X., Song, H., Sun, T., Wan, J., 2018. Preparation of RuO$_2$-TiO$_2$/Nano-graphite composite anode for electrochemical degradation of ceftriaxone sodium. J. Hazard. Mater. 351, 250–259.

Liang, C., Su, H.W., 2009. Identification of sulfate and hydroxyl radicals in thermally activated persulfate. Ind. Eng. Chem. Res. 48, 5558–5562. https://doi.org/10.1021/ie9002848.

Liang, C., Bruell, C.J., Marley, M.C., Sperry, K.L., 2004. Persulfate oxidation for in situ remediation of TCE. I. Activated by ferrous ion with and without a persulfate-thiosulfate redox couple. Chemosphere 55, 1213–1223. https://doi.org/10.1016/j.chemosphere.2004.01.029.

Liang, C., Huang, C.F., Mohanty, N., Kurakalva, R.M., 2008. A rapid spectrophotometric determination of persulfate anion in ISCO. Chemosphere 73, 1540–1543. https://doi.org/10.1016/j.chemosphere.2008.08.043.

Lu, M.C., 2000. Oxidation of chlorophenols with hydrogen peroxide in the presence of goethite. Chemosphere 40, 125–130. https://doi.org/10.1016/S0045-6535(99)00213-1.

Neta, P., Madhavan, V., Zemel, H., Fessenden, R.W., 1977. Rate constants and mechanism of reaction of SO$_4$ with aromatic compounds. J. Am. Chem. Soc. 99, 163–164. https://doi.org/10.1021/ja00443a030.

Norte, T.H.D.O., Marcelino, R.B.P., Medeiros, F.H.A., Moreira, R.P.L., Amorim, C.C., Lago, R.M., 2018. Ozone oxidation of β-lactam antibiotic molecules and toxicity decrease in aqueous solution and industrial wastewaters heavily contaminated. Ozone Sci. Eng. 40 (5), 385–391.

Oh, S.Y., Kang, S.G., Kim, D.W., Chiu, P.C., 2011. Degradation of 2,4-dinitrotoluene by persulfate activated with iron sulfides. Chem. Eng. J. 172, 641–646. https://doi.org/10.1016/j.cej.2011.06.023.

Owens, M.H., Dash, K.A., 2003. Ceftriaxone sodium: Comprehensive profile. Profiles Drug Subst. Excipients Relat. Methodol 36 (1), 1–84.

Pignatello, J.J., Oliveros, E., MacKay, A., 2006. Advanced oxidation processes for organic contaminant destruction based on the Fenton reaction and related chemistry. Crit. Rev. Environ. Sci. Technol. 36 (1), 1–84.

Rastogi, A., Al-Abed, S.R., Dionysiou, D.D., 2009. Sulfate radical-based ferrous-peroxymonosulfate oxidative system for PCBs degradation in aqueous and sediment systems. Appl. Catal. B Environ. 85, 171–179. https://doi.org/10.1016/j.apcatb.2008.07.010.

Sacco, O., Vaiano, V., Rizzo, L., Sannino, D., 2019.). Intensification of ceftriaxone degradation under UV and solar light irradiation in presence of phosphors based structured catalyst. Chem. Eng. Process. Process Intensif. 137, 12–21.

Takdastan, A., Kakavandi, B., Azizi, M., Golshan, M., 2018. Efficient activation of peroxymonosulfate by using ferroferric oxide supported on carbon/UV/US system: a new approach into catalytic degradation of bisphenol A. Chem. Eng. J. 331, 729–743.

Tsitonaki, A., Petri, B., Crimi, M., Mosbæk, H., Siegrist, R.L., Bjerg, P.L., 2010. In situ chemical oxidation of contaminated soil and groundwater using persulfate: a review. Crit. Rev. Environ. Sci. Technol. 40 (1), 55–91.

Verlicchi, P., Al Aukidy, M., Zambello, E., 2012. Occurrence of pharmaceutical compounds in urban wastewater: removal, mass load and environmental risk after a secondary treatment—a review. Sci. Total Environ. 429, 123–155.

Wang, S., Zhou, N., 2016. Removal of carbamazepine from aqueous solution using sono-activated persulfate process. Ultrason. Sonochem. 29, 156–162.

Wojcieszyńska, D., Domaradzka, D., Hupert-Kocurek, K., Guzik, U., 2014. Bacterial degradation of naproxen - undisclosed pollutant in the environment. J. Environ. Manag. 145, 157–161. https://doi.org/10.1016/j.jenvman.2014.06.023.

Xue, X., Hanna, K., Abdelmoula, M., Deng, N., 2009. Adsorption and oxidation of PCP on the surface of magnetite: kinetic experiments and spectroscopic investigations. Appl. Catal. B Environ. 89, 432–440. https://doi.org/10.1016/j.apcatb.2008.12.024.

Zhang, R., Somasundaran, P., 2006. Advances in adsorption of surfactants and their mixtures at solid/solution interfaces. Adv. Colloid Interf. Sci. 123, 213–229.

Zhao, J.Y., Zhang, Y.B., Quan, X., Zhao, Y.Z., 2010. Sodium peroxydisulfate activation by heat and Fe (II) for the degradation of 4-CP. Huanjing Kexue 31, 1233–1238.

Zhao, Y., Liu, F., Qin, X., 2017. Adsorption of diclofenac onto goethite: adsorption kinetics and effects of pH. Chemosphere 180, 373–378.

Research article

UV-assisted chemical oxidation of antihypertensive losartan in water

Balpreet Kaur [*], Niina Dulova

Department of Materials and Environmental Technology, Tallinn University of Technology, Ehitajate tee 5, 19086, Tallinn, Estonia

ABSTRACT

Population growth and deteriorating health issues have led to an increase in the consumption of angiotensin receptor blockers (ARBs), such as losartan (LOR), for treating high blood pressure and, as a result, to the frequent detection of these drugs in water and wastewater. The present study focuses on the oxidation of LOR by UV photolysis, UV(/Fe^{2+})-activated persulfate (PS) and hydrogen peroxide (H$_2$O$_2$) systems. The effects of operating parameters including pH value, reaction time, concentration of oxidant and activator on the efficacy of treatment were studied. The target compound degradation by direct UV photolysis, UV/PS and UV/H$_2$O$_2$ systems proved to be efficient and followed a pseudo-first-order kinetic model. The application of UV/oxidant systems even at lower PS or H$_2$O$_2$ concentrations resulted in more than 95% of LOR degradation in 10 min. In addition, the use of UV/Fe^{2+}-activated oxidant systems led to a further increase in the k_{obs} by improving the LOR oxidation in aqueous solution. The effectiveness of LOR mineralization based on total organic carbon (TOC) removal was also considered. The optimized results of the studied systems obtained in ultrapure water were used in groundwater to assess the effectiveness of LOR decomposition in more complex environmental matrix. Moreover, the acute toxicity of LOR solutions before and after the UV/Fe^{2+}-activated PS and H$_2$O$_2$ oxidation to luminous bacteria (*Vibrio fischeri*) was investigated.

1. Introduction

The population growth leads to an increase in the production and consumption of pharmaceutical products, and, as a result, to a more frequent detection of these substances, such as antibiotics, analgesics, β-blockers, antidepressants, antihypertensives, in the environment. According to World Health Organization over one billion people are suffering from hypertension worldwide and this number would rise to 1.5 billion by 2020 (Padmanabhan et al., 2012). Sartans, angiotensin receptor blockers (ARBs), are prescribed to treat high blood pressure. Once consumed, similar to the majority of pharmaceuticals, sartans are only partially metabolized, and thus a significant amount of antihypertensive substances is excreted as the parent compound. As a result, ARBs were detected in seawater (0.60–8.70 ng L^{-1}) (Cortez et al., 2018), wastewater treatment plants influent (19.7–2760 ng L^{-1}) (Ashfaq et al., 2017; Botero-Coy et al., 2018; Casado et al., 2014; Wang et al., 2018), rivers (149 ng L^{-1}) (Mandaric et al., 2017), hospital effluent (Azuma et al., 2019a) and wetlands (22.9 µg L^{-1}) (Nuel et al., 2018). The conventional treatment methods, such as biological processes, have been successfully applied for the elimination of ARBs using biochar (Blum et al., 2019), biofilm (Muter et al., 2017) and activated sludge process

(Kern et al., 2010). However, during the biological treatment some antihypertensives, such as losartan (LOR), can undergo structural modification to generate valsartan-acid and end up in activated sludge. The latter is a persistent pollutant and accumulate in various environment compartments (Carpinteiro et al., 2019; Nödler et al., 2013).

The application of advanced oxidation processes (AOPs) has demonstrated great potential for the treatment of water and wastewater in order to eliminate toxic, non-biodegradable and recalcitrant organic compounds (Dimitriadou et al., 2019; Dulova and Trapido, 2011; Kulik et al., 2007; Matzek and Carter, 2016). AOPs generate hydroxyl (HO•) and sulfate (SO$_4$•$^-$) radicals, which decompose organic pollutants with the formation of more short-chain and simpler organic compounds virtually until complete mineralization as presented in Eq. (1).

Organic species + HO•/SO$_4$•$^-$ → intermediates → CO$_2$ + H$_2$O + inorganic ions (1)

Traditionally, AOPs involved the generation of HO• (E^0 = 2.73 V), as for example in the case of the UV/H$_2$O$_2$ system (Eq. (2)), where photolysis plays a vital role contributing to the generation of HO• by rupturing the O–O bond of H$_2$O$_2$ (Lado Ribeiro et al., 2019)

$$H_2O_2 + h\upsilon \rightarrow 2HO^\bullet \tag{2}$$

The reaction mechanism of $HO^\bullet$ with organic pollutants (R) can be explained in three main pathways: radical addition (Eq. (3)), hydrogen abstraction (Eq. (4)), in which organic compounds react with $HO^\bullet$ to form an organic radical ($R^\bullet$), and electron transfer (Eq. (5)) (Lado Ribeiro et al., 2019). In general, $HO^\bullet$ is a non-selective oxidant and therefore commonly react on a competitive basis with both the target pollutant and background organic or inorganic compounds in complex aqueous matrices.

$$HO^\bullet + R \rightarrow ROH \tag{3}$$

$$HO^\bullet + RH \rightarrow R^\bullet + H_2O \tag{4}$$

$$HO^\bullet + RX \rightarrow RX^{\bullet-} + OH^- \tag{5}$$
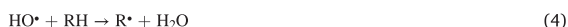
Recently, much attention has been paid to AOPs based on the activation of a strong oxidant persulfate ion ($S_2O_8^{2-}$, PS) with the formation of sulfate radicals. As shown in Eqs. (6)–(8), the $SO_4^{\bullet-}$ can be generated by activation of PS with the aid of heat, transition metal, ultrasonic and light radiation and is effective over a wide pH range (Tsitonaki et al., 2010).

$$S_2O_8^{2-} + 2e^- \rightarrow 2SO_4^{2-} \tag{6}$$

$$S_2O_8^{2-} + heat \rightarrow 2SO_4^{\bullet-} \tag{7}$$

$$S_2O_8^{2-} + h\upsilon \rightarrow 2SO_4^{\bullet-} \tag{8}$$

The high redox potential ($E^0 = 2.5$–3.1 V) and aqueous stability of sulfate radicals, makes activated PS oxidation a promising choice among the AOPs. Moreover, the $SO_4^{\bullet-}$ predominantly undergoes electron transfer mechanism and is more selective than the hydroxyl radical with respect to target pollutants (Matzek and Carter, 2016).

In addition, under basic conditions, sulfate radicals can react with water to form hydroxyl radicals (Eq. (9) and (10)), while at a neutral pH value, both $SO_4^{\bullet-}$ and $HO^\bullet$ radicals are present in the aqueous solution.

$$SO_4^{\bullet-} + H_2O \rightarrow SO_4^{2-} + HO^\bullet + H^+ \tag{9}$$

$$SO_4^{\bullet-} + OH^- \rightarrow SO_4^{2-} + HO^\bullet \tag{10}$$

According to the available literature, several $HO^\bullet$-based AOPs such as sonochemical process (Dimitriadou et al., 2019), photo-electro-Fenton system (Martínez-Pachón et al., 2019), electrochemical process (Salazar et al., 2016), photocatalysis (Zhou et al., 2018), and ozonation (Azuma et al., 2019b) have proved promising for degradation of LOR in aqueous matrices. However, scare literature is available on the application of sulfate radical-based oxidation processes for LOR degradation and identification of reaction intermediates.

The objective of the current study was to investigate and compare the efficiency of UV- and UV/Fe^{2+}-activated persulfate and hydrogen peroxide systems for the degradation and mineralization of LOR. The effect of the operating parameters, including the pH value, the concentration of oxidant and activator as well as the composition of groundwater matrix, on the efficiency of the selected treatment processes was evaluated. It is anticipated that the results of this study could provide fundamental support for the treatment of LOR-contaminated water, and especially the remediation of groundwater using these oxidation processes in practical applications.

2. Materials and methods

2.1. Chemicals and materials

Losartan ($C_{22}H_{22}ClKN_6O$, ≥99%, molecular weight 422.9 g mol^{-1}, Fig. 1), sodium persulfate ($Na_2S_2O_8$, ≥99%), ferrous sulfate heptahydrate ($FeSO_4 \cdot 7H_2O$, ≥99%), potassium iodide (KI, ≥99%), sodium hydrogen carbonate ($NaHCO_3$, 99%), sodium sulfite (Na_2SO_3, ≥98%)

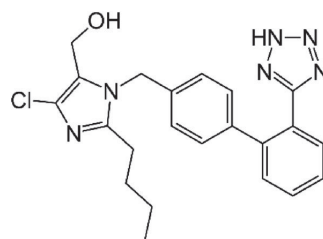**Fig. 1.** Molecular structure of losartan.

and sodium chloride (NaCl, ≥99%) were purchased from Sigma-Aldrich. Acetonitrile (CH_3CN, LiChrosolv®), formic acid (CH_2O_2, 99%), tert-butyl alcohol ((CH_3)$_3COH$, TBA, ≥99%) and ethanol (C_2H_6O, EtOH, 99%) were obtained from Merck KGaA.

All the chemicals were of analytical grade used without further purification. All stock solutions were prepared in ultrapure water (Millipore Simplicity®UV System, Merck) or in twice-distilled water (>18.2 MΩ cm).

2.2. Properties of groundwater

Groundwater (GW) collected from a borehole of 19 m depth (Harjumaa, Estonia) was used without preceding purification as a real aqueous matrix for LOR degradation. The groundwater samples were stored at 4 °C. The main parameters of GW are presented in Table 1.

2.3. Experiment procedure

The laboratory-scale experiments on the photochemical LOR oxidation were performed in batch mode at ambient room temperature (23 ± 1 °C). LOR solutions (40 μM, 0.8 L) were treated in a 1.0-L cylindrical glass reactor for 2 h with a permanent agitation speed (400 rpm) sufficient for uniform distribution and complete dissolution of iron activator. The treatment trials were carried out in non-buffered solutions at pH 6.1 ± 0.2 (UW) and 7.7 ± 0.2 (GW). The solid form of activator (FeSO$_4 \cdot 7H_2O$), if necessary, was added first and, after its complete dissolution, the oxidation was initiated by adding oxidant (PS or H_2O_2) and exposure to the UV lamp. A low-pressure mercury germicidal lamp (11 W, Philips TUV PL-S) located in a quartz tube inside the reactor were used as an UVC source. The average irradiance entering the solution in the reactor measured by spectrometer (Ocean Optics USB2000+) equipped with SpectraSuite software was 2.7 mW cm^{-2}. The lamp was turned on at least 5 min prior the trial to provide a constant output. A water cooling jacket was used to keep the constant temperature in the reactor. The LOR/oxidant molar ratios of 1/1, 1/5, 1/10, 1/20, corresponding to a molar concentration of oxidants ranging between 40 and 800 μM, were studied. The molar concentration of Fe^{2+} was in range of 20–80 μM in the UV/oxidant/Fe^{2+} systems. The experiments on LOR oxidation with non-activated PS or H_2O_2 as well as dark PS/Fe^{2+} and

Table 1
Chemical composition and main parameters of groundwater sample.

Parameter	Unit	Value
pH		7.71
Alkalinity	mgCaCO$_3$ L^{-1}	350
Conductivity	μS cm^{-1}	820
Total organic carbon (TOC)	mg L^{-1}	2.21
Fe^{2+}	mg L^{-1}	0.012
Total Fe	mg L^{-1}	0.175
Cl$^-$	mg L^{-1}	83.54
NO$_2^-$	mg/L	0.82
NO$_3^-$	mg L^{-1}	2.08
SO$_4^{2-}$	mg L^{-1}	33.95

H_2O_2/Fe^{2+} systems were conducted in identical reactor and treatment condition for the respective UV-activated oxidation trials. Sample aliquots were withdrawn at pre-determined time intervals. The oxidation quenching was done by the addition of EtOH (sample/EtOH volume ratio of 10/1) for HPLC, and by the addition of Na_2SO_3 ([oxidant]$_0$/[SO_3^{2-}] molar ratio of 1/10) for TOC analysis.

All experiments were duplicated. The results of the analysis are presented as the mean with a standard deviation of at least three parallel replicates less than 5%.

2.4. Analytical methods

LOR concentration was quantified using a high performance liquid chromatography combined with diode array detector (HPLC-PDA, Shimadzu, Japan) equipped with a Phenomenex Gemini (150 × 2.0 mm, 1.7 mm) NX-C18 (110 Å, 5 µm) column. The analysis was performed using an isocratic method with a mobile phase mixture of 40% acetonitrile (with 0.3% formic acid) and 60% formic acid (0.3%) aqueous solution. The flow rate was kept at 0.2 mL min^{-1}. Samples (75 µL) were analyzed at $\lambda = 210$ nm.

The pH was measured using a digital pH/Ion meter (Mettler Toledo S220). The electrical conductivity was measured using a digital EC meter (HQ 430d flexi, HACH Company). The total organic carbon (TOC) was measured by a TOC analyzer multi N/C® 3100 (Analytik Jena). The concentration of anions was measured using ion chromatography with chemical suppression of the eluent conductivity (761 Compact IC, Metrohm Ltd.). The alkalinity of groundwater was measured by titration with hydrochloric acid (0.1 M) in the presence of methyl orange. The residual hydrogen peroxide concentration in the treated samples was measured spectrophotometrically at $\lambda = 410$ nm with titanium sulfate by a H_2O_2–Ti^{4+} complex formation (Eisenberg, 1943) by a GENESYS 10S spectrophotometer (Thermo Scientific). The measurement of residual PS concentration in the treated samples (0.4 mL) was done spectrophotometrically (Genesys 10S, Thermo Scientific) at $\lambda = 352$ nm by an excess KI reaction with PS towards the formation of I_2 (Liang et al., 2008). The residual concentration of PS was determined by using the standard multipoint calibration.

2.5. Identification of the main radical species

The main active radicals involved in the degradation of LOR by the UV/PS and UV/PS/Fe^{2+} processes have been identified using radical scavengers. To differentiate the role of hydroxyl and sulfate radicals in LOR oxidation by the selected systems two radical probes, TBA and EtOH, were used. An excessive amount of scavenger was spiked into the reaction solutions before the addition of activator and oxidant at a LOR/scavenger molar ratio of 1/500. In the case of UV/Fe^{2+} process, the addition of TBA at a [TBA]$_0$ = 20 mM was studied.

2.6. Acute toxicity test

The acute toxicity was investigated using the Microtox® method (Model 500 Analyzer SDI) (ISO 11348–3:2007) (ISO (International Organization for Standardization), 2007). The reconstitution solution was prepared and used to activate freeze-dried *Vibrio fischeri*. To maintain the osmotic pressure of the test bacteria suspension, concentrated salt solution (2% NaCl) was used to achieve 2% salinity (Kahru et al., 1996). The salt solution was used as control. The initial LOR solution (40 µM) and treated LOR solutions after a 2-h oxidation by the UV/PS/Fe^{2+} and UV/H_2O_2/Fe^{2+} system were used as samples. Each toxicity test was performed in 10 dilutions, and the luminescence was measured after 15 min of exposure. The bacterial luminescence inhibition (INH%) was calculated using Eqs. (11) and (12).

$$INH\% = 100 - \frac{IT_{15}}{KF^*IT_0}*100 \tag{11}$$

$$KF = \frac{IC_{15}}{IC_0} \tag{12}$$

Where: KF - correction factor, IC$_{15}$ - luminescence intensity of control after contact time (15 min), IC$_0$ - initial luminescence intensity of control sample, IT$_{15}$ - luminescence intensity of test sample after contact time (15 min), and IT$_0$ - initial luminescence intensity of the test sample.

2.7. Identification of LOR transformation products

The samples from selected trails were analyzed by the high-performance liquid chromatography combined with a mass spectrometer (HPLC-MS, Shimadzu LC-MS, 2020). Phenomenex Gemini NX-C18 column was used with an isocratic eluent mixture, 0.3% formic acid aqueous solution (60%, v/v) and acetonitrile (40%, v/v) with a total flow rate of 0.2 mL min^{-1}. Mass spectra were acquired in full-scan mode (scanning in the range 50–500 m/z). The instrument was operated in positive ESI mode, and the results obtained with MS detector were handled using Shimadzu Lab Solutions software.

3. Results and discussion

3.1. UV photolysis, UV/PS and UV/H_2O_2 systems for LOR degradation

To evaluate the effect of UV photolysis on activation of PS and H_2O_2, the initial trials were performed using the target compound concentration of 40 µM in UW at pH$_0$ = 6.1 ± 0.2. The concentration of the oxidants ranged from 40 to 800 µM, which corresponds to LOR/PS and LOR/H_2O_2 molar ratios of 1/1, 1/5, 1/10, 1/20.

Accordingly, the direct UV photolysis and studied UV-induced oxidation systems proved to be effective and resulted in more than 95% of LOR degradation in 60 min. The obtained results indicated that LOR degradation in the UV-assisted systems followed a pseudo-first-order kinetics law (r$^2 \geq 0.95$) and may be described with regard to the LOR concentration through Eq. (13).

$$\frac{dC_{LOR}}{dt} = -k_{obs} \times C_{LOR} \tag{13}$$

Where k$_{obs}$ is the observed pseudo-first-order rate constant and C_{LOR} is the LOR concentration. As shown in Fig. 2, the k$_{obs}$ values were calculated from the slopes of the straight lines by plotting ln (C_t/C_0) as a function of time t through linear regression.

The direct PS and H_2O_2 oxidation at a [PS]$_0$ = [H_2O_2]$_0$ = 400 µM resulted in a negligible LOR degradation and mineralization with 99% of residual oxidant concentration in both systems after a 2-h treatment. On the other hand, the application of direct UV photolysis for the removal of LOR showed complete decomposition of the target compound (k$_{obs}$ of 0.081 min^{-1}), but low mineralization extent (8%).

The addition of UV radiation to PS and H_2O_2 oxidation to form UV/PS and UV/H_2O_2 systems substantially improved the LOR elimination efficiency, as depicted in Fig. 3. Irrespective of the oxidant used, the increase in its concentration led to more rapid degradation of LOR along with more complete mineralization in the studied UV/PS and UV/H_2O_2 systems. This observation can be explained by the fact that photolysis of raised oxidants dosages led to an increase in the formation of radicals according to equations (2) and (8), which, in turn, led to an improvement in the removal of LOR.

Accordingly, the application of the lowest studied [oxidant]$_0$ of 40 µM at a to LOR/oxidant molar ratio of 1/1 in the UV/PS and UV/H_2O_2 processes resulted in the k$_{obs}$ value of 0.132 min^{-1} and 0.095 min^{-1} and the TOC removal of 11% and 8.5%, respectively. A further 10-fold increase in oxidants molar concentration to 400 µM, corresponding to LOR/oxidant molar ratio of 1/10, facilitated LOR degradation with k$_{obs}$ of 0.283 min^{-1} and 0.249 min^{-1} along with 45% and 51% TOC removal, respectively.
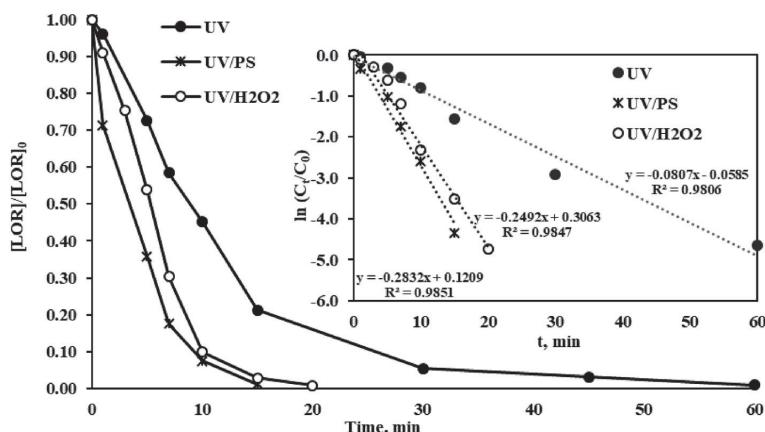
Fig. 2. LOR degradation by the UV photolysis, UV/PS and UV/H$_2$O$_2$ processes ([LOR]$_0$ = 40 μM, [PS]$_0$ = [H$_2$O$_2$] = 200 μM).
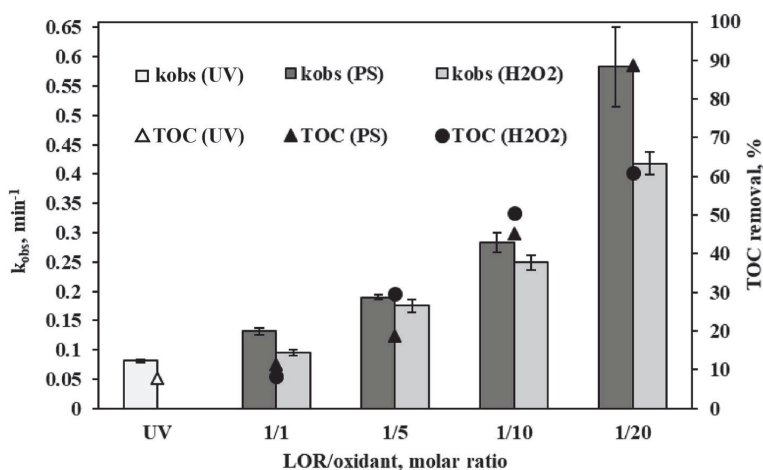

Fig. 3. LOR degradation observed reaction rate constants and TOC removal by the UV photolysis, UV/PS and UV/H$_2$O$_2$ processes at different LOR/oxidant molar ratios ([LOR]$_0$ = 40 μM, t = 2 h).

As can be seen from the results presented in Fig. 3, the target compound degradation was in general faster in UV/PS systems compared to the UV/H$_2$O$_2$ oxidation with the same [oxidant]$_0$ used, which indicates the important role of sulfate radicals in the decomposition of LOR. Accordingly, the highest k$_{obs}$ value of 0.583 min^{-1} and TOC removal of 89% were observed in the UV/PS process at a LOR/PS molar ratio of 1/20. Whereas, at the same [oxidant]$_0$ of 800 μM used in the UV/H$_2$O$_2$ system, the k$_{obs}$ value of 0.418 min^{-1} along with 61% TOC removal were obtained.

As shown in Table 2, the utilization of oxidants in the studied UV-assisted PS and H$_2$O$_2$ systems was more complete at higher dosages of the oxidizing agent used. On the other hand, regardless of the studied LOR/oxidant moral ratio, PS consumption was always higher than H$_2$O$_2$ at the same [oxidant]$_0$ applied in the UV/oxidant system. Accordingly, an almost 3-fold lower oxidant utilization was observed at a LOR/oxidant molar ratio of 1/1 in the UV/H$_2$O$_2$ system (10%) compared to the UV/PS system (28%). A further increase in the initial concentration of the oxidant to 200 μM resulted in 20% and 49% of the oxidizing agent consumption after a 2-h oxidation in the UV/H$_2$O$_2$ and UV/PS system, respectively. Overall, the highest PS and H$_2$O$_2$ utilization was observed

Table 2
Residual oxidant concentration and final pH (pH$_F$) at different UV/PS and UV/H$_2$O$_2$ molar ratios ([LOR]$_0$ = 40 μM, t = 2 h).

Process	LOR/[oxidant]$_0$, molar ratio	pH$_0$	pH$_F$	[oxidant]$_0$, % utilized
UV/PS	1/1	6.29	4.13	28
	1/5	6.11	3.62	49
	1/10	6.18	3.21	66
	1/20	6.11	2.92	93
UV/H$_2$O$_2$	1/1	6.24	4.61	10
	1/5	6.12	4.25	20
	1/10	6.01	3.79	55
	1/20	6.16	4.70	81

at a LOR/oxidant molar ratio of 1/20 with 7% and 19% of residual oxidant concentration, respectively.

To assess changes in pH during oxidation of the target compound, the initial (pH$_0$) and final (pH$_F$) were measured for all studied systems (Table 2). The pH drop observed both in UV/PS (pH$_F$ = 3–4.10) and UV/H$_2$O$_2$ systems (pH$_F$ = 4–4.70) was mainly caused by the formation of acidic intermediates and acidity of the oxidizing agents used.

Overall, based on the obtained k_{obs} values, the efficacy of oxidant utilization and TOC removal, it can be assumed that the application of the UV/PS system has the highest potential for the effective degradation of LOR in UW.

3.2. UV/PS/Fe²⁺ and UV/H₂O₂/Fe²⁺ systems for LOR degradation

To further improve the removal of LOR from UW, the dual UV/Fe²⁺ activation of oxidants, corresponding to UV/PS/Fe²⁺ and UV/H₂O₂/Fe²⁺ systems, was evaluated. Accordingly, the UV/Fe²⁺/oxidant systems with oxidants concentrations in the range of 40–800 μM (LOR/oxidant molar ratios were 1/1, 1/5, 1/10, 1/20) were studied. To effect of the concentration of homogeneous ferrous ions on the degradation and mineralization of LOR was studied at $[Fe^{2+}]_0 = 20$–80 μM and at pH_0 of 6.1 ± 0.2.

The dark trials of the PS/Fe²⁺ and H₂O₂/Fe²⁺ system at a LOR/oxidant/Fe²⁺ molar ratio of 1/10/1 resulted in only 28% and 51% of LOR degradation, respectively, after a 2-h treatment. The oxidant utilization was 6 times higher in the PS/Fe²⁺ (~90%) process compared to H₂O₂/Fe²⁺ (~15%) system. However, TOC removal results showed a negligible LOR mineralization in both systems studied.

The effectiveness of the UV/Fe²⁺ system for the degradation of LOR at a LOR/Fe²⁺ molar ratio of 1/1 was also evaluated. Accordingly, the k_{obs} value of 0.118 min⁻¹ and 21% of TOC removal after a 2-h treatment was observed. A comparison of the results of the UV/Fe²⁺ system (Fig. 4) and UV photolysis (Fig. 3) shows that the addition of ferrous ions to the system positively affected the oxidation efficiency of the target compound. The addition of oxidant (PS or H₂O₂) into the UV/Fe²⁺ system led to a further improvement in the decomposition and mineralization of LOR (Fig. 4).

Moreover, as compared to the UV/oxidant systems, higher k_{obs} values and TOC removal were observed in the studied UV/oxidant/Fe²⁺ systems with the same $[oxidant]_0$ used, except TOC at a $[PS]_0 = 800$ μM. Similar to the results of the use of UV/oxidant systems, an increase in the dosage of the oxidant at a fixed activator concentration led to higher k_{obs} values and LOR mineralization extent in the UV/oxidant/Fe²⁺ systems. Accordingly, at the lowest studied initial oxidant concentration of 40 μM, corresponding to a LOR/oxidant/Fe²⁺ molar ratio of 1/1/1, the k_{obs} value was 0.113 min⁻¹ and 0.135 min⁻¹ for the UV/PS/Fe²⁺ and UV/H₂O₂/Fe²⁺ system, respectively. Similarly, the TOC removal result for the UV/PS/Fe²⁺ system was slightly lower (22%) compared with the UV/H₂O₂/Fe²⁺ system (27%). A further 5-fold

increase in the oxidant concentration to 200 μM with a fixed $[Fe^{2+}]_0 = 40$ μM resulted in the k_{obs} value of 0.293 min⁻¹ and 0.279 min⁻¹ for the UV/PS/Fe²⁺ and UV/H₂O₂/Fe²⁺ system, respectively. The highest k_{obs} values of 1.031 min⁻¹ and 0.751 min⁻¹ and around 85% of LOR mineralization were obtained by the application of UV/Fe²⁺- activated PS and H₂O₂ oxidation, respectively, at a LOR/oxidant/Fe²⁺ molar ratio of 1/20/1.

The effect of activator dosage on LOR degradation and TOC removal was also investigated at a fixed LOR/oxidant molar ratio of 1/5 and different LOR/Fe²⁺ molar ratios of 1/0.5, 1/1 and 1/2 (Fig. 4). An increase in the concentration of ferrous ions from 20 to 40 μM improved the removal of the target compound in both systems. However, a further 2-fold increase in the activator concentration was less pronounced in the UV/PS/Fe²⁺ and UV/H₂O₂/Fe²⁺ system, which indicated the need for careful optimization of ferrous ions in order to increase the cost-effectiveness of the UV/oxidant/Fe²⁺ systems.

In order to evaluate the efficiency of radicals generation through the effective activation of oxidants, the residual concentrations of PS and H₂O₂ were measured and the results are presented in Table 3.

The obtained data showed an improvement in the utilization of oxidants with an increase in $[oxidant]_0$ in both systems. Accordingly, the oxidant consumption was 56% and 88% in the UV/Fe²⁺-activated PS and H₂O₂ process, respectively, at a LOR/oxidant/Fe²⁺ molar ratio of 1/1/1. A further increase in $[oxidant]_0$–200 μM improved the oxidant utilization to 91% in the UV/PS/Fe²⁺ system and 95% in the UV/H₂O₂/

Table 3
Residual oxidant concentration and final pH (pH_F) at different UV/PS/Fe²⁺ and UV/H₂O₂/Fe²⁺ molar ratios ($[LOR]_0 = 40$ μM, t = 2 h).

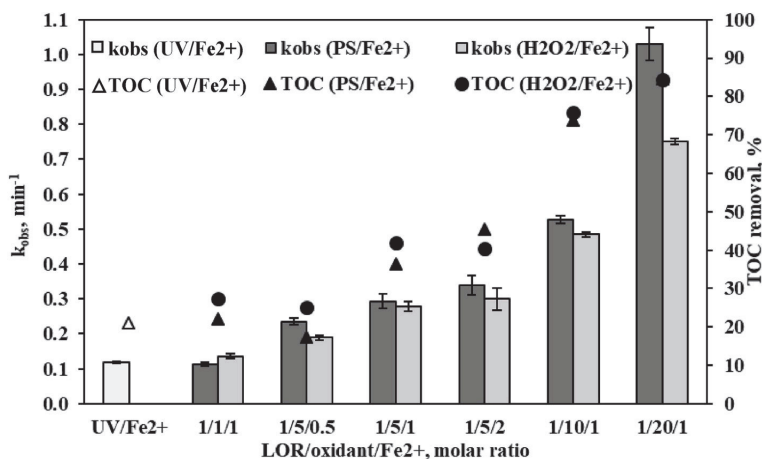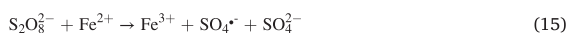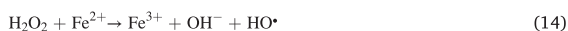| Process	LOR/[oxidant], molar ratio	pH_0	pH_F	[oxidant], % utilized
UV/PS/Fe²⁺	1/1/1	6.24	3.85	56
	1/5/0.5	6.20	3.36	98
	1/5/1	6.24	4.59	91
	1/5/2	6.14	3.42	98
	1/10/1	6.10	3.23	89
	1/20/1	6.03	2.90	96
UV/H₂O₂/Fe²⁺	1/1/1	6.12	4.26	88
	1/5/0.5	6.16	4.38	95
	1/5/1	6.30	4.27	95
	1/5/2	6.04	4.04	96
	1/10/1	6.10	4.36	92
	1/20/1	6.33	4.36	99

Fig. 4. LOR degradation observed reaction rate constants and TOC removal by the UV/Fe²⁺ system ($[Fe^{2+}]_0 = 40$ μM), UV/PS/Fe²⁺ and UV/H₂O₂/Fe²⁺ processes at different LOR/oxidant/Fe²⁺ molar ratios ($[LOR]_0 = 40$ μM, t = 2 h).

Fe^{2+} system. The highest oxidant utilization ˃96% was observed in both systems at a LOR/oxidant/Fe^{2+} molar ratio of 1/20/1. A comparison of the results of the UV/oxidant/Fe^{2+} (Table 3) and UV/oxidant (Table 2) systems shows that the addition of ferrous ions to the system enhanced the utilization of oxidants under the same treatment conditions.

The observed higher efficacy of the UV/oxidant/Fe^{2+} systems compared to the UV/oxidant and oxidant/Fe^{2+} systems in LOR degradation can be explained by the rapid generation of $HO^\bullet$ and $SO_4^{\bullet-}$ radicals using Fe^{2+} as a catalyst according to following Eqs. (14) and (15) and accumulation of iron forming hydroxide complex (Fe^{3+}) (Eq. (16) and (17)). In the case of complete oxidant utilization, Fe^{3+} slowly reduced to Fe^{2+} by the reaction with organic radicals ($R^\bullet$) as shown in Eq. (18) or reduced to Fe^{2+} through photo-Fenton process (19) (Pignatello et al., 2006).

$$H_2O_2 + Fe^{2+} \rightarrow Fe^{3+} + OH^- + HO^\bullet \qquad (14)$$

$$S_2O_8^{2-} + Fe^{2+} \rightarrow Fe^{3+} + SO_4^{\bullet-} + SO_4^{2-} \qquad (15)$$

$$SO_4^{\bullet-} + Fe^{2+} \rightarrow Fe^{3+} + SO_4^{2-} \qquad (16)$$

$$HO^\bullet + Fe^{2+} \rightarrow Fe^{3+} + OH^- \qquad (17)$$

$$R^\bullet + Fe^{3+} \rightarrow Fe^{2+} + \text{intermediates} \qquad (18)$$

$$Fe^{3+} + H_2O + h\nu \rightarrow Fe^{2+} + HO^\bullet + H^+ \qquad (19)$$

The measured pH_F of the solutions treated by both UV/oxidant/Fe^{2+} systems was around 3, mainly due to the acidity of the activator and oxidant as well as the formation of acidic intermediates during the degradation of LOR.

Overall, the UV/Fe^{2+}-activated PS system proved to be more effective than the UV/H_2O_2/Fe^{2+} system at elevated oxidant concentrations. Nevertheless, both UV/oxidant/Fe^{2+} systems can be considered promising methods for removing LOR from UW. Notably, to quantify the interaction between different processes in combined systems, such as UV/PS/Fe^{2+} and UV/H_2O_2/Fe^{2+}, the degree of synergy (S) was calculated based on the methodology proposed by (Frontistis, 2018) and resulted in 43.5% and 38.5%, respectively (Table S2).

3.3. Identification of active radical species

It is well known fact that in certain conditions, the generated $SO_4^{\bullet-}$ can convert to $HO^\bullet$ radicals (Tsitonaki et al., 2010). Thus as shown in Eqs. (9) and (10), both $SO_4^{\bullet-}$ and $HO^\bullet$ radicals can be predominant at neutral pH in the activated PS systems. In order to identify the predominant oxidative species and gain a further understanding of the reaction mechanism of LOR degradation by the UV/PS and UV/PS/Fe^{2+} processes, scavenging studies using two radical probes were carried out. The trials were conducted with the addition of TBA, which is more effective scavenger for $HO^\bullet$ (3.8–7.6) $\times$ 10^8 M^{-1} s^{-1} than for $SO_4^{\bullet-}$ (4–9.1) $\times$ 10^5 M^{-1} s^{-1}, and EtOH, reacting at comparable rates with $SO_4^{\bullet-}$ (1.6–7.7) $\times$ 10^7 M^{-1} s^{-1} and $HO^\bullet$ (1.2–2.8) $\times$ 10^9 M^{-1} s^{-1} (Anipsitakis and Dionysiou, 2004). Based on these characteristics, the presence of $HO^\bullet$ was identified by adding an excess of TBA to the UV photolysis, UV/PS and UV/PS/Fe^{2+} systems. The effect of sulfate radicals was evaluated by comparing the differences between the LOR degradation efficacy after adding an excess of TBA and EtOH to the UV/PS and UV/PS/Fe^{2+} systems.

As shown in Table 4, the addition of excess TBA decreased the efficiency of LOR degradation by 32% and 25% in the UV/PS and UV/PS/Fe^{2+} system, respectively, indicating the active participation of $HO^\bullet$ in the oxidation process.

On the other hand, the addition of excess EtOH substantially inhibited the decomposition of LOR in the UV/PS (50%) and UV/PS/Fe^{2+} (52%) system, which, in turn, indicated the important role of sulfate radicals in the degradation of the target compound. The remaining amount of LOR decomposition after adding excess EtOH was most likely

Table 4
Degradation of LOR by the UV photolysis, UV/PS and UV/PS/Fe^{2+} systems ($[LOR]_0 = [Fe^{2+}]_0 = 40$ μM, $[PS]_0 = 200$ μM, $[TBA]_0 = [EtOH]_0 = 20$ mM, $t = 7$ min).

Process	$[LOR]_t/[LOR]_0$,%		
	Without scavenger	TBA	EtOH
UV	54	29	–
UV/PS	78	46	28
UV/PS/Fe^{2+}	92	67	40

due to the presence of other reactive oxygen species in the studied systems.

The findings of scavenging studies suggested that both $SO_4^{\bullet-}$ and $HO^\bullet$ contributed to the degradation of LOR in the UV/PS/Fe^{2+} system, while hydroxyl radicals proved more dominant oxidative species in the UV/PS system.

3.4. Effect of water matrix on LOR oxidation

To evaluate the applicability of the studied systems to remove LOR from real water matrices, some experiments were repeated in groundwater samples artificially contaminated with LOR (40 μM). Accordingly, the most promising and cost-effective treatment conditions selected based on the results obtained in the UW trials, namely $[PS]_0 = [H_2O_2]_0 = 400$ μM and $[Fe^{2+}]_0 = 40$ μM, were studied in GW (pH$_0$ = 7.71 ± 0.2).

As shown in Fig. 5, LOR degradation in GW by the direct UV photolysis was more efficient than in UW and resulted in the k_{obs} value of 0.106 min^{-1} along with 25% of TOC removal. As shown in Table 1, the chloride anions present in the groundwater matrix can generate additional radicals by reacting with available hydroxyl radicals (Eqs. 20–24) to promote LOR and formed intermediates degradation.

$$HO^\bullet + Cl^- \rightarrow HOCl^- \rightarrow Cl^\bullet + HO^- \qquad (20)$$

$$Cl^- + Cl^\bullet \rightarrow Cl_2^{\bullet-} \qquad (21)$$

$$Cl^\bullet + H_2O \rightarrow HO^\bullet + HCl \qquad (22)$$

$$Cl_2^{\bullet-} + H_2O \rightarrow HO^\bullet + Cl^- + H^+ \qquad (23)$$

$$Cl_2^{\bullet-} + HO^- \rightarrow HO^\bullet + 2Cl^- \qquad (24)$$

In contrast, the application of UV- and UV/Fe^{2+}-activated PS and H_2O_2 systems resulted in slower LOR degradation with the same oxidant concentrations as compared with UW trials results suggesting inhibitory effect of water matrix of the studied AOPs efficacy. For example, k_{obs} of 0.152 min^{-1} and 0.192 min^{-1} were obtained in GW during the UV/PS/Fe^{2+} and UV/H_2O_2/Fe^{2+} oxidation, respectively, compared to 0.526 min^{-1} and 0.485 min^{-1} in UW. Similarly, the TOC removal was 32/74% and 30/76% after a 2-h UV/PS/Fe^{2+} and UV/H_2O_2/Fe^{2+} oxidation, respectively, in GW/UW.

Notably, no improvement in LOR degradation was observed with the addition of ferrous ion activator to the UV/PS and UV/H_2O_2 systems in GW. Accordingly, the obtained k_{obs} values were 0.159 min^{-1} and 0.152 min^{-1} for the UV/PS and UV/PS/Fe^{2+} system, respectively. In the case of the UV/H_2O_2 and UV/H_2O_2/Fe^{2+} oxidation, a slight decrease in the k_{obs} value from 0.214 min^{-1} to 0.192 min^{-1} was observed. In general, the results obtained in the UV/Fe^{2+}-activated PS and H_2O_2 systems indicate a strong impact of the buffered groundwater matrix on the efficiency of radical formation mainly due to the removal of the activator from the system by precipitation in the form of ferric hydroxide complex. This assumption is confirmed by the fact that in all GW experiments only a slight change in pH$_F$ value was observed, for example, pH$_F$ = 7.7 ± 0.1 for UV photolysis and pH$_F$ = 7.1 ± 0.2 for UV(/Fe^{2+})-activated systems. In addition, moderate (in the range of 54–66%) utilization of oxidants was obtained after 2 h of treatment by the studied systems.
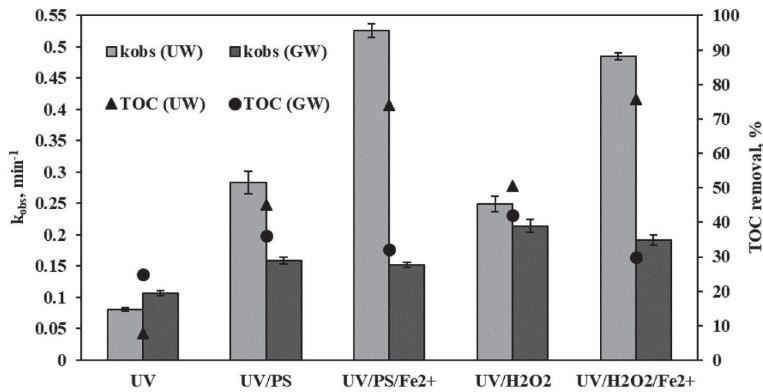
Fig. 5. LOR degradation observed reaction rate constants and TOC removal by the UV photolysis, UV/PS, UV/PS/Fe^{2+}, UV/H$_2$O$_2$ and UV/H$_2$O$_2$/Fe^{2+} processes in different water matrices ([LOR]$_0$ = [Fe^{2+}]$_0$ = 40 μM, [PS]$_0$ = [H$_2$O$_2$]$_0$ = 400 μM).

The observed lower LOR degradation efficiency in the GW matrix can also be explained by the influence of natural organic matter (NOM), which is ubiquitous in natural water. NOM is a well-known absorber of UV radiation and competes with the generated radicals, as shown in Eqs. (25) and (26), to produce reactive intermediates, thereby reducing the target compound degradation efficiency.

$$NOM + SO_4^{\bullet -} \rightarrow products \tag{25}$$

$$NOM + HO^{\bullet} \rightarrow products \tag{26}$$
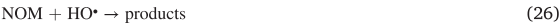
Moreover, the inorganic anions such as carbonate (CO$_3^{2-}$) and bicarbonate (HCO$_3^-$) present in natural water may act as radical scavenger and generate less reactive carbonate radicals as shown in Eq. (27–30).

$$SO_4^{\bullet -} + CO_3^{2-} \rightarrow CO_3^{\bullet -} + SO_4^{2-} \tag{27}$$

$$HO^{\bullet} + CO_3^{2-} \rightarrow CO_3^{\bullet -} + OH^- \tag{28}$$

$$SO_4^{\bullet -} + HCO_3^- \rightarrow CO_3^{\bullet -} + SO_4^{2-} + H^+ \tag{29}$$

$$HO^{\bullet} + HCO_3^- \rightarrow CO_3^{\bullet -} + H_2O \tag{30}$$

Finally, to assess the economic feasibility of the applied treatment systems, the operating costs were calculated (Table S1). Irrespective of the water matrices studied, the UV/oxidant(/Fe^{2+}) systems were more cost-effective for LOR degradation that direct UV photolysis. While the operational costs of the UV/H$_2$O$_2$(/Fe^{2+}) systems were lower compared to the UV/PS(/Fe^{2+}) systems under the same treatment conditions.

3.5. Identification of transformation products and their acute toxicity

In addition to the efficacy of decomposition and mineralization of the target compound, the transformation products (TPs) were identified during the oxidation of LOR by the UV/PS, UV/H$_2$O$_2$, UV/PS/Fe^{2+}, and UV/H$_2$O$_2$/Fe^{2+} systems using LC-MS analysis and are presented in Table 5. Due to the higher response in the positive mode for both LOR and TPs, a positive ESI mode was used in the MS analysis.

According to the results of the radical scavenging studies, both SO$_4^{\bullet -}$ and HO$^{\bullet}$ were responsible for the decomposition of LOR in the UV/PS and UV/PS/Fe^{2+} systems. Nevertheless, the identified TPs were similar for the studied activated persulfate and hydrogen peroxide oxidation processes. Regardless of the oxidation system used, the initial step in the decomposition of LOR was presumably the reaction between HO$^{\bullet}$ and the alcohol moiety of LOR with the formation of TP1 (Serna-Galvis et al., 2019). With a high probability, the primary TP may also be formed by addition of HO$^{\bullet}$ to the carbon double bond, forming several isomers of biphenyl hydroxylation (TP2) (Martínez-Pachón et al., 2019), or by

Table 5
Proposed structures of transformation products for the degradation of LOR by the UV/PS, UV/PS/Fe^{2+}, UV/H$_2$O$_2$ and UV/H$_2$O$_2$/Fe^{2+} processes by LC-MS analysis.

Compound	MS (m/z)/MW (g mol^{-1})	Proposed elemental composition	Reaction pathway proposed	Chemical structure proposed
TP1	421/420	C$_{22}$H$_{22}$N$_6$OCl	Alcohol moiety oxidation	
TP2	439/438	C$_{22}$H$_{24}$N$_6$O$_2$Cl	Isomer of biphenyl hydroxylation	
TP3	439/438	C$_{22}$H$_{24}$N$_6$O$_2$Cl	Hydroxylation/oxidation of alkyl chain	
TP4	437/436	C$_{22}$H$_{20}$N$_6$O$_2$Cl	Hydroxylation/oxidation of alkyl chain	
TP5	389/388	C$_{22}$H$_{24}$N$_6$O	Removal of chlorine	
TP6	394/393	C$_{21}$H$_{24}$N$_5$O$_3$	Hydroxylation of carbon in the imidazole ring	
TP7	335/334	C$_{19}$H$_{23}$N$_6$	Opening of imidazole ring	
TP8	336/335	C$_{19}$H$_{22}$N$_5$O	Opening of imidazole ring	

hydroxylation of the alkyl chain (TP3) followed by its oxidation (TP4) (Gao et al., 2016). TP5 is formed by the removal of chlorine, and the hydroxylation of carbon atoms 2 and 5 in the imidazole ring leads to the formation of TP6. Similarly, TP7 and TP8 are isomers formed from the opening of the imidazole ring (Carpinteiro et al., 2019). All the identified TPs were previously reported in the literature as the LOR degradation intermediates by other AOPs.

Further, to assess the formation of toxic intermediates, the acute toxicity of LOR aqueous solutions treated by the UV/PS/Fe^{2+} and UV/H_2O_2/Fe^{2+} system at a LOR/oxidant/Fe^{2+} molar ratio of 1/5/1 was studied. Accordingly, a *Vibrio fischeri* bioluminescence inhibition assay was used to evaluate ecotoxicity. The EC_{20} of the initial LOR solution was low (55.6% of the sample). The application of UV/H_2O_2/Fe^{2+} treatment led to detoxification of the LOR solution (EC_{20} at >100% of the solution). On the other hand, the sample treated with the UV/PS/Fe^{2+} system showed an increase in the inhibition of *Vibrio fischeri* bioluminescence (EC_{20} at 16.5% of the solution). This observation can be explained by the toxic effect of residual PS concentration in the system (Moreno-Andrés et al., 2019). Therefore, unused PS must be removed from treated water/wastewater prior to discharge into receiving water bodies.

4. Conclusions

This study examined the application of UV(/Fe^{2+})-activated PS and H_2O_2 processes for LOR degradation and mineralization in aqueous solution. The addition of Fe^{2+} substantially improved the LOR removal by the UV/oxidant/Fe^{2+} processes compared to UV/oxidant systems. The overall efficacy in the target compound degradation and mineralization was as follows: UV/PS/Fe^{2+} system ˃ UV/H_2O_2/Fe^{2+} system ˃ UV/PS system ˃ UV/H_2O_2 system. Regardless of the system used, LOR mineralization was incomplete. The highest k_{obs} values obtained in the UV/oxidant/Fe^{2+} at a LOR/oxidant/Fe^{2+} molar ratio of 1/20/1 were 1.031 min^{-1} and 0.751 min^{-1} along with 85% and 84% TOC removal for PS and H_2O_2, respectively. The composition of GW matrix showed an inhibitory effect on the decomposition of LOR by the studied UV- and UV/Fe^{2+}-activated PS and H_2O_2 systems. The results of radical scavenging studies suggested that $HO^•$ and $SO_4^{•-}$ contributed to the degradation of LOR in the UV/PS and UV/PS/Fe^{2+} systems. The transformation products of LOR oxidation by the studied systems were identified and the ecotoxicity of treated LOR solutions to *Vibrio fischeri* was assessed. The findings of this study provide valuable information for practicable application of UV(/Fe^{2+})-activated PS and H_2O_2 processes for the degradation of LOR in water/wastewater and groundwater.

CRediT authorship contribution statement

Balpreet Kaur: Validation, Formal analysis, Investigation, Writing - original draft, Writing - review & editing, Visualization. **Niina Dulova:** Conceptualization, Methodology, Validation, Formal analysis, Writing - original draft, Resources, Writing - review & editing, Visualization, Supervision, Project administration, Funding acquisition.

Acknowledgements

Appendix A. Supplementary data

Supplementary data to this article can be found online at https://doi.org/10.1016/j.jenvman.2020.110170.

References

Anipsitakis, G.P., Dionysiou, D.D., 2004. Radical generation by the interaction of transition metals with common oxidants. Environ. Sci. Technol. 38, 3705–3712. https://doi.org/10.1021/es035121o.

Ashfaq, M., Li, Y., Wang, Y., Chen, W., Wang, H., Chen, X., Wu, W., Huang, Z., Yu, C.-P., Sun, Q., 2017. Occurrence, fate, and mass balance of different classes of pharmaceuticals and personal care products in an anaerobic-anoxic-oxic wastewater treatment plant in Xiamen, China. Water Res. 123, 655–667. https://doi.org/10.1016/j.watres.2017.07.014.

Azuma, T., Otomo, K., Kunitou, M., Shimizu, M., Hosomaru, K., Mikata, S., Ishida, M., Hisamatsu, K., Yunoki, A., Mino, Y., Hayashi, T., 2019a. Environmental fate of pharmaceutical compounds and antimicrobial-resistant bacteria in hospital effluents, and contributions to pollutant loads in the surface waters in Japan. Sci. Total Environ. 657, 476–484. https://doi.org/10.1016/j.scitotenv.2018.11.433.

Azuma, T., Otomo, K., Kunitou, M., Shimizu, M., Hosomaru, K., Mikata, S., Mino, Y., Hayashi, T., 2019b. Removal of pharmaceuticals in water by introduction of ozonated microbubbles. Separ. Purif. Technol. 212, 483–489. https://doi.org/10.1016/j.seppur.2018.11.059.

Blum, K.M., Gallampois, C., Andersson, P.L., Renman, G., Renman, A., Haglund, P., 2019. Comprehensive assessment of organic contaminant removal from on-site sewage treatment facility effluent by char-fortified filter beds. J. Hazard Mater. 361, 111–122. https://doi.org/10.1016/j.jhazmat.2018.08.009.

Botero-Coy, A.M., Martínez-Pachón, D., Boix, C., Rincón, R.J., Castillo, N., Arias-Marín, L.P., Manrique-Losada, L., Torres-Palma, R., Moncayo-Lasso, A., Hernández, F., 2018. An investigation into the occurrence and removal of pharmaceuticals in Colombian wastewater'. Sci. Total Environ. 642, 842–853. https://doi.org/10.1016/j.scitotenv.2018.06.088.

Carpinteiro, I., Castro, G., Rodríguez, I., Cela, R., 2019. Free chlorine reactions of angiotensin II receptor antagonists: kinetics study, transformation products elucidation and in-silico ecotoxicity assessment. Sci. Total Environ. 647, 1000–1010. https://doi.org/10.1016/j.scitotenv.2018.08.082.

Casado, J., Rodríguez, I., Ramil, M., Cela, R., 2014. Selective determination of antimycotic drugs in environmental water samples by mixed-mode solid-phase extraction and liquid chromatography quadrupole time-of-flight mass spectrometry. J. Chromatogr. A 1339, 42–49. https://doi.org/10.1016/j.chroma.2014.02.087.

Cortez, F.S., Souza, L. da S., Guimarães, L.L., Almeida, J.E., Pusceddu, F.H., Maranho, L. A., Mota, L.G., Nobre, C.R., Moreno, B.B., Abessa, D.M. de S., Cesar, A., Santos, A.R., Pereira, C.D.S., 2018. Ecotoxicological effects of losartan on the brown mussel Perna perna and its occurrence in seawater from Santos Bay (Brazil). Sci. Total Environ. 637–638, 1363–1371. https://doi.org/10.1016/j.scitotenv.2018.05.069.

Dimitriadou, S., Frontistis, Z., Petala, A., Bampos, G., Mantzavinos, D., 2019. Carbocatalytic activation of persulfate for the removal of drug diclofenac from aqueous matrices. Catal. Today. https://doi.org/10.1016/j.cattod.2019.02.025.

Dulova, N., Trapido, M., 2011. Application of fenton's reaction for food-processing wastewater treatment. J. Adv. Oxid. Technol. 14 https://doi.org/10.1515/jaots-2011-0101.

Eisenberg, G., 1943. Colorimetric determination of hydrogen peroxide. Ind. Eng. Chem. Anal. Ed. 15, 327–328. https://doi.org/10.1021/i560117a011.

Frontistis, Z., 2018. Degradation of the nonsteroidal anti-inflammatory drug piroxicam by iron persulfate: the role of water matrix and ultrasound synergy. Int. J. Environ. Res. Publ. Health 15, 2600. https://doi.org/10.3390/ijerph15112600.

Gao, Y., Ji, Y., Li, G., An, T., 2016. Theoretical investigation on the kinetics and mechanisms of hydroxyl radical-induced transformation of parabens and its consequences for toxicity: influence of alkyl-chain length. Water Res. https://doi.org/10.1016/j.watres.2015.12.056.

ISO (International Organization for Standardization), 2007. Water Quality-Determination of the Inhibitory Effect of Water Samples on Te Light Emission of vibrio Fischeri (Luminescent Bacteria Test)- Part 3: Method Using Freeze-Dried Bacteria. ISO 11348-32007.

Kahru, A., Kurvet, M., Külm, I., 1996. Toxicity of phenolic wastewater to luminescent bacteria and activated sludges. Water Sci. Technol. 33 https://doi.org/10.1016/0273-1223(96)00291-0.

Kern, S., Baumgartner, R., Helbling, D.E., Hollender, J., Singer, H., Loos, M.J., Schwarzenbach, R.P., Fenner, K., 2010. A tiered procedure for assessing the formation of biotransformation products of pharmaceuticals and biocides during activated sludge treatment. J. Environ. Monit. 12, 2100. https://doi.org/10.1039/c0em00238k.

Kulik, N., Panova, Y., Trapido, M., 2007. The Fenton chemistry and its combination with coagulation for treatment of dye solutions. In: Separation Science and Technology. https://doi.org/10.1080/01496390701290185.

Lado Ribeiro, A.R., Moreira, N.F.F., Li Puma, G., Silva, A.M.T., 2019. Impact of water matrix on the removal of micropollutants by advanced oxidation technologies. Chem. Eng. J. 363, 155–173. https://doi.org/10.1016/j.cej.2019.01.080.

Liang, C., Huang, C.-F., Mohanty, N., Kurakalva, R.M., 2008. A rapid spectrophotometric determination of persulfate anion in ISCO. Chemosphere 73, 1540–1543. https://doi.org/10.1016/j.chemosphere.2008.08.043.

Mandaric, L., Diamantini, E., Stella, E., Cano-Paoli, K., Valle-Sistac, J., Molins-Delgado, D., Bellin, A., Chiogna, G., Majone, B., Diaz-Cruz, M.S., Sabater, S., Barcelo, D., Petrovic, M., 2017. Contamination sources and distribution patterns of pharmaceuticals and personal care products in Alpine rivers strongly affected by tourism. Sci. Total Environ. 590–591, 484–494. https://doi.org/10.1016/j.scitotenv.2017.02.185.

Martínez-Pachón, D., Espinosa-Barrera, P., Rincón-Ortíz, J., Moncayo-Lasso, A., 2019. Advanced oxidation of antihypertensives losartan and valsartan by photo-electro-Fenton at near-neutral pH using natural organic acids and a dimensional stable

anode-gas diffusion electrode (DSA-GDE) system under light emission diode (LED) lighting. Environ. Sci. Pollut. Res. 26, 4426–4437. https://doi.org/10.1007/s11356-018-2645-3.

Matzek, L.W., Carter, K.E., 2016. Activated persulfate for organic chemical degradation: a review. Chemosphere 151, 178–188. https://doi.org/10.1016/j.chemosphere.2016.02.055.

Moreno-Andrés, J., Farinango, G., Romero-Martínez, L., Acevedo-Merino, A., Nebot, E., 2019. Application of persulfate salts for enhancing UV disinfection in marine waters. Water Res. https://doi.org/10.1016/j.watres.2019.114866.

Muter, O., Perkons, I., Svinka, V., Svinka, R., Bartkevics, V., 2017. Distinguishing the roles of carrier and biofilm in filtering media for the removal of pharmaceutical compounds from wastewater. Process Saf. Environ. Protect. 111, 462–474. https://doi.org/10.1016/j.psep.2017.08.010.

Nödler, K., Hillebrand, O., Idzik, K., Strathmann, M., Schiperski, F., Zirlewagen, J., Licha, T., 2013. Occurrence and fate of the angiotensin II receptor antagonist transformation product valsartan acid in the water cycle – a comparative study with selected β-blockers and the persistent anthropogenic wastewater indicators carbamazepine and acesulfame. Water Res. 47, 6650–6659. https://doi.org/10.1016/j.watres.2013.08.034.

Nuel, M., Laurent, J., Bois, P., Heintz, D., Wanko, A., 2018. Seasonal and ageing effect on the behaviour of 86 drugs in a full-scale surface treatment wetland: removal efficiencies and distribution in plants and sediments. Sci. Total Environ. 615, 1099–1109. https://doi.org/10.1016/j.scitotenv.2017.10.061.

Padmanabhan, S., Newton-Cheh, C., Dominiczak, A.F., 2012. Genetic basis of blood pressure and hypertension. Trends Genet. 28, 397–408. https://doi.org/10.1016/j.tig.2012.04.001.

Pignatello, J.J., Oliveros, E., MacKay, A., 2006. Advanced oxidation processes for organic contaminant destruction based on the fenton reaction and related chemistry. Crit. Rev. Environ. Sci. Technol. 36, 1–84. https://doi.org/10.1080/10643380500326564.

Salazar, C., Contreras, N., Mansilla, H.D., Yáñez, J., Salazar, R., 2016. Electrochemical degradation of the antihypertensive losartan in aqueous medium by electro-oxidation with boron-doped diamond electrode. J. Hazard Mater. 319, 84–92. https://doi.org/10.1016/j.jhazmat.2016.04.009.

Serna-Galvis, E.A., Isaza-Pineda, L., Moncayo-Lasso, A., Hernández, F., Ibáñez, M., Torres-Palma, R.A., 2019. Comparative degradation of two highly consumed antihypertensives in water by sonochemical process. Determination of the reaction zone, primary degradation products and theoretical calculations on the oxidative process. Ultrason. Sonochem. 58, 104635. https://doi.org/10.1016/j.ultsonch.2019.104635.

Tsitonaki, A., Petri, B., Crimi, M., Mosbk, H., Siegrist, R.L., Bjerg, P.L., 2010. In situ chemical oxidation of contaminated soil and groundwater using persulfate: a review. Crit. Rev. Environ. Sci. Technol. https://doi.org/10.1080/10643380802039303.

Wang, Yuwen, Li, Y., Hu, A., Rashid, A., Ashfaq, M., Wang, Yinhan, Wang, H., Luo, H., Yu, C.-P., Sun, Q., 2018. Monitoring, mass balance and fate of pharmaceuticals and personal care products in seven wastewater treatment plants in Xiamen City, China. J. Hazard Mater. 354, 81–90. https://doi.org/10.1016/j.jhazmat.2018.04.064.

Zhou, D., Dong, S., Ki, D., Rittmann, B.E., 2018. Photocatalytic-induced electron transfer via anode-respiring bacteria (ARB) at an anode that intimately couples ARB and a TiO2 photocatalyst. Chem. Eng. J. 338, 745–751. https://doi.org/10.1016/j.cej.2018.01.094.

RESEARCH ARTICLE

Insights into nonylphenol degradation by UV-activated persulfate and persulfate/hydrogen peroxide systems in aqueous matrices: a comparative study

Balpreet Kaur[1] · Eneliis Kattel[1] · Niina Dulova[1]

Abstract

Nonylphenol ethoxylates are widely used industrial surfactants. Once released into environment compartments, these chemicals undergo degradation and generate more toxic short chain artificial compound nonylphenol (NP). The latter is a known endocrine disrupting compound and persistent micropollutant. In the present study, the performance of NP degradation in UV-induced PS, PS/Fe^{2+}, PS/H$_2$O$_2$, and PS/H$_2$O$_2$/Fe^{2+} systems was examined. The effect of concentration of oxidant and activators on the efficiency of target compound decomposition was studied. The trials were conducted in ultrapure water and groundwater to assess the influence of matrix composition. The obtained results indicated that NP degradation by all the systems studied followed a pseudo-first-order kinetics. The application of UV-activated PS at lower concentrations of the oxidant improved NP oxidation in both water matrices. The addition of iron activator at a cost-effective concentration showed slight improvement in the studied PS-based systems. The application of UV-induced dual oxidant PS/H$_2$O$_2$ system demonstrated promising results in NP oxidation. In turn, the addition of Fe^{2+} to the UV/PS/H$_2$O$_2$ system accelerated the target compound oxidation at an optimized dose of iron activator. The radicals scavenging studies indicated that HO$^\bullet$ was the predominant radical in all UV-induced PS-based systems. The results of this research could provide significant information for the removal of NP from different water matrices by means of UV-induced persulfate-based oxidation processes.

Keywords Endocrine disrupting compound · Persulfate oxidation · Fenton process · Photo-Fenton process · Groundwater

Introduction

The rapid expansion of agricultural and industrial areas has led to an extensive use of synthetic organic contaminants. Nonylphenol ethoxylates (NPEs) are one such common phenolic ring containing non-ionic surfactants used as emulsifiers, detergents, dispersants, lubricants, etc. contributing to 60% of total surfactant market (Loyo-Rosales et al. 2010).

NPEs end up in wastewater treatment plants (WWTPs) or directly into the environment from industrial discharges. Moreover, further aerobic and anaerobic degradation of NPEs in the environment or at WWTPs can generate more toxic short chain, synthetic compounds such as nonylphenol (NPs), nonylphenol ethoxylate (NP1EO), nonylphenol diethoxylate (NP2EO), and nonylphenoxyacetic acid (NP2EC) (Ying et al. 2002). Previous studies have indicated the toxic and carcinogenic effect of NPs, which mimic natural hormones estrogen and are responsible for the multiplication of breast cancer cells as well as the hormonal disruption in animals (Guenther et al. 2002; Lee and Lee 1996). NPs were listed as priority pollutant in the European Union Water Framework Directive in 2001 as a result the production and use of NPs was restricted (Bertanza et al. 2011). The application of conventional treatment methods such as physical and chemical proved inefficient for NPs degradation in different water matrices. Moreover, biological treatment usually results in incomplete degradation of NPs due to limited oxygen supply and bioavailability (Giger et al. 1984; Hesselsøe et al.

✉ Balpreet Kaur
   bakaur@taltech.ee

✉ Niina Dulova
   niina.dulova@taltech.ee

[1] Department of Materials and Environmental Technology, Tallinn University of Technology, Ehitajate tee 5, 19086 Tallinn, Estonia

2001). NPs are persistent pollutants that have endocrine disruptive properties, and bioaccumulation of which leads to their constant detection in the natural environment, which requires efficient technologies for removing NPs from effluents entering the environment.

Great attention has been paid to advanced oxidation technologies (AOTs) for the degradation of contaminants, since they are relatively fast and cost-effective compared with other used processes of chemical, physical, and biological treatment. Typically, AOTs comprise application of various systems or combination of systems based on ozone (O_3), hydrogen peroxide (H_2O_2), and persulfate (PS). These technologies have been implemented to decompose various organic pollutants by generating hydroxyl ($HO^\bullet$) and sulfate radicals ($SO_4^{\bullet-}$) from strong oxidants using different activators, such as transition metals, UV, and ultrasound radiation (Kulik et al. 2007; Pignatello et al. 2006; Takdastan et al. 2018, Waclawek et al. 2017).

Notably, hydroxyl radicals ($E^0 = 2.73$) generated, for example, by photocatalytic dissociation of H_2O_2 in aqueous matrices (Eq. 1) have high reaction rates and involve in nonselective oxidation making $HO^\bullet$-AOT, a promising system for multiple contaminants degradation (Litter and Quici 2010).

$$H_2O_2 + h\upsilon \rightarrow 2HO^\bullet \tag{1}$$

The widely studied $HO^\bullet$-AOTs system, the classical Fenton process, involves Fe^{2+} as a catalyst and generates $HO^\bullet$ from H_2O_2 according to Eq. (2). According to Eq. (3), the reduction of Fe^{3+} by hydrogen peroxide allows the regeneration of activator (Pignatello et al. 2006).

$$Fe^{2+} + H_2O_2 \rightarrow Fe^{3+} + OH^- + HO^\bullet \tag{2}$$

$$Fe^{3+} + H_2O_2 \rightarrow Fe^{2+} + HO_2^\bullet + H^+ \tag{3}$$
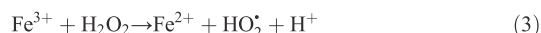
The generated Fe^{3+} can be reduced to Fe^{2+} through photo-Fenton process (Eq. 4) (Pignatello et al. 2006).

$$Fe^{3+} + H_2O + h\upsilon \rightarrow Fe^{2+} + HO^\bullet + H^+ \tag{4}$$

However, the conventional Fenton system has limitations, such as operation at a narrow pH and formation of iron sludge, which demands optimization of oxidant and activators dose (Babuponnusami and Muthukumar 2014; Dulova and Trapido 2011; Liu et al. 2018).

Over the last decade, technologies based on sulfate radicals ($SO_4^{\bullet-}$-AOTs) have received much attention. The sulfate radicals have a high oxidation-reduction potential ($E^0 = 2.5$–3.1 V) and are comparatively stable in aqueous matrices as well as selective for oxidizing of the contaminants (Matzek and Carter 2016). The common $SO_4^{\bullet-}$ precursor persulfate (PS, $E^0 = 2.01$ V) can directly react with organic contaminants; however, degree of removal is lower comparing with

the activated persulfate (Eq. 5) (Matzek and Carter 2016).

$$S_2O_8^{2-} + activator \rightarrow SO_4^{\bullet-} + \left(SO_4^{\bullet-} \text{ or } SO_4^{2-} \right) \tag{5}$$
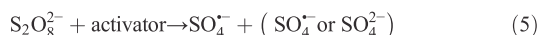
For example, activation of PS via heat (Eq. 6), UV (Eq. 7), or ultrasound radiation, generates two sulfate radicals by cleavage of the peroxide bond (Waldemer et al. 2007).

$$S_2O_8^{2-} + energy \rightarrow 2SO_4^{\bullet-} \tag{6}$$

$$S_2O_8^{2-} + h\upsilon \rightarrow 2SO_4^{\bullet-} \tag{7}$$

The most widely studied transition metal for $SO_4^{\bullet-}$ generation, iron in its ferrous form (Fe^{2+}) (Eq. 8), is comparatively cheap, non-toxic, and more environment friendly than other transition metals (Waclawek et al. 2017). The iron concentration is important parameter in the PS/Fe^{2+} system as an insufficient amount of iron can lead to a lower persulfate consumption while sulfate radical scavenging occurs at a higher concentration of activator finally decreasing effectiveness of the system (Hori et al. 2005).

$$S_2O_8^{2-} + Fe^{2+} \rightarrow Fe^{3+} + SO_4^{\bullet-} + SO_4^{2-} \tag{8}$$
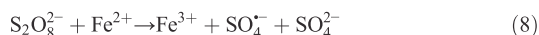
Recently, AOTs, such as ultra-sonication (ElShafei et al. 2017; Ince et al. 2009; Yim et al. 2003), ozonation (Kim et al. 2005), combined ozonation-electrooxidation (Barrera-Díaz et al. 2018) and, photochemical oxidation (Dulov et al. 2013; Naya et al. 2013), have been successfully applied for the degradation of NPs in different water matrices. Additionally, numerous studies proved that photo-Fenton systems can be effectively used to degrade toxic compounds such as pharmaceutically active compounds (PhACs) (Kümmerer 2009), phenols (Messele et al. 2012), and nonylphenol ethoxylates (Karci et al. 2013). However, there is limited literature on the use of UV-activated PS-based systems to decompose NPs in water matrices.

Therefore, the aim of the present study was to investigate and compare the efficiency of UV and/or Fe^{2+}-assisted PS and PS/H_2O_2 system in NP degradation. The effect of operating parameters such as pH, activator dosage, and oxidant concentration was evaluated in ultrapure water (UW) and compared with the results obtained in groundwater (GW). To the best of our knowledge, the application and comparison of the efficiencies of selected AOTs have not been previously studied for the removal of NPs from water matrices.

Materials and methods

Chemicals and materials

4-n-Nonylphenol ($C_{15}H_{24}O$, $\geq 99\%$, molecular weight 220.356 g mol^{-1}), sodium persulfate ($Na_2S_2O_8$, $\geq 99\%$), hydrogen peroxide (H_2O_2, PERDROGEN™, $\geq 30\%$), ferrous

sulfate heptahydrate (FeSO$_4$·7H$_2$O, ≥ 99%), potassium iodide (KI, ≥ 99%), sodium hydrogen carbonate (NaHCO$_3$, 99%), humic acid sodium salt (C$_9$H$_8$Na$_2$O$_4$, tech. 50–60% as humic acid), sodium chloride (NaCl, ≥ 99%), sodium sulfite (Na$_2$SO$_3$, ≥ 98%), sodium hydroxide (NaOH, ≥ 98%), and sulfuric acid (H$_2$SO$_4$, 95–98%) were purchased from Sigma-Aldrich. Acetonitrile (CH$_3$CN, LiChrosolv®), formic acid (CH$_2$O$_2$, 99%), ethanol (C$_2$H$_6$O, EtOH, 99%), tert-butyl alcohol ((CH$_3$)$_3$COH, t-BuOH, ≥ 99%), and methanol (CH$_4$O, > 99%) were obtained from Merck KGaA.

All the chemicals were of analytical grade used without further purification. The solutions were prepared in ultrapure water (Millipore Simplicity®UV System, Merck) or in twice-distilled water (~ 18.2 MΩ cm). A stock NP solution of 4.54 mM was prepared in 100-mL methanol and stored in the dark at 4 °C. The working solutions with initial NP concentration of 50 μM were prepared by dilution of the stock in twice-distilled water. The solution was stirred until complete NP dissolution.

Properties of groundwater

Groundwater was collected from a 19-m borehole (Harjumaa, Estonia) and used without preceding purification as a real aqueous matrix for NP degradation. The groundwater samples were stored at 4 °C. The main parameters of GW are presented in Table 1.

Experimental procedure

All the laboratory scale experiments of the photochemical NP oxidation were performed in batch mode at ambient room temperature (23 ± 1 °C). NP solutions (50 μM, 0.8 L) were treated in a 1.0-L cylindrical glass reactor for a period of 3 h with permanent stirring at a speed sufficient to evenly distribute and completely dissolve the iron activator. The treatment

Table 1 Chemical composition and main parameters of water samples

Parameter	Unit	Groundwater
pH		7.94
Alkalinity	mgCaCO$_3$ L^{-1}	342
Conductivity	μS cm^{-1}	763
Total organic carbon (TOC)	mg L^{-1}	16.40
Fe^{2+}	mg L^{-1}	0.005
Total Fe	mg L^{-1}	0.038
F$^-$	mg L^{-1}	0.269
Cl$^-$	mg L^{-1}	73.57
NO$_2^-$	mg L^{-1}	0.627
NO$_3^-$	mg L^{-1}	1.127
SO$_4^{2-}$	mg L^{-1}	34.94

trials were carried out in UW at an initial pH of 5.8 ± 0.25 as well as in GW at an initial pH of 7.94 ± 0.2. The iron activator (FeSO$_4$·7H$_2$O) was added first, and after its complete dissolution, the oxidation was initiated by adding PS and exposing to UV radiation. In the case of combined PS/H$_2$O$_2$ system, both oxidants were added to the working solution simultaneously. A low-pressure mercury germicidal lamp (11 W, Philips TUV PL-S) located in a quartz tube inside the reactor was used as an UV source. The average irradiance entering the solution in the reactor measured by spectrometer (Ocean Optics USB2000+) equipped with SpectraSuite software was 2.7 mW cm^{-2}. The lamp was turned on at least 5 min prior the trial to provide a constant output. A water cooling jacket was used to keep the constant temperature in the reactor. The molar concentration of PS used varied between 50 and 1000 μM in the UV/PS systems. The UV/PS/Fe^{2+} oxidation trials were conducted at different concentrations of PS ranging from 50 to 1000 μM along with varying activator molar concentrations ([Fe^{2+}]$_0$ = 12.5–500 μM). In the case of UV-induced dual oxidant (PS/H$_2$O$_2$) systems, the oxidation was conducted at fixed [PS]$_0$ = 50 μM but different concentrations of H$_2$O$_2$ in the range of 5–50 μM. The non-activated PS and H$_2$O$_2$ as well as dark PS/Fe^{2+} and H$_2$O$_2$/Fe^{2+} experiments on NP degradation were conducted in identical reactor and treatment condition for the respective UV-activated oxidation trials. Samples were withdrawn at pre-determined time intervals and the oxidation quenching was done by the addition of EtOH (sample/EtOH volume ratio of 10/1). All experiments were duplicated; the results of the analysis are presented as the mean with a standard deviation of at least two parallel replicates less than 5% error.

Identification of active radical species

Radical scavengers were applied to identify the main radical species involved in the decomposition of NP by the UV/PS, UV/PS/Fe^{2+}, UV/PS/H$_2$O$_2$, and UV/PS/H$_2$O$_2$/Fe^{2+} processes. Two radical probes, t-BuOH and EtOH, were used to differentiate the role of HO$^•$ and SO$_4^{•-}$ in NP degradation by the studied systems. An excess concentration of scavenger was spiked into the reaction solutions before the oxidant addition at a NP/[t-BuOH]$_0$ and NP/[EtOH]$_0$ M ratio of 1/500.

Analytical methods

NP concentration was quantified using high-performance liquid chromatography combined with a diode array detector (HPLC-PDA, Shimadzu) and equipped with a Phenomenex Gemini (150 × 2.0 mm, 1.7 mm) NX-C18 (110 Å, 5 μm) column. The analysis was performed using an isocratic method with a mobile phase mixture of 85% acetonitrile (with 0.3% formic acid) and 15% formic acid (0.3%) aqueous solution. Samples (75 μL) were analyzed at a flow rate of 0.2 mL min^{-1}

and a wavelength of 210 nm. The initial and final (after a 3-h treatment) pH value of NP solution was measured using a digital pH/Ion meter (Mettler Toledo S220). The electrical conductivity of GW was measured using a digital EC meter (HQ 430d flexi, HACH Company). The concentration of anions in GW was measured using ion chromatography with chemical suppression of the eluent conductivity (761 Compact IC, Metrohm Ltd.). The measurement of residual persulfate concentration in the treated samples (0.4 mL) was done spectrophotometrically (Genesys 10S, Thermo Scientific) at a wavelength of 352 nm by an excess KI reaction with PS towards the formation of I_2 (Liang et al. 2008). The residual concentration of PS was determined by using the standard multipoint calibration. The residual hydrogen peroxide concentration in the trials conducted was measured spectrophotometrically (GENESYS 10S, Thermo Scientific) at a wavelength of 410 nm with titanium sulfate by a hydrogen peroxide-Ti^{4+} complex formation (Eisenberg 1943). The alkalinity of GW was measured by titration with hydrochloric acid (0.1 M) in the presence of methyl orange (Mosteo et al. 2010). The total organic carbon (TOC) was measured by a TOC analyzer multi N/C® 3100 (Analytik Jena).

Results and discussion

UV-induced PS oxidation

The results of non-activated persulfate oxidation at $[PS]_0 = 500$ μM showed < 15% NP degradation with low PS utilization (< 10%) in UW and GW after a 3-h treatment. This clearly indicated the need to activate PS, e.g., by UV radiation, to improve NP degradation efficacy. The application of only UV photolysis resulted in ≥ 90% NP decomposition in both matrices after 3 h of treatment. Furthermore, the performance of UV-induced PS system in NP degradation was evaluated. The effect of oxidant concentration on the decomposition of the target compound was studied at a fixed $[NP]_0 = 50$ μM. Experiments with the UV/PS system were performed using $[PS]_0 = 50, 100, 200, 500, 1000$ μM, which corresponds to NP/PS molar ratios from 1/1 to 1/20. The obtained results revealed that NP degradation in UV photolysis and all studied UV/PS systems followed a pseudo-first-order kinetics law and may be described with regard to the NP concentration through Eq. 9.
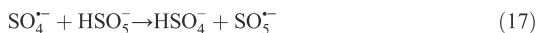
$$\frac{dC_{NP}}{dt} = -k_{obs} \times C_{NP} \qquad (9)$$

where k_{obs} is the observed pseudo-first-order rate constant and C_{NP} is the NP concentration. The k_{obs} values were calculated from the slopes of the straight lines by plotting $\ln(C_t/C_0)$ as a function of time t through linear regression (Fig. 1).

A comparison of k_{obs} values obtained for only UV photolysis in studied water matrices showed that NP decomposed faster in UW ($k_{obs} = 0.017$ min^{-1}) compared with GW ($k_{obs} = 0.012$ min^{-1}). A similar tendency was observed in the results of the UV/PS system application.
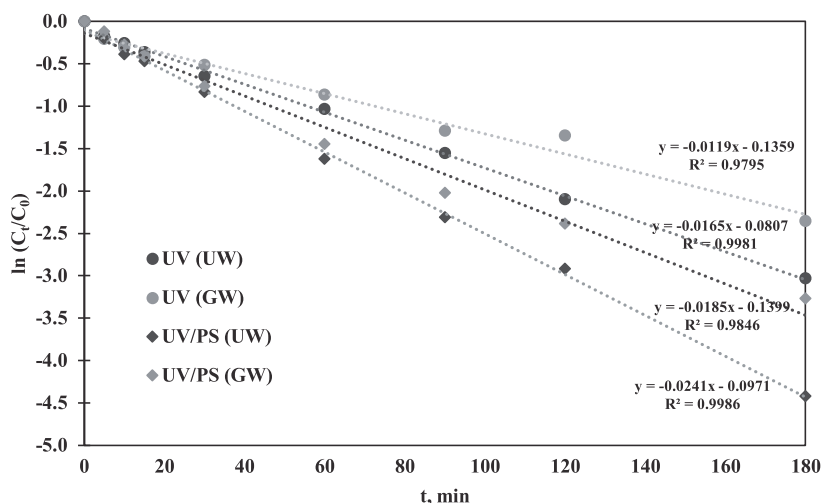
The effect of PS dosage on the treatment efficacy of UV/PS system is presented in Fig. 2. The obtained results indicated improvement in k_{obs} values of NP oxidation with increase in oxidant concentration from 50 to 200 μM in both water matrices. For instance, in UW, the k_{obs} values of 0.019 min^{-1} and 0.024 min^{-1} were obtained at $[PS]_0 = 50$ μM and 200 μM, respectively. Similarly, the UV/PS oxidation of NP in GW at the same oxidant concentrations resulted in the k_{obs} values of 0.014 min^{-1} and 0.019 min^{-1}, respectively. However, further increase in oxidant dosage up to 500 μM lowered the k_{obs} values in both water matrices. To prove the observed tendency, a trial with $[PS]_0 = 1000$ μM, corresponding to a NP/PS molar ratio of 1/20, was conducted in UW and resulted in a further decrease in k_{obs} value (0.015 min^{-1}).

This observation can be explained by the fact that the addition of excess oxidant leads to the scavenging of active radical species, SO$_4^{\bullet-}$ and HO$^\bullet$ (Eq. 10), as presented in Eqs. 11–13 and/or self-combination reactions among radicals take place as presented in Eqs. 14–19 (Matzek and Carter 2016; Waclawek et al. 2017).

$$SO_4^{\bullet-} + H_2O \rightarrow HO^\bullet + SO_4^{2-} + H^+ \qquad (10)$$

$$SO_4^{\bullet-} + S_2O_8^{2-} \rightarrow SO_4^{2-} + S_2O_8^{\bullet-} \qquad (11)$$

$$HO^\bullet + S_2O_8^{2-} \rightarrow S_2O_8^{\bullet-} + OH^- \qquad (12)$$

$$S_2O_8^{\bullet-} \rightarrow 2SO_4^{2-} \qquad (13)$$

$$SO_4^{\bullet-} + SO_4^{\bullet-} \rightarrow S_2O_8^{2-} \qquad (14)$$

$$HO^\bullet + HO^\bullet \rightarrow H_2O_2 \qquad (15)$$

$$SO_4^{\bullet-} + HO^\bullet \rightarrow HSO_5^- \qquad (16)$$

$$SO_4^{\bullet-} + HSO_5^- \rightarrow HSO_4^- + SO_5^{\bullet-} \qquad (17)$$

$$HO^\bullet + HSO_5^- \rightarrow SO_5^{\bullet-} + H_2O \qquad (18)$$

$$2SO_5^{\bullet-} \rightarrow S_2O_8^{2-} + O_2 \qquad (19)$$

Comparison of the results of applying the UV-induced PS system in the two matrices studied showed that NP decomposition was faster in UW than in GW. This observation can be explained by the fact that characteristic composition of GW can influence the oxidation efficiency of the target compound. Therefore, the generated sulfate and hydroxyl radicals might react with natural organic matter (NOM) or effluent organic matter, which are usually present in water and is persistent after conventional treatment processes (Frontistis 2019). The chemical structure of NOM contains numerous aromatic and oxygen functional groups. Therefore, NOM is recognized as a remarkable absorber of light that can produce reactive
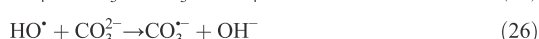
Fig. 1 NP degradation observed reaction rate constants by UV photolysis and UV/PS processes in different water matrices ($[NP]_0 = 50\ \mu M$, $[PS]_0 = 200\ \mu M$)

$y = -0.0119x - 0.1359$
$R^2 = 0.9795$

$y = -0.0165x - 0.0807$
$R^2 = 0.9981$

$y = -0.0185x - 0.1399$
$R^2 = 0.9846$

$y = -0.0241x - 0.0971$
$R^2 = 0.9986$

intermediates thus inhibiting the photo-degradation of micropollutants (Hua et al. 2019). Moreover inorganic anions such as bicarbonate (HCO_3^-), carbonate (CO_3^{2-}), chloride (Cl^-), and nitrate (NO_3^-) present in water can influence the degradation of target compound (Hu et al. 2019; McKay et al. 2016). Numerous studies have shown the negative effect of these anions on the effectiveness of AOTs by the formation of less reactive radicals (Eqs. 20–28), and thus reducing the efficiency of decomposition of the target compound (Fang et al. 2012; Lutze et al. 2015).
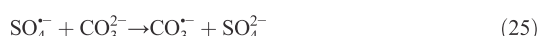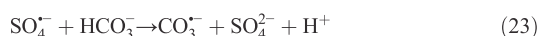
$$SO_4^{\bullet-} + Cl^- \rightarrow SO_4^{2-} + Cl^{\bullet} \tag{20}$$

$$Cl^- + Cl^{\bullet} \rightarrow Cl_2^{\bullet-} \tag{21}$$

$$HO^{\bullet} + Cl^- \rightarrow HOCl^- \tag{22}$$

$$SO_4^{\bullet-} + HCO_3^- \rightarrow CO_3^{\bullet-} + SO_4^{2-} + H^+ \tag{23}$$

$$HO^{\bullet} + HCO_3^- \rightarrow CO_3^{\bullet-} + H_2O \tag{24}$$

$$SO_4^{\bullet-} + CO_3^{2-} \rightarrow CO_3^{\bullet-} + SO_4^{2-} \tag{25}$$

$$HO^{\bullet} + CO_3^{2-} \rightarrow CO_3^{\bullet-} + OH^- \tag{26}$$

$$SO_4^{\bullet-} + NO_3^- \rightarrow NO_3^{\bullet} + SO_4^{2-} \tag{27}$$

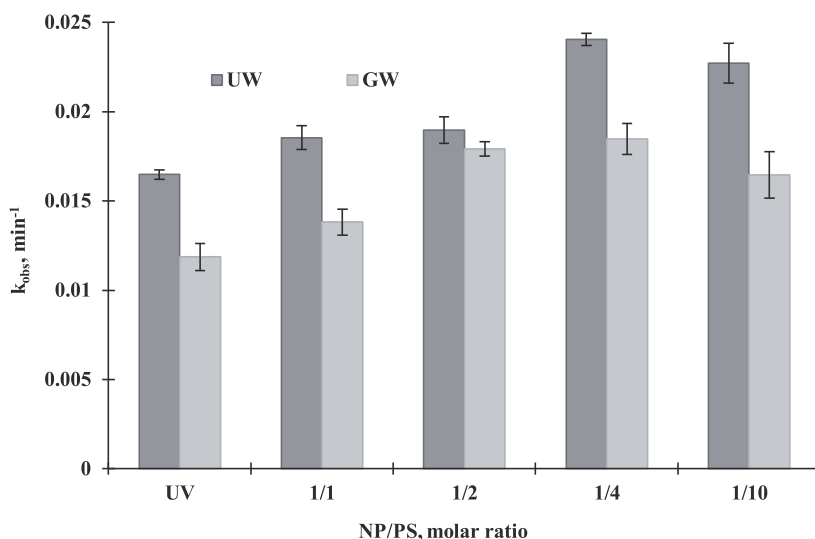$$HO^{\bullet} + NO_3^- \rightarrow NO_3^{\bullet} + OH^- \tag{28}$$
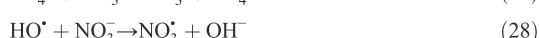
Fig. 2 NP degradation observed reaction rate constants by UV photolysis and UV/PS processes at different NP/PS molar ratios ($[NP]_0 = 50\ \mu M$)

As shown in Fig. S1, the effect of the addition of chlorides and bicarbonates on NP oxidation of PS in ultrapure water was investigated. Based on the results obtained, it can be assumed that chlorides have a neutral or positive effect on the rate of NP degradation, at least within the concentrations studied in this work. The presence of HCO_3^- at a concentration of 200 mg L^{-1} slightly increased the rate of NP degradation, while an inhibition effect was observed at 500 mg L^{-1}. The effect of the presence of NOM (humic acids) on NP degradation by the UV/PS system was also studied (Fig. S2). In contrast to experiments with inorganic anions, the presence of NOM considerably inhibited the target compound oxidation. Accordingly, 80%, 44%, and 20% of NP were decomposed after 60 min of reaction in ultrapure water, 5 mg C L^{-1}, and 10 mg L^{-1} NOM-containing solution, respectively.

To obtain a further insight into reaction mechanism in the studied UV-induced PS-based systems, the concentration of residual persulfate was also measured. The oxidant consumption has steadily increased with an increase in the amount of added oxidant in both matrices, even though the efficiency of NP decomposition decreases at elevated PS dosages. Accordingly, PS utilization increased from < 10% and 61% at $[PS]_0 = 50$ μM to 82% and 90% at $[PS]_0 = 500$ μM during the UV/PS treatment in GW and UW, respectively. The higher residual PS concentration observed in the GW trials can be explained by the more complex composition of a real sample of natural water, where UV radiation is also absorbed by other components of the matrix.

The influence of the water matrix composition on the pH value of the treated solution was also examined. As a result, after a 3-h UV/PS treatment in UW, a drop in pH from an initial value of 5.8 ± 0.25 to 3.85 ± 0.2 was observed. On the other hand, only a negligible change in pH value was observed in GW ($pH_{initial} = 7.9 \pm 0.2$ and $pH_{final} = 7.3 \pm 0.3$), mainly due to the buffering capacity of the natural water sample (Table 1).

Overall, considering all the studied UV/PS systems in both water matrices, the PS dosage of 200 μM (NP/PS molar ratio of 1/4) proved the most efficient for NP degradation. These results were used further to evaluate the effectiveness of NP decomposition in the dual-activated UV/PS/Fe^{2+} system.

UV-induced Fe^{2+}-activated PS oxidation

To investigate the performance of NP degradation in the UV/PS/Fe^{2+} system, trials were first conducted with a variable molar concentration of PS ranging from 50 to 1000 μM at a fixed molar concentration of activator ($[Fe^{2+}]_0 = 50$ μM) as presented in Fig. 3. Similar to the UV/PS system trials, the obtained results indicated that the NP degradation in the UV/Fe^{2+}-activated PS systems followed a pseudo-first-order kinetics, and thus k_{obs} values were calculated.

Irrespective of the applied PS concentration, NP degradation was slower in the UV/PS/Fe^{2+} system as compared with the results of UV/PS treatment in UW. Thus, the UV-induced PS/Fe^{2+} and PS oxidation at the same NP/PS molar ratio of 1/1 resulted in a k_{obs} value of 0.015 min^{-1} and 0.019 min^{-1}, respectively. A slight improvement in the efficiency of NP degradation was observed at a NP/PS/Fe^{2+} molar ratio of 1/4/1 with a k_{obs} value of 0.016 min^{-1}. However, a further increase in the concentration of the oxidant, as in the case of UV-induced PS process, led to a slower rate of NP degradation in the UV/PS/Fe^{2+} system. As a result, k_{obs} values of 0.006 min^{-1} and 0.005 min^{-1} were obtained at NP/PS/Fe^{2+} molar ratios of 1/10/1 and 1/20/1, respectively. The lower efficacy of the UV/PS/Fe^{2+} systems compared with the UV-activated PS process at an oxidant concentration in the range 50–200 μM can be explained by the fact that the added Fe^{2+} scavenges HO$^{\bullet}$ and SO$_4^{\bullet-}$ (Eqs. 29–30) and, as a result, reduces the target contaminant degradation efficiency (Liang et al. 2004; Matzek and Carter 2016; Vicente et al. 2011).

$$SO_4^{\bullet-} + Fe^{2+} \rightarrow Fe^{3+} + SO_4^{2-} \qquad (29)$$

$$HO^{\bullet} + Fe^{2+} \rightarrow Fe^{3+} + OH^- \qquad (30)$$

In the case of elevated PS concentrations (> 200 μM), similar to the UV/PS systems, the decrease in treatment efficacy is mainly due to the scavenging reactions between PS and SO$_4^{\bullet-}$/HO$^{\bullet}$ (Eqs. 11–13) as well as due to the recombination of radicals (Eqs. 14–16).

The effectiveness of the UV/PS/Fe^{2+} system in terms of NP decomposition was also studied in GW (Fig. 3). The data obtained showed that the chemical composition of the GW matrix also has an inhibitory effect on the oxidation rate of the target compound in the combined system, but to a lesser extent than in the case of the UV-activated PS process. Thus, k_{obs} values of 0.016 min^{-1} and 0.014 min^{-1} were obtained at a NP/PS/Fe^{2+} molar ratio of 1/4/1 in UW and GW, respectively. On the other hand, similar to the UW tests, the NP degradation efficiency was lower in the dual-activated PS system compared with the UV/PS system. Accordingly, the addition of Fe^{2+} to the UV/PS system, provided that all other treatment conditions were unchanged, resulted in a 1.4-fold decrease in the k_{obs} value.

Overall, the utilization of PS in the studied UV/PS/Fe^{2+} systems was increasing along with the increase in oxidant concentration in UW. Accordingly, 69% and 93% of initial concentration of PS was consumed after a 3-h treatment at a NP/PS/Fe^{2+} molar ratio of 1/1/1 and 1/4/1, respectively. At the same molar ratio of 1/4/1 used in GW, about 70% of the initial PS concentration was consumed, which indicates a higher stability of the oxidant in the real water matrix compared with the artificial solution. In general, by comparing the efficiency of NP decomposition and PS consumption, it can be assumed that the

Fig. 3 Effect of PS concentration NP degradation observed reaction rate constants by UV/PS and UV/PS/Fe^{2+} processes in different water matrices ([NP]$_0$ = [Fe^{2+}]$_0$ = 50 μM)
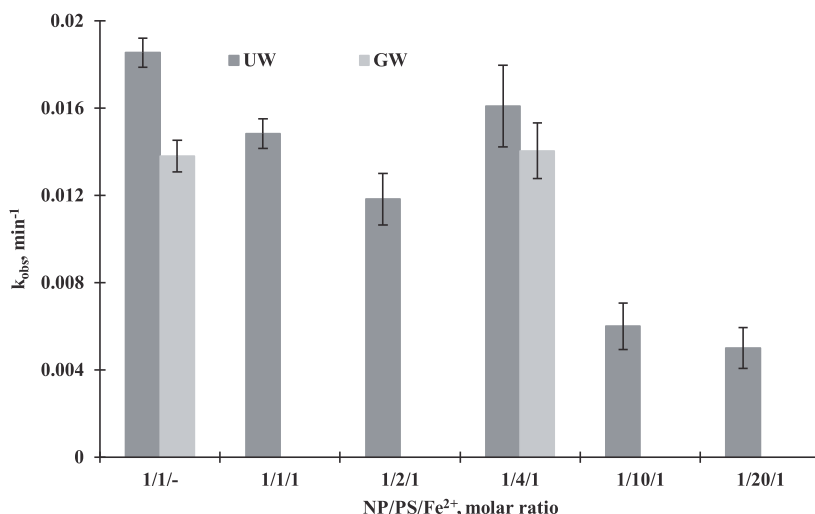
application of dual UV/Fe^{2+} activation of PS lead to irrational over-consumption of the added oxidant.

In order to prove this assertion, the ferrous ion-activated PS oxidation at a NP/PS/Fe^{2+} molar ratio of 1/10/1 corresponding to [PS]$_0$ = 500 μM was also studied in both matrices. The results showed that around 30% and 40% NP were degraded after 3 h of dark oxidation in UW and GW, respectively, in contrast to 82% obtained in the UV-induced PS/Fe^{2+} system at the same NP/PS/Fe^{2+} molar ratio in UW. In turn, the use of PS without additional UV activation was more than moderate, and about 85–90% of residual oxidant was present in the system. Low oxidant consumption and moderate decomposition of the target compound can be explained not only by the absence of additional UV activation, but also by the limited availability of ferrous iron in the PS/Fe^{2+} system. Accordingly, the results of measuring Fe^{2+} concentration in both of the studied matrices showed that approximately 35% and 14% of the initial concentration of ferrous ions were available in the system after 5 min and 3 h of treatment, respectively. This observation is consistent with the previously reported studies and could be explained by rapid generation of SO$_4^{\bullet-}$ through the Fe^{2+}-activated dissociation of S$_2$O$_8^{2-}$. This resulted in fast accumulation of Fe^{3+}, which is most likely subsequently slowly reduced in the reaction with organic radicals (R$^{\bullet}$) as presented in Eq. (31) (Liang et al. 2004; Wu et al. 2014):

$$R^{\bullet} + Fe^{3+} \rightarrow Fe^{2+} + \text{intermediates} \qquad (31)$$

In the case of the UV-induced PS/Fe^{2+} system, more than 50% and 95% of the initial concentration of Fe^{2+} were available in the solution after 5 min and 3 h of treatment,

respectively, mainly due to effective regeneration of the ferrous iron activator through Eq. 4.

Furthermore, to investigate the influence of Fe^{2+} activator dosage on NP degradation, the UV/PS/Fe^{2+} oxidation trials were conducted at a fixed molar concentration of oxidant ([PS]$_0$ = 500 μM) along with varying molar concentration of Fe^{2+} (5–500 μM) as showed in Fig. 4.

The results showed an inverse proportionality between the efficiency of NP degradation and the added dose of iron. Thus, the UV/PS/Fe^{2+} treatment at a NP/PS/Fe^{2+} molar ratio of 1/10/0.25 resulted in the highest k_{obs} value of 0.010 min^{-1}. A further increase in the concentration of [Fe^{2+}]$_0$ by 4 and 8 times led to a slowdown in the decomposition of the target compound with a k_{obs} value of 0.006 min^{-1} and 0.003 min^{-1}, respectively. It is noteworthy that in all the systems studied, after 3 h of oxidation, almost complete (~95%) PS utilization and high (~95%) availability of Fe^{2+} was observed along with the acidic (~3.2) final solution pH. The latter can be explained by the acidic nature of the activator and oxidant as well as formation of acidic intermediate products during a 3-h treatment (Liang et al. 2004).

The findings of this study suggest that the UV-induced PS/Fe^{2+} system can potentially be applied for effective NP decomposition in different water matrices, but a prudent optimization of the iron activator and oxidant dosage will be required to suppress the radicals scavenging reactions with excess of Fe^{2+} and/or PS.

UV-induced combined PS/H$_2$O$_2$ oxidation

In the UV-activated dual oxidant (PS/H$_2$O$_2$) system, the high reactivity of hydrogen peroxide and the water stability of

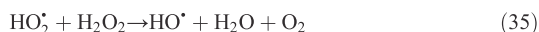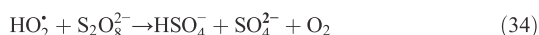**Fig. 4** Effect of Fe^{2+} concentration on NP degradation observed reaction rate constants by UV/PS/Fe^{2+} process in UW ([NP]$_0$ = 50 μM, [PS]$_0$ = 500 μM)
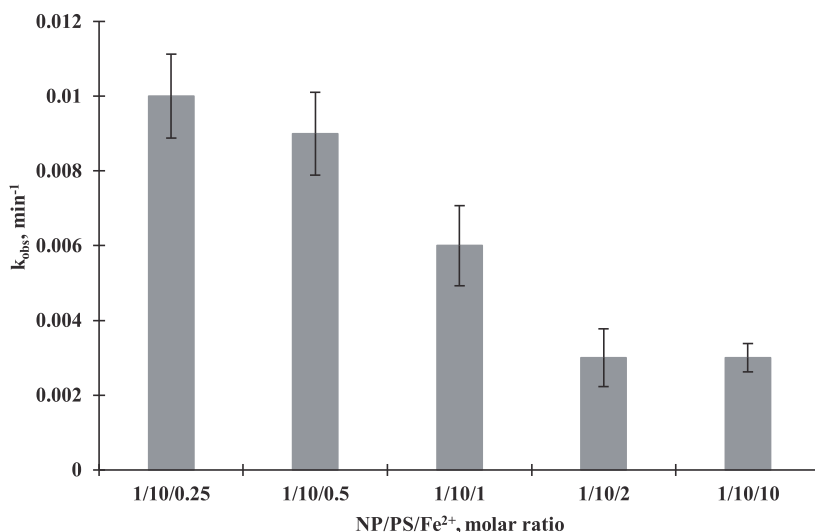
persulfate make it possible to simultaneously generate $HO^\bullet$ and $SO_4^{\bullet-}$. The formation of radicals follows a series of reactions and begins with the thermal decomposition of PS, as represented in Eq. 6. Chu et al. (2011) suggested that the simultaneous presence of PS and H_2O_2 plays a role in initiating the decomposition of PS to $SO_4^{\bullet-}$ by direct peroxide activation (Eq. 32).

$$S_2O_8^{2-} + H_2O_2 \rightarrow SO_4^{\bullet-} + HO_2^\bullet + HSO_4^- \qquad (32)$$
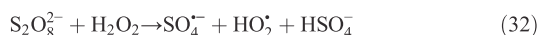
A further mechanism can be described as represented in Eqs. 33–35:

$$HO^\bullet + H_2O_2 \rightarrow H_2O + HO_2^\bullet \qquad (33)$$

$$HO_2^\bullet + S_2O_8^{2-} \rightarrow HSO_4^- + SO_4^{2-} + O_2 \qquad (34)$$

$$HO_2^\bullet + H_2O_2 \rightarrow HO^\bullet + H_2O + O_2 \qquad (35)$$

Accordingly, the efficacy of NP degradation by dual UV-activated PS/H_2O_2 and combined UV/PS and photo-Fenton systems were studied in UW and under optimized treatment conditions in GW. The effect of hydrogen peroxide concentration on the efficiency of the UV/PS/H_2O_2 system was considered at a fixed [PS]$_0$ = 50 μM and varying [H_2O_2]$_0$ = 5–50 μM, as presented in Fig. 5. The application of UV-induced dual oxidant process demonstrated ≥ 90% NP degradation in all studied systems in a 3-h treatment.

Firstly, the photolysis of H_2O_2 was carried out at [H_2O_2]$_0$ = 50 μM, corresponding to a NP/H_2O_2 molar ratio of 1/1, and the results showed 96% NP degradation. The obtained k_{obs} value (0.024 min^{-1}) was comparable with the results obtained for the UV-induced PS system at a NP/PS molar ratio of 1/4

(0.024 min^{-1}) in UW, indicating a higher efficiency of the UV/H_2O_2 process compared with UV/PS system at the same concentration of oxidant. Notably, the direct H_2O_2 oxidation conducted at [H_2O_2]$_0$ = 50 μM resulted in only 15% NP degraded with more than 90% residual H_2O_2 in both matrices after a 3-h oxidation.

The application of combined UV/PS/H_2O_2 treatment at [PS]$_0$ = 50 μM along with [H_2O_2]$_0$ = 5 μM resulted in a k_{obs} value of 0.02 min^{-1}, indicating a negligible improvement in NP degradation compared with the UV/PS system at a NP/PS molar ratio of 1/1 (0.019 min^{-1}). A 2.5-fold increase in [H_2O_2]$_0$ to 12.5 μM, corresponding to a NP/PS/H_2O_2 molar ratio of 1/1/0.25, slightly improved the efficacy of NP decomposition and the obtained k_{obs} value was 0.022 min^{-1}. A further increase in the concentration of hydrogen peroxide led to a slowdown in the degradation of NP and proved unreasonable. Most likely, an increase in the dosage of H_2O_2 provokes an escalation of the scavenging reactions between the generated free radicals and the oxidant (Lin et al. 2016).

The performance of NP degradation in the UV/PS/H_2O_2 system in GW was studied at a NP/PS/H_2O_2 molar ratio of 1/1/0.25 (Fig. 5). The composition of the real water matrix clearly hindered the target compound decomposition by the combined system, since the calculated k_{obs} value of 0.006 min^{-1} was 3 times lower than the k_{obs} value (0.014 min^{-1}) obtained in the UV/PS system at a NP/PS molar ratio of 1/1.

Overall, the results of UV-activated PS/H_2O_2 system at a NP/PS/H_2O_2 molar ratio of 1/1/0.25 conducted in both water matrices (more than 98% NP degradation) were considerably

Fig. 5 NP degradation observed reaction rate constants by UV/PS/H_2O_2 and UV/PS/H_2O_2/Fe^{2+} processes at different H_2O_2 concentrations in different water matrices ($[NP]_0 = [PS]_0 = 50$ μM, $[Fe^{2+}]_0 = 12.5$ μM)
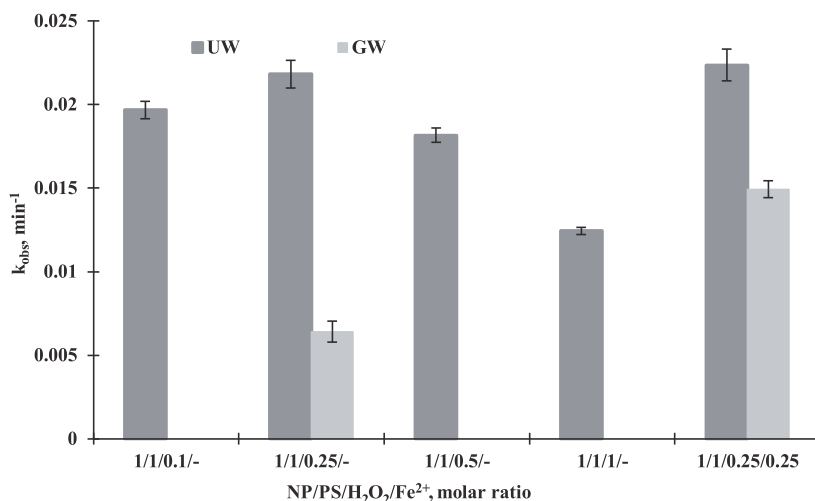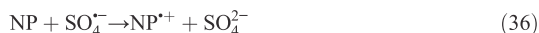
better than in the dark PS/H_2O_2 oxidation at the same treatment conditions (28% in UW and 6% in GW).

The finding of this study showed that the efficacy of NP degradation in the UV-activated PS/H_2O_2 system was considerably enhanced compared with the UV/PS/Fe^{2+} process. Therefore, the combined UV/PS/H_2O_2/Fe^{2+} system at a NP/PS/H_2O_2/Fe^{2+} at molar ratio of 1/1/0.25/0.25 was also studied (Fig. 5). Accordingly, no notable improvement in treatment efficacy was observed in UW, indicating a limited effect of the additional activator on improving NP degradation in a model un-buffered solution. In the case of GW, a 2.5-fold increase in the k_{obs} value (0.015 min^{-1}) was obtained compared with the UV/PS/H_2O_2 treatment at a NP/PS/H_2O_2 molar ratio of 1/1/0.25, which indicates a more efficient generation of HO$^{\bullet}$ and SO$_4^{\bullet-}$ using the supplied Fe^{2+}. Notably, the application of dark PS/H_2O_2/Fe^{2+} oxidation under the same treatment conditions in UW and GW showed substantially lower efficiency (26% and 33% NP degradation, respectively) after 3 h of treatment compared with the combined UV-induced system.

The utilization of H_2O_2 was measured in the UV/PS/H_2O_2 and UV/PS/H_2O_2/Fe^{2+} systems in both water matrices. However, it should be noted that due to interference caused by the presence of hydrogen peroxide the residual concentrations of persulfate were not measured in the studied systems. In contrast, the presence of residual PS still allowed the measurement of un-dissociated H_2O_2 and showed incomplete oxidant utilization after 3 h treatment in the UV/PS/H_2O_2 systems. Overall, the results showed a slight improvement in the utilization of H_2O_2 with increasing $[H_2O_2]_0$ concentration in the UV/PS/H_2O_2 systems. Accordingly, at a NP/PS/H_2O_2 molar ratio of 1/1/0.25, only 17% and 12% of initial concentration of H_2O_2 was utilized in UW and GW, respectively. A further 4-fold increase in the dose of H_2O_2, corresponding to

a NP/PS/H_2O_2 molar ratio of 1/1/1, demonstrated a 2-fold improvement (28%) in the consumption of H_2O_2 in UW. Irrespective of the water matrix studied, the highest H_2O_2 utilization was observed in the UV/PS/H_2O_2/Fe^{2+} system in UW and GW with 52% and 32% oxidant consumed, respectively, which in turn indicates the predominance of different radicals scavenging reactions over NP oxidation reactions (Eqs. 36–39).

$$NP + SO_4^{\bullet-} \rightarrow NP^{\bullet+} + SO_4^{2-} \tag{36}$$

$$NP^{\bullet+} + H_2O \rightarrow (HO)NP^{\bullet} + H^+ \tag{37}$$

$$NP + HO^{\bullet} \rightarrow (HO)NP^{\bullet} \tag{38}$$

$$(HO)NP^{\bullet} \rightarrow intermediate\ products \rightarrow CO_2 + H_2O \tag{39}$$

Overall, comparing the results of all UV-induced PS/H_2O_2 and combined persulfate/Fenton systems studied in both UW and GW, it can be concluded that the application of carefully adjusted UV/PS/H_2O_2/Fe^{2+} treatment is a promising solution for the abatement of NP contamination in different water matrices.

Identification of active radical species

To identify the predominant radical species responsible for the degradation of NP in the UV/PS, UV/PS/Fe^{2+}, UV/PS/H_2O_2, and UV/PS/H_2O_2/Fe^{2+} systems, scavenging studies using two radical probes were carried out. The experiments were conducted with the addition of *t*-BuOH, which is more effective scavenger for HO$^{\bullet}$ (3.8×10^8–7.6×10^8 $M^{-1} \cdot s^{-1}$) than for SO$_4^{\bullet-}$ (4×10^5–9.1×10^5 $M^{-1}\ s^{-1}$), and EtOH, reacting at high and comparable rates with HO$^{\bullet}$ (1.2×10^9–2.8×10^9 $M^{-1}\ s^{-1}$) and SO$_4^{\bullet-}$ (1.6×10^7–7.7×10^7 $M^{-1}\ s^{-1}$) (Anipsitakis and

Dionysiou 2004.). Thus, the presence of HO$^{\bullet}$ was identified by adding excess t-BuOH to the studied systems. While the existence and role of SO$_4^{\bullet-}$ was estimated by comparing the difference between the decomposition efficiency of NP after adding excess t-BuOH and EtOH.

The results indicated that the addition of excess t-BuOH decreased the efficacy of NP degradation by about 17%, 3%, 13%, and 14% in the UV/PS, UV/PS/Fe^{2+}, UV/PS/H$_2$O$_2$, and UV/PS/H$_2$O$_2$/Fe^{2+} systems, respectively, suggesting that HO$^{\bullet}$ was involved in the oxidation of the target compound by all processes (Table 2).

Irrespective of the studied system, the addition of excess EtOH led to only 1–2% supplementary inhibition of the decomposition of NP compared to the use of t-BuOH. These findings suggested that both HO$^{\bullet}$ and SO$_4^{\bullet-}$ contributed to the degradation of NP in the studied systems, while HO$^{\bullet}$ turned out to be the predominant radical species.

Conclusion

The focus of the present study was the application of UV-induced PS-based processes for NP oxidation in ultrapure water and groundwater matrices. The efficacy of the performance of studied UV-induced processes in NP degradation was as follows: the UV/PS system ≥ the UV/PS/H$_2$O$_2$/Fe^{2+} system ≈ the UV/PS/H$_2$O$_2$ system ≥ the UV/PS/Fe^{2+} system. The application of UV/PS treatment resulted in near to complete target compound degradation (> 90%) after 3 h oxidation with the highest k$_{obs}$ of 0.24 min^{-1} and 0.019 min^{-1} obtained at a NP/PS molar ratio of 1/4 ([PS]$_0$ = 200 μM) in UW and GW, respectively. The use of UV/PS/Fe^{2+} systems showed promising results for NP degradation at controlled oxidant and activator dosages. However, an increase in oxidant dosages showed an antagonistic effect on the rate of NP decomposition. Thus, the highest k$_{obs}$ value of 0.016 min^{-1} was obtained at a NP/PS/Fe^{2+} molar ratio of 1/4/1 in UW. The dual oxidant UV/PS/H$_2$O$_2$ system proved more favorable for NP

degradation in UW that in GW. As a result, a higher k$_{obs}$ (0.021 min^{-1}) was obtained in UW compared with GW (0.006 min^{-1}) at a NP/PS/H$_2$O$_2$ molar ratio of 1/1/0.25. However, the presence of ≥ 70% of unused hydrogen peroxide in the solution after 3 h of UV/PS/H$_2$O$_2$ treatment indicated the possibility of further optimization of this combined system to improve the decomposition of the target compound. The UV/PS/H$_2$O$_2$/Fe^{2+} process has proven to be a very promising solution to reduce NP pollution in both the model and real water matrices. The data obtained in this study clearly indicated the negative effect of the chemical composition of the GW on the efficiency of NP degradation in all studied systems. Nevertheless, the results of UW trials can be reliably used to predict the treatment efficacy of the studied processes in GW. The findings of this study suggest that the UV-activated PS system, both alone and in combination with H$_2$O$_2$/Fe^{2+}, is an effective technology for NP-contaminated water and groundwater treatment.

References

Anipsitakis GP, Dionysiou DD (2004) Radical generation by the interaction of transition metals with common oxidants. Environ Sci Technol 38:3705–3712. https://doi.org/10.1021/es035121o

Babuponnusami A, Muthukumar K (2014) A review on Fenton and improvements to the Fenton process for wastewater treatment. J Environ Chem Eng 2:557–572. https://doi.org/10.1016/j.jece.2013.10.011

Barrera-Díaz CE, Frontana-Uribe BA, Rodríguez-Peña M, Gomez-Palma JC, Bilyeu B (2018) Integrated advanced oxidation process, ozonation-electrodegradation treatments, for nonylphenol removal in batch and continuous reactor. Catal Today 305:108–116. https://doi.org/10.1016/j.cattod.2017.09.003

Bertanza G, Pedrazzani R, Dal Grande M, Papa M, Zambarda V, Montani C, Steimberg N, Mazzoleni G, Di Lorenzo D (2011) Effect of biological and chemical oxidation on the removal of estrogenic compounds (NP and BPA) from wastewater: an integrated assessment procedure. Water Res 45:2473–2484. https://doi.org/10.1016/j.watres.2011.01.026

Chu W, Wang YR, Leung HF (2011) Synergy of sulfate and hydroxyl radicals in UV/S2O82−/H2O2 oxidation of iodinated X-ray contrast medium iopromide. Chem Eng J 178:154–160. https://doi.org/10.1016/j.cej.2011.10.033

Dulov A, Dulova N, Trapido M (2013) Photochemical degradation of nonylphenol in aqueous solution: the impact of pH and hydroxyl

Table 2 Degradation of NP by UV-induced PS-based systems ([NP]$_0$ = 50 μM, [PS]$_0$ = 50 μM, [H$_2$O$_2$]$_0$ = 12.5 μM, [Fe^{2+}]$_0$ = 50 μM (in the UV/PS/Fe^{2+} system), [Fe^{2+}]$_0$ = 12.5 μM (in the UV/PS/H$_2$O$_2$/Fe^{2+} system), [t-BuOH]$_0$ = [EtOH]$_0$ = 25 mM, t = 15 min)

Process	[NP]/[NP]$_0$, %		
	Without scavenger	t-BuOH	EtOH
UV/PS	63	80	82
UV/PS/Fe^{2+}	68	72	73
UV/PS/H$_2$O$_2$	67	80	81
UV/PS/H$_2$O$_2$/Fe^{2+}	58	72	73

radical promoters. J Environ Sci 25:1326–1330. https://doi.org/10.1016/S1001-0742(12)60205-8

Dulova N, Trapido M (2011) Application of Fenton's reaction for food-processing wastewater treatment. J Adv Oxid Technol 14:9–16. https://doi.org/10.1515/jaots-2011-0101

Eisenberg G (1943) Colorimetric determination of hydrogen peroxide. Ind Eng Chem Anal Ed 15:327–328. https://doi.org/10.1021/i560117a011

ElShafei GMS, Yehia FZ, Eshaq G, ElMetwally AE (2017) Enhanced degradation of nonylphenol at neutral pH by ultrasonic assisted-heterogeneous Fenton using nano zero valent metals. Sep Purif Technol 178:122–129. https://doi.org/10.1016/j.seppur.2017.01.028

Fang G-D, Dionysiou DD, Wang Y, Al-Abed SR, Zhou D-M (2012) Sulfate radical-based degradation of polychlorinated biphenyls: effects of chloride ion and reaction kinetics. J Hazard Mater 227-228:394–401. https://doi.org/10.1016/j.jhazmat.2012.05.074

Frontistis Z (2019) Degradation of the nonsteroidal anti-inflammatory drug piroxicam from environmental matrices with UV-activated persulfate. J Photochem Photobiol A Chem 378:17–23. https://doi.org/10.1016/j.jphotochem.2019.04.016

Giger W, Brunner PH, Schaffner C (1984) 4-Nonylphenol in sewage sludge: accumulation of toxic metabolites from nonionic surfactants. Science 225:623–625. https://doi.org/10.1126/science.6740328

Guenther K, Heinke V, Thiele B, Kleist E, Prast H, Raecker T (2002) Endocrine disrupting nonylphenols are ubiquitous in food. Environ Sci Technol 36:1676–1680. https://doi.org/10.1021/es010199v

Hesselsøe M, Jensen D, Skals K, Olesen T, Moldrup P, Roslev P, Mortensen GK, Henriksen K (2001) Degradation of 4-nonylphenol in homogeneous and nonhomogeneous mixtures of soil and sewage sludge. Environ Sci Technol 35:3695–3700. https://doi.org/10.1021/es010024l

Hori H, Yamamoto A, Hayakawa E, Taniyasu S, Yamashita N, Kutsuna S, Kiatagawa H, Arakawa R (2005) Efficient decomposition of environmentally persistent perfluorocarboxylic acids by use of persulfate as a photochemical oxidant. Environ Sci Technol 39:2383–2388. https://doi.org/10.1021/es0484754

Hu J, Wang C, Ye Z, Dong H, Li M, Chen J, Qiang Z (2019) Degradation of iodinated disinfection byproducts by VUV/UV process based on a mini-fluidic VUV/UV photoreaction system. Water Res 158:417–423. https://doi.org/10.1016/j.watres.2019.03.056

Hua Z, Kong X, Hou S, Zou S, Xu X, Huang H, Fang J (2019) DBP alteration from NOM and model compounds after UV/persulfate treatment with post chlorination. Water Res 158:237–245. https://doi.org/10.1016/j.watres.2019.04.030

Ince NH, Gültekin I, Tezcanli-Güyer G (2009) Sonochemical destruction of nonylphenol: effects of pH and hydroxyl radical scavengers. J Hazard Mater 172:739–743. https://doi.org/10.1016/j.jhazmat.2009.07.058

Karci A, Arslan-Alaton I, Bekbolet M (2013) Oxidation of nonylphenol ethoxylates in aqueous solution by UV-C photolysis, H2O2/UV-C, Fenton and photo-Fenton processes: are these processes toxicologically safe? Water Sci Technol 68:1801–1809. https://doi.org/10.2166/wst.2013.422

Kim J, Korshin G, Velichenko A (2005) Comparative study of electro-chemical degradation and ozonation of nonylphenol. Water Res 39:2527–2534. https://doi.org/10.1016/j.watres.2005.04.070

Kulik N, Panova Y, Trapido M (2007) The Fenton chemistry and its combination with coagulation for treatment of dye solutions. Sep Sci Technol 42:1521–1534. https://doi.org/10.1080/01496390701290185

Kümmerer K (2009) The presence of pharmaceuticals in the environment due to human use–present knowledge and future challenges. J Environ Manag 90:2354–2366. https://doi.org/10.1016/j.jenvman.2009.01.023

Lee P-C, Lee W (1996) In vivo estrogenic action of nonylphenol in immature female rats. Bull Environ Contam Toxicol 57:341–348. https://doi.org/10.1007/s001289900196

Liang C, Bruell CJ, Marley MC, Sperry KL (2004) Persulfate oxidation for in situ remediation of TCE. I. Activated by ferrous ion with and without a persulfate–thiosulfate redox couple. Chemosphere 55:1213–1223. https://doi.org/10.1016/j.chemosphere.2004.01.029

Liang C, Huang C-F, Mohanty N, Kurakalva RM (2008) A rapid spectrophotometric determination of persulfate anion in ISCO. Chemosphere 73:1540–1543. https://doi.org/10.1016/j.chemosphere.2008.08.043

Lin CK, Bashir MJK, Abu Amr SS, Sim LC (2016) Post-treatment of palm oil mill effluent (POME) using combined persulphate with hydrogen peroxide (S2O82−/H2O2) oxidation. Water Sci Technol 74:2675–2682. https://doi.org/10.2166/wst.2016.458

Litter IM, Quici N (2010) Photochemical advanced oxidation processes for water and wastewater treatment. Recent Patents Eng 4:217–241. https://doi.org/10.2174/187221210794578574

Liu X, Zhou Y, Zhang J, Luo L, Yang Y, Huang H, Peng H, Tang L, Mu Y (2018) Insight into electro-Fenton and photo-Fenton for the degradation of antibiotics: mechanism study and research gaps. Chem Eng J 347:379–397. https://doi.org/10.1016/j.cej.2018.04.142

Loyo-Rosales JE, Rice CP, Torrents A (2010) Fate and distribution of the octyl- and nonylphenol ethoxylates and some carboxylated transformation products in the Back River, Maryland. J Environ Monit 12:614–621. https://doi.org/10.1039/B913229E

Lutze HV, Kerlin N, Schmidt TC (2015) Sulfate radical-based water treatment in presence of chloride: formation of chlorate, inter-conversion of sulfate radicals into hydroxyl radicals and influence of bicarbonate. Water Res 72:349–360. https://doi.org/10.1016/j.watres.2014.10.006

Matzek LW, Carter KE (2016) Activated persulfate for organic chemical degradation: a review. Chemosphere 151:178–188. https://doi.org/10.1016/j.chemosphere.2016.02.055

McKay G, Couch KD, Mezyk SP, Rosario-Ortiz FL (2016) Investigation of the coupled effects of molecular weight and charge-transfer interactions on the optical and photochemical properties of dissolved organic matter. Environ Sci Technol 50:8093–8102. https://doi.org/10.1021/acs.est.6b02109

Messele SA, Stüber F, Bengoa C, Fortuny A, Fabregat A, Font J (2012) Phenol degradation by heterogeneous Fenton-like reaction using Fe supported over activated carbon. Procedia Eng 42:1373–1377. https://doi.org/10.1016/j.proeng.2012.07.529

Mosteo R, Miguel N, Ormad Maria P, Ovelleiro JL (2010) Effect of advanced oxidation processes on nonylphenol removal with respect to chlorination in drinking water treatment. Water Sci Technol Water Supply 10:51–57. https://doi.org/10.2166/ws.2010.726

Naya S, Nikawa T, Kimura K, Tada H (2013) Rapid and complete removal of nonylphenol by gold nanoparticle/rutile titanium(IV) oxide plasmon photocatalyst. ACS Catal 3:903–907. https://doi.org/10.1021/cs400169u

Pignatello JJ, Oliveros E, MacKay A (2006) Advanced oxidation processes for organic contaminant destruction based on the Fenton reaction and related chemistry. Crit Rev Environ Sci Technol 36:1–84. https://doi.org/10.1080/10643380500326564

Takdastan A, Kakavandi B, Azizi M, Golshan M (2018) Efficient activation of peroxymonosulfate by using ferroferric oxide supported on carbon/UV/US system: a new approach into catalytic degradation of bisphenol A. Chem Eng J 331:729–743. https://doi.org/10.1016/j.cej.2017.09.021

Vicente F, Santos A, Romero A, Rodriguez S (2011) Kinetic study of diuron oxidation and mineralization by persulphate: effects of temperature, oxidant concentration and iron dosage method. Chem Eng J 170:127–135. https://doi.org/10.1016/j.cej.2011.03.042

Waclawek S, Lutze HV, Grübel K, Padil VVT, Černík M, Dionysiou DD (2017) Chemistry of persulfates in water and wastewater treatment:

a review. Chem Eng J 330:44–62. https://doi.org/10.1016/j.cej.2017.07.132

Waldemer RH, Tratnyek PG, Johnson RL, Nurmi JT (2007) Oxidation of chlorinated ethenes by heat-activated persulfate: kinetics and products. Environ Sci Technol 41:1010–1015. https://doi.org/10.1021/es062237m

Wu X, Gu X, Lu S, Xu M, Zang X, Miao Z, Qiu Z, Sui Q (2014) Degradation of trichloroethylene in aqueous solution by persulfate activated with citric acid chelated ferrous ion. Chem Eng J 255:585–592. https://doi.org/10.1016/j.cej.2014.06.085

Yim B, Yoo Y, Maeda Y (2003) Sonolysis of alkylphenols in aqueous solution with Fe(II) and Fe(III). Chemosphere 50:1015–1023. https://doi.org/10.1016/S0045-6535(02)00665-3

Ying G-G, Williams B, Kookana R (2002) Environmental fate of alkylphenols and alkylphenol ethoxylates—a review. Environ Int 28:215–226. https://doi.org/10.1016/S0160-4120(02)00017-X

CURRICULUM VITAE

Personal data

Name: Balpreet Kaur
Date of birth: 13.11.1988
Place of birth: Faridkot, India
Citizenship: India

Contact data

E-mail: bakaur@taltech.ee

Education

2015–2017   Tallinn University of Technology, MSc in Engineering
2011–2013   Lovely Professional University, MSc in Biotechnology
2008–2011   Lovely Professional University, BSc in Biotechnology
1993–2007   High school, Dasmesh Public School

Language competence

Punjabi   mother tongue
Hindi   native speaker
English   fluent
French   beginner

Professional employment

2017–2019 Tallinn University of Technology, Department of Materials and Environmental Technology, Early Stage Researcher

Defended thesis

Master's Degree: Degradation of amoxicillin in aqueous solution by photo-activated persulfate, Tallinn University of Technology School of Engineering, Department of Materials and Environmental Technology, 2017, Supervisors: Niina Dulova, Eneliis Kattel

Main areas of scientific work

1. Biosciences and Environment; 1.8. Research relating to the State of the Environment and to Environmental Protection; CERCS CLASSIFICATION: T270 Environmental technology, pollution control

1. Biosciences and Environment; 1.9. Research into Substances Hazardous to the Environment; CERCS CLASSIFICATION: P305 Environmental chemistry

4. Natural Sciences and Engineering; 4.11. Chemistry and Chemical Technology; CERCS CLASSIFICATION: T350 Chemical technology and engineering

Involvement in research projects

PRG776 Innovative energy-efficient abatement of aqueous and airborne hazardous pollutants combining pulsed corona discharge plasma with catalysis/photocatalysis

IUT1-7 Chemical engineering approach to removal of priority pollutants and emerging micropollutants from water/wastewater and soil: implementation and optimization of advanced oxidation technologies

Awards

2019 FMDTK scholarship for the participation in the 3rd European Summer School of Environmental Applications on Advanced Oxidation Processes, 3-7 June 2019, Alcoy, Spain

2019 Dora Plus programme (activity 1) scholarship for the participation in the 6th European Conference on Environmental Applications of Advanced Oxidation Processes (EAAOP-6), 26-30 June 2019, Portoroz-Portorose, Slovenia

2019 Association of Chemistry and the Environment (ACE) scholarship for the participation in the 20th European Meeting on Environmental Chemistry (EMEC 20), 2-5 December 2019, Lodz, Poland

2018 Dora Plus programme (activity 1) scholarship for the participation in the 4th International Conference on Photocatalytic and Advanced Oxidation Technologies for the Treatment of Water, Air, Soil and Surfaces (PAOT-4), 10-13 July 2018, Porto, Portugal

Supervised dissertations

Kaie Eha, Master's Degree, 2020, (sup) Niina Dulova; Balpreet Kaur, Photochemical oxidation of losartan in aqueous solution, Tallinn University of Technology, Department of Materials and Environmental Technology

Svetlana Puustusmaa, Master's Degree, 2019, (sup) Niina Dulova; Balpreet Kaur Photochemical oxidation of endocrine disrupting compound in artificial and natural water matrix, Tallinn University of Technology, Department of Materials and Environmental Technology

ELULOOKIRJELDUS

Isikuandmed

Nimi: Balpreet Kaur
Sünniaeg: 13.11.1988
Sünnikoht: Faridkot, India
Kodakondsus: India

Kontaktandmed

E-mail: bakaur@taltech.ee

Hariduskäik

2015–2017 Tallinn Tehnikaülikool, tehnikateaduste magistrikraad
2011–2013 Lovely Professional ülikool, biotehnoloogia magistrikraad
2008–2011 Lovely Professional ülikool, biotehnoloogia bakalaureusekraad
1993–2007 Dasmesh Public School, keskharidus

Keelteoskus

Pandžabi keel   emakeel
Hindi keel   emakeel
Inglise keel   kõrgtase
Prantsuse keel   algtase

Teenistuskäik

2017–2019 Tallinna Tehnikaülikool, Materjali- ja keskkonnatehnoloogia instituut, doktorant-nooremteadur

Kaitstud lõputööd

Tehnikateaduste magistrikraad: Amoksitsilliini lagundamine vesilahuses foto-aktiveeritud persulfaadiga, Tallinna Tehnikaülikool, Materjali- ja keskkonnatehnoloogia instituut, 2017, juhendajad: Niina Dulova, Eneliis Kattel

Uurimistöö põhisuunad

1. Bio- ja keskkonnateadused; 1.8. Keskkonnaseisundit ja keskkonnakaitset hõlmavad uuringud; CERCS KLASSIFIKAATOR: T270 Keskkonnatehnoloogia, reostuskontroll
1. Bio- ja keskkonnateadused; 1.9. Keskkonnaohtlikke aineid käsitlevad uuringud; CERCS KLASSIFIKAATOR: P305 Keskkonnakeemia
4. Loodusteadused ja tehnika; 4.11. Keemia ja keemiatehnika; CERCS KLASSIFIKAATOR: T350 Keemiatehnoloogia ja -masinaehitus

Osalemine uurimisprojektides

PRG776 Ohtlike vee ja õhu saasteainete lagundamine innovatiivse energiatõhusa kombineeritud impulss-koroona elektrilahenduse ja katalüüsi/fotokatalüüsiga.

IUT1-7 Keemiatehnikapõhine lähenemisviis prioriteetsete saasteainete ja uute esilekerkivate mikrosaasteainete kõrvaldamisele veest/reoveest ja pinnasest: täiustatud oksüdatsioonitehnoloogiate kasutamine ja optimeerimine

Tunnustused

2019 FMDTK välislähetuste stipendium osalemiseks suvekoolis 3rd European Summer School of Environmental Applications on Advanced Oxidation Processes, 3.-7. juuni 2019, Alcoy, Hispaania

2019 Dora Pluss (tegevus 1) stipendium osalemiseks konverentsil 6th European Conference on Environmental Applications of Advanced Oxidation Processes (EAAOP-6), 26.-30. juuni 2019, Portoroz-Portorose, Sloveenia

2019 Association of Chemistry and the Environment (ACE) stipendium osalemiseks konverentsil 20th European Meeting on Environmental Chemistry (EMEC 20), 2.-5. detsember 2019, Lodz, Poola

2018 Dora Pluss (tegevus 1) stipendium osalemiseks konverentsil 4th International Conference on Photocatalytic and Advanced Oxidation Technologies for the Treatment of Water, Air, Soil and Surfaces (PAOT-4), 10.-13. juuli 2018, Porto, Portugal

Juhendatud magistritööd

Kaie Eha, magistrikraad, 2020, (juh) Niina Dulova; Balpreet Kaur, Losartaani fotokeemiline oksüdatsioon vesilahuses, Tallinna Tehnikaülikool, Materjali- ja keskkonnatehnoloogia instituut

Svetlana Puustusmaa, magistrikraad, 2019, (juh) Niina Dulova; Balpreet Kaur, Endokriinsüsteemi häiriva ühendi fotokeemiline oksüdatsioon kunstlikus ja looduslikus vesikeskkonnas, Tallinna Tehnikaülikool, Materjali- ja keskkonnatehnoloogia instituut